UNIWERSYTET W BIAŁYMSTOKU

WYDZIAŁ CHEMII

mgr Justyna Czyrko-Horczak

Rozprawa doktorska – monotematyczny zbiór publikacji pod tytułem:

„*Charakterystyka biochemiczna i strukturalna hydrolaz S-adenozylo-ʟ-homocysteiny pochodzących z wybranych mikroorganizmów*"

Praca doktorska wykonana
w Laboratorium Biochemii i Biologii Strukturalnej
pod kierunkiem
dr hab. Krzysztofa Brzezińskiego

Białystok 2020

Pragnę serdecznie podziękować

dr hab. Krzysztofowi Brzezińskiemu

*za opiekę promotorską, nieocenioną pomoc i wsparcie udzielone
w trakcie przygotowywania niniejszej pracy, przekazanie ogromnej
wiedzy, wyrozumiałość, cierpliwość oraz motywację do krytycznego
spojrzenia na problematykę badawczą.*

oraz

Prof. dr hab. Mariuszowi Jaskólskiemu

dr hab. Edycie Nalewajko-Sieliwoniuk

dr Barbarze Imiołczyk

dr Joannie Śliwiak

za cenne dyskusje, życzliwość i wyrozumiałość.

Wykaz publikacji wchodzących w skład cyklu stanowiącego podstawę do ubiegania się o nadanie stopnia doktora.

D1. Brzezinski, K., **Czyrko, J.**, Sliwiak, J., Nalewajko-Sieliwoniuk, E., Jaskolski, M., Nocek, B., Dauter, Z. *S*-adenosyl-L-homocysteine hydrolase from a hyperthermophile (*Thermotoga maritima*) is expressed in *Escherichia coli* in inactive form - Biochemical and structural studies. (2017). *International Journal of Biological Macromolecules* **104,** 584-596.

D2. Czyrko, J., Sliwiak, J., Imiolczyk, B., Gdaniec, Z., Jaskolski, M., Brzezinski, K. Metal-cation regulation of enzyme dynamics is a key factor influencing the activity of *S*-adenosyl-L-homocysteine hydrolase from *Pseudomonas aeruginosa*. (2018). *Scientific Reports* **8,** 11334.

D3. Czyrko, J., Jaskolski, M., Brzezinski, K. Crystal structure of *S*-adenosyl-L-homocysteine hydrolase from *Cytophaga hutchinsonii*, a case of combination of crystallographic and non-crystallographic symmetry. (2018). *Croatica Chemica Acta* **91,** 153-162.

Wyniki badań przedstawionych w publikacji D1 były podstawą do opracowania dwóch zgłoszeń patentowych z dnia 8 września 2016.

WP1. Sposób syntezy enzymatycznej *S*-adenozylo-L-homocysteiny.

Numer zgłoszenia: P.418595

WP2. Sposób uzyskania rekombinowanego enzymu bakteryjnego z *Thermotoga maritima*, hydrolazy *S*-adenozylo-L-homocysteiny.

Numer zgłoszenia: P.418596

Struktura krystaliczna zdeponowana w bazie struktur makrocząsteczek biologicznych PDB wraz z hiperłączem do metadanych dla eksperymentalnego zbioru danych zdeponowanego w repozytorium RepOD przy Interdyscyplinarnym Centrum Modelowania Matematycznego i Komputerowego Uniwersytetu Warszawskiego, powiązana z osiągnięciem naukowym (publikacja **D3**) stanowiącym podstawę do ubiegania się o nadanie stopnia doktora:

6GBN   Crystal structure of *S*-adenosyl-ʟ-homocysteine hydrolase from *Cytophaga hutchinsonii* in complex with adenosine

Ponadto, wyniki badań wchodzących w zakres pracy doktorskiej zaprezentowałam w formie następujących referatów ustnych lub posterowych na międzynarodowych i krajowych konferencjach naukowych:

1. **Czyrko-Horczak, J.**, Brzeziński, K. Effect of monovalent cations on the activity of *S*-adenosyl-L-homocysteine hydrolase. 6th International Caucasian Symposium on Polymers and Advanced Materials, Batumi, Gruzja 17-20.06.2019. **Referat ustny.**

2. **Czyrko, J.,** Jaskólski, M., Brzeziński, K. Struktura krystaliczna hydrolazy *S*-adenozylo-L-homocysteiny z *Cytophaga hutchinsonii*. 60 Konwersatorium Krystalograficzne, Instytut Niskich Temperatur i Badań Strukturalnych PAN, Wrocław 27-29.06.2018. **Referat ustny.**

3. **Czyrko, J.**, Sliwiak, J., Imiolczyk, B., Gdaniec, Z., Jaskólski, Brzeziński, K. Kationy metali regulatorem aktywności enzymatycznej i kluczowym czynnikiem wpływającym na aktywność hydrolazy *S*-adenosylo-L-homocysteiny z *Pseudomonas aeruginosa.* 60 Konwersatorium Krystalograficzne, Instytut Niskich Temperatur i Badań Strukturalnych PAN, Wrocław 27-29.06.2018. **Poster.**

4. **Czyrko, J.**, Brzeziński, K. Metal-cation-based regulation of enzyme dynamics influences the activity of *S*-adenosyl-L-homocysteine hydrolase from *Pseudomonas aeruginosa*. 3rd Conference "Analytical methods to study oxidative damage, antioxidants and drugs. Advanced analytical chemistry for life sciences", Uniwersytet Medyczny w Białymstoku, Białystok 24-26.05.2018. **Poster.**

5. **Czyrko, J.**, Brzeziński, K. Termoaktywacja hydrolazy z ekstermofilnej bakterii – badania biochemiczne i strukturalne. V Konferencja Związki biologicznie czynne: aktywność, struktura, synteza, Uniwersytet w Białymstoku, Białystok 9-11.06.2017. **Poster.**

6. **Czyrko, J.**, Brzeziński, K. Investigating the mechanism of substrate delivery to the active site of SAH hydrolase from microbial pathogens. "Nanocomposites - Characterization and properties - training school", Uniwersytet w Białymstoku, Białystok 12-15.06.2017. **Poster.**

7. **Czyrko, J.**, Brzeziński, K. Klonowanie, ekspresja i oczyszczanie hydrolazy *S*-adenozylo-L-homocysteiny z *Cytophaga hutchinsonii*. Ogólnopolskie Studenckie Mikrosympozjum Chemików 2017, Koło Naukowe Chemików UwB POZYTON, Uniwersytet w Białymstoku, Białystok 30.03.2017. **Referat ustny.**

Spis skrótów

2′-dAdo	2′-deoksyadenozyna
Ado	adenozyna
ADP	indywidualne atomowe parametry przemieszczenia
ChSAHaza	hydrolaza *S*-adenozylo-L-homocysteiny z *Cytophaga hutchinsonii*
DTNB	5,5′-disulfanodiylobis(kwas 2-nitrobenzoesowy)
DLS	dynamiczne rozpraszanie światła
EDTA	kwas etylenodiaminotetraoctowy
Hcy	L-homocysteina
IMAC	chromatografia powinowactwa do unieruchomionych jonów metali
ITC	izotermiczna kalorymetria miareczkowa
iTmSAHaza	nieaktywna forma hydrolazy *S*-adenozylo-L-homocysteiny z *Thermotoga maritima*
LIC	klonowanie bez użycia ligazy DNA
MT	metylotransferaza
mtnN	nukleozydaza 5′-metylotioadenozyny/*S*-adenozylo-L-homocysteiny
NAD$^+$	utleniona forma kofaktora nikotynamidoadeninowego
NADH	zredukowana forma kofaktora nikotynamidoadeninowego
PaSAHaza	hydrolaza *S*-adenozylo-L-homocysteiny z *Pseudomonas aeruginosa*
PCR	reakcja łańcuchowa polimerazy
PIPE	klonowanie oparte na niekompletnym wydłużeniu startera polimerazy
PDB	baza struktur makrocząsteczek biologicznych
PEG	glikol polietylenowy
SAH	*S*-adenozylo-L-homocysteina
SAHaza	hydrolaza *S*-adenozylo-L-homocysteiny
sahh	gen kodujący hydrolazę *S*-adenozylo-L-homocysteiny
SAM	*S*-adenozylo-L-metionina
SAM-MT	metylotransferaza zależna od *S*-adenozylo-L-homocysteiny
TmSAHaza	aktywna forma hydrolazy *S*-adenozylo-L-homocysteiny z *Thermotoga maritima*
TEV	wirus wżerkowej plamistości tytoniu
tNCS	niekrystalograficzna symetria translacyjna
TLS	parametry opisujące anizotropię drgań bryły sztywnej
TPEN	*N,N,N′,N′*-tetrakis(pirydyn-2-ylometylo)etano-1,2-diamina

STRESZCZENIE

Przedstawione osiągnięcie naukowe stanowiące podstawę do nadania stopnia doktora dotyczy badań biochemicznych i strukturalnych bakteryjnych hydrolaz *S*-adenozylo-L-homocysteiny (SAHazy) pochodzących z *Thermotoga maritima*, *Pseudomonas aeruginosa* i *Cytophaga hutchinsonii*. SAHazy regulują kluczowe dla metabolizmu komórki reakcje metylacji zależne od *S*-adenozylo-L-metioniny (SAM), poprzez kontrolę stężenia *S*-adenozylo-L-homocysteiny (SAH), silnego inhibitora szeregu procesów metylacyjnych. Enzymy te są najczęściej aktywne w formie homotetrameru, w którym każda z podjednostek: (i) ma budowę trójdomenową oraz (ii) wiąże po jednej cząsteczce substratu i kofaktora nikotynoamidowoadeninowego w formie utlenionej (NAD$^+$). Obecność kofaktora jest konieczna do przeprowadzenia reakcji enzymatycznej. W trakcie cyklu katalitycznego, każda z podjednostek oscyluje pomiędzy dwiema konformacjami – otwartą i zamkniętą, co wynika z ruchu dwóch głównych domen w trakcie wiązania substratu i uwalniania produktu. Prezentowane przeze mnie badania miały na celu poszerzenie wiedzy dotyczącej tej grupy enzymów. Interdyscyplinarność badań opisanych w niniejszym osiągnięciu naukowym pozwoliła mi na rozwiązanie wielu problemów pojawiających się w trakcie realizacji poszczególnych etapów badawczych, a co za tym idzie, pozwoliło na osiągnięcie założonych celów.

W trakcie prowadzenia badań nad hipertermofilną SAHazą z *T. maritima* wykazałam, że rekombinowane białko uzyskane w temperaturze pokojowej nie wykazuje aktywności katalitycznej. Analiza modelu krystalograficznego wskazywała, że poszczególne podjednostki przyjmują dwie nietypowe konformacje, wykluczające aktywność enzymatyczną tak zwiniętego białka. Dodatkowo, tylko dwie z czterech podjednostek wiążą kofaktor, który ponadto występuje głównie w formie zredukowanej (NADH), co również uniemożliwia katalityczny rozkład SAH. W oparciu o opracowaną przeze mnie procedurę pomiaru aktywności enzymatycznej tej SAHazy wykazałam, że białko zyskuje pełną aktywność katalityczną w wysokiej temperaturze, jedynie w obecności utlenionej formy kofaktora. W oparciu o porównanie modeli krystalograficznych SAHazy z *T. maritima* w formie nieaktywnej i aktywnej wyjaśniłam

podłoże molekularne procesu termoaktywacji tego białka, polegające na przestrzennej rearanżacji poprawnie ufałdowanych domen.

W ramach badań związanych z SAHazą z *P. aeruginosa* zwróciłam uwagę na to, że aktywność katalityczna tego enzymu mocno zależy od typu jonu metalu alkalicznego obecnego w mieszaninie reakcyjnej. Wykazałam, że enzym osiągał najwyższą aktywność w obecności kationów K^+ poprzez odpowiedni wpływ na dynamikę białka. Ponadto wykazałam, że wiązanie innych kationów wpływających na dynamikę tego białka może również prowadzić do inhibicji aktywności katalitycznej SAHazy. Zaobserwowałam to dla kationów Rb^+ i Zn^{2+}, które hamują aktywność enzymatyczną w sposób niekompetycyjny.

W ramach badań scharakteryzowałam biochemicznie i krystalograficznie SAHazę z *C. hutchinsonii*. Badania strukturalne oparte o metody biokrystalografii dotyczyły enzymu w konformacji zamkniętej w kompleksie z kofaktorem w formie utlenionej (NAD^+), adenozyną (produkt reakcji rozkładu SAH) oraz kationem Na^+ związanym w pobliżu kieszeni wiążącej substrat. Dodatkowo, przeanalizowałam sposób upakowania cząsteczek białka w sieci krystalicznej, zwracając uwagę na interesujący przypadek generowania homotetramerów odpowiadających aktywnej formie enzymu w oparciu o kombinację elementów symetrii krystalograficznej oraz translacyjnej symetrii niekrystalograficznej.

Podsumowując, uzyskane rezultaty stanowią nowe odkrycia i pozwalają na szersze zrozumienie aspektów biochemicznych i strukturalnych hydrolazy *S*-adenozylo-L-homocysteiny, dotyczących zwłaszcza nieznanych mechanizmów regulacji aktywności katalitycznej tej grupy enzymów.

SUMMARY

The scientific achievement, described therein, which constitutes the basis for being conferred a doctoral degree, concerns the biochemical and structural characterization of *S*-adenosyl-L-homocysteine hydrolases (SAHases) from various bacteria, such as *Thermotoga maritima*, *Pseudomonas aeruginosa* and *Cytophaga hutchinsonii*. SAHase is an essential element of cell metabolism, involved in the regulation of methylation reactions that utilize *S*-adenosyl-L-methionine (SAM) as a methyl group donor. SAM-Dependent methylation generates equimolar amounts of *S*-adenosyl-L-homocysteine (SAH), a potent inhibitor of SAM-dependent methylation processes. Therefore, cellular concentration of SAH has to be strictly controlled, and this function is fulfilled by SAHase. The enzyme is usually active as a homotetramer with a subunit folded into three domains. Each subunit binds one substrate and one nicotinamide adenine dinucleotide cofactor in its oxidized state (NAD^+). A presence of the cofactor is required for the enzyme activity. Two principal domains, involved in substrate and cofactor binding, are connected by a two-part hinge element and the enzyme oscillates between two conformational states: open (ligand-free) and closed (with ligand bound) during the catalytic cycle. The studies presented herein were performed to broaden a biochemical and structural knowledge about SAHases. The interdisciplinary nature of the research were of key importance for the success of the research.

In the course of research on hyperthermophilic SAHase from *T. maritima*, I revealed that a recombinant protein expressed and purified at room temperature is not active. A closer inspection of a crystallographic model of the protein showed, that individual subunits adopt two distinct and atypical conformations, which do not permit a protein folded in such manner to be enzymatically active. In addition, only two of the four subunits bind the cofactor, however, mainly in its reduced form (NADH). This fact also precludes the enzymatic degradation of SAH. I have developed a new assay that indicated that the protein could gain a full catalytic activity only at a high temperature in the presence of the oxidized form of the cofactor (NAD^+). Based on crystallographic models of both, active and inactive forms of SAHase from *T. maritima*, I elucidated a mechanism of

thermoactivation of the enyzme that is based on a spatial rearrangement of properly folded domains.

While conducting research related to SAHase from *P. aeruginosa*, I noticed that the catalytic activity of the enzyme varies considerably, depending on the alkali metal ion present in the reaction mixture. Among tested cations, the K^+ ion stimulates the highest enzymatic activity. An explanation of this phenomenon is that K^+, but not other alkali cations, enables unique dynamic properties of the enzyme to ensure its maximum catalytic activity. The enzymatic activity can be influenced *via* regulation of protein dynamics, which depends on the type of coordinated cation. This mechanism can also be exploited for noncompetitive inhibition of the enzyme, as I observed for reactions performed in a presence of Rb^+ and Zn^{2+} cations.

The interdisciplinary research was also aimed at biochemical and structural characterization of SAHase from *C. hutchinsonii*. Within the study, I presented the crystal structure of recombinant enzyme in a ternary complex with NAD^+, a reaction product/substrate (adenosine). Additionally, a sodium cation was identified in close proximity of the active site. The crystal contains two translational NCS-related dimers in the asymmetric unit. Two complete tetrameric enzyme molecules are generated from these dimers within the crystal lattice through the operation of two separate crystallographic twofold axes.

To summarize, the results obtained are new discoveries, which allow a deeper understanding of numerous biochemical and structural aspects of *S*-adenosyl-ʟ-homocysteine hydrolase, especially these related to previously unknown regulation mechanisms of the enzyme activity.

OPIS OSIĄGNIĘCIA NAUKOWEGO STANOWIĄCEGO PODSTAWĘ DO NADANIA STOPNIA DOKTORA

1. Wstęp

Reakcje metylacji należą do najstarszych, podstawowych i powszechnych procesów chemicznych zachodzących we wszystkich żywych komórkach [1]. Głównym donorem grupy metylowej jest *S*-adenozylo-ʟ-metionina (SAM), a reakcja przeniesienia grupy metylowej jest katalizowana przez metylotransferazy (MT) zależne od SAM (SAM-MT) [2],[3]. W reakcjach katalizowanych przez SAM-zależne metylotranferazy, akceptorami grupy metylowej są makromolekuły, takie jak kwasy nukleinowe, białka i polisacharydy, jak również szereg małocząsteczkowych metabolitów pierwotnych i wtórnych [3]. U patogennych bakterii reakcje metylacji zależne od SAM odpowiedzialne są za szereg procesów molekularnych zapewniających im wysoki poziom wirulentności i oporności na szereg czynników zewnętrznych. Przykładowo, u *Pseudomonas aeruginosa* reakcje katalizowane przez SAM-MT odpowiadają za niektóre etapy biosyntezy: (i) lipopolisacharydu [4], chroniącego komórki bakteryjne przed czynnikami zewnętrznymi (antybiotyki, układ immunologiczny gospodarza czy środki dezynfekujące) oraz (ii) niektórych cząsteczek sygnalnych uczestniczących w procesie „porozumiewania się" komórek bakterii w trakcie rozwijania się infekcji (tzw. *quorum sensing*) [5]. SAM-zależne reakcje metylacji bakteryjnego DNA stanowią jeden z głównych mechanizmów obrony przed obcym, nie metylowanym DNA, wprowadzanym do komórek bakteryjnych np. w trakcie infekcji bakteriofagami [6].

Przeniesieniu grupy metylowej na cząsteczkę akceptora towarzyszy wytworzenie *S*-adenozylo-ʟ-homocysteiny (SAH). Związek ten jest silnym inhibitorem SAM-MT, przez co jego akumulacja zahamowuje większość komórkowych procesów metylacyjnych. Dlatego wewnątrzkomórkowe stężenie SAH (lub precyzyjniej - stosunek stężenia SAM do stężenia SAH w komórce, będący wskaźnikiem aktywności metylacyjnej) musi być dokładnie regulowane [7],[8],[9]. Rozkład SAH w komórkach jest katalizowany przez dwa różne enzymy: (i) nukleozydazę 5′-metylotioadenozyny/*S*-adenozylo-ʟ-homocysteiny (mtnN) oraz (ii) hydrolazę *S*-adenozylo-ʟ-homocysteiny (SAHazę). Pierwszy z enzymów hydrolizuje SAH do adeniny i *S*-rybozylo-ʟ-homocysteiny, natomiast drugi enzym rozkłada

SAH do adenozyny (Ado) i L-homocysteiny (Hcy) [10]. Reakcja katalizowana przez SAHazę jest odwracalna, a równowaga tej reakcji jest mocno przesunięta w kierunku syntezy SAH. Dodatkowo, aktywność tego enzymu jest hamowana przez jeden z produktów rozkładu SAH – adenozynę [11],[12]. Jednak w warunkach fizjologicznych, zarówno Ado jak i Hcy są szybko włączane w inne szlaki metaboliczne, przez co wypadkową reakcją w komórce jest rozkład SAH [3]. W zależności od organizmu, genom może kodować oba enzymy lub tylko jeden z nich [10]. Przykładowo, genomy hipertermofilnej bakterii *Thermotoga maritima* [13] i bakterii glebowej rozkładającej celulozę *Cytophaga hutchinsoni* [14] zawierają po jednej kopii genu kodującego białko mtnN i SAHazę, podczas gdy genom *P. aeruginosa* posiada tylko jeden gen kodujący SAHazę [15]. Dlatego u *P. aeruginosa* SAHaza jest jedynym enzymem regulującym procesy metylacyjne w komórce tej bakterii. Podobna sytuacja ma miejsce w komórkach ludzkich, których genom pozbawiony jest genu *mtnN*, posiada natomiast kilka kopii genów *sahh* kodujących SAHazę [10].

Analiza strukturalna SAHaz oparta jest przede wszystkich na badaniach krystalograficznych. Jak dotąd, w literaturze opisano kilkanaście struktur tych enzymów pochodzenia eukariotycznego i bakteryjnego [16],[17],[18],[19],[20],[21],[22],[23],[24]. Podjednostkę SAHazy tworzą dwie duże, połączone dwoma tzw. „zawiasami molekularnymi", domeny: (i) wiążąca substrat oraz (ii) wiążąca kofaktor (NAD$^+$), który jest niezbędny do jednego z kroków reakcji rozkładu SAH, oraz jedna niewielka C-końcowa domena (Rys. 1A), która uczestniczy w oligomeryzacji podjednostek enzymu, przechodząc z jednej podjednostki białka do sąsiedniej, tworząc tzw. ścisły dimer (Rys. 1B). Co ciekawe, forma ścisłego dimeru nie jest zwykle preferowana w roztworze. Jak dotąd, jedynym przykładem SAHazy aktywnej jako homodimer jest enzym roślinny pochodzący z łubinu żółtego (*Lupinus luteus*) [20]. Podstawową aktywną formą oligomeryczną w roztworze jest homotetramer, a określając dokładniej – dimer dimerów (AB-A'B') (Rys. 1C). Ponadto, w SAHazach pochodzenia eukariotycznego oraz u części SAHaz bakteryjnych, domena C-końcowa uczestniczy w oddziaływaniach z cząsteczką kofaktora związanego w sąsiedniej podjednostce enzymu. Taką sytuację obserwujemy na przykład w SAHazie z *C. hutchinsoni* (ChSAHaza) i *P. aeruginosa* (PaSAHaza). Z drugiej strony, oddziaływania te nie występują w SAHazach obecnych w komórkach

organizmów ekstremofilnych, w tym u *T.maritima* (TmSAHaza) [23]. W trakcie cyklu katalitycznego, białko oscyluje pomiędzy dwiema konformacjami - otwartą (brak substratu związanego w centrum aktywnym) i zamkniętą (kompleks enzymu z substratem związanym w centrum aktywnym) [16],[17]. Zmiana konformacji białka oparta jest na przemieszczeniu domeny wiążącej substrat w kierunku domeny wiążącej kofaktor. W ruch domeny wiążącej substrat, zaangażowane są oba „zawiasy molekularne" (Rys. 1A). Dodatkowo, jeden z zawiasów, zlokalizowany w pobliżu miejsca wiązania substratu, uczestniczy w koordynacji jonu metalu alkalicznego [20] (najczęściej Na^+ lub K^+), ewentualnie w wiązaniu jonu amonowego [21]. Przegląd struktur SAHaz zdeponowanych w bazie struktur białkowych PDB (ang. *Protein Data Bank*) [25] pokazuje, że obecność poszczególnych kationów zależy jedynie od warunków krystalizacji danego enzymu.
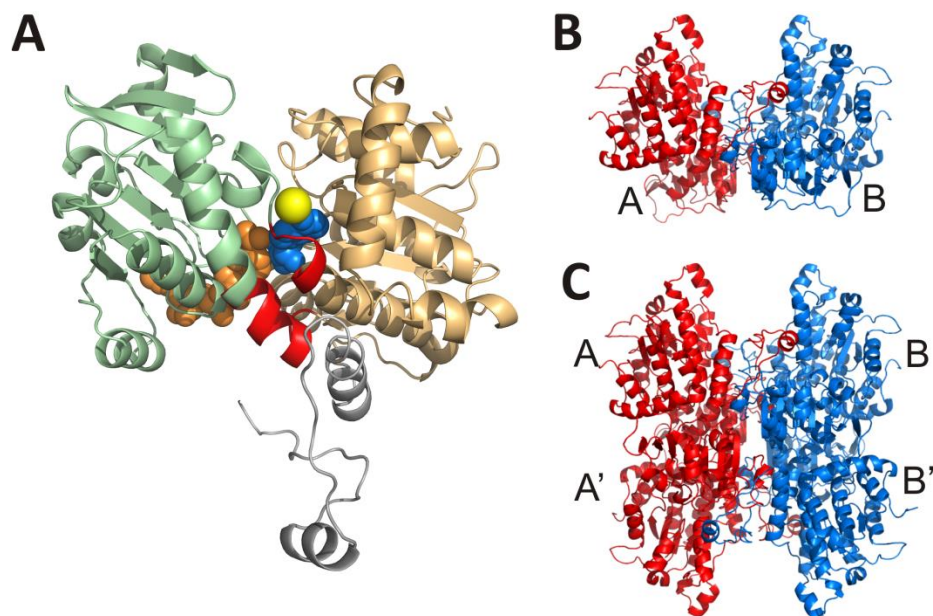
Rysunek 1. Model wstęgowy podjednostki SAHazy z *C. hutchinsonii* w konformacji zamkniętej (A). Podjednostka jest utworzona przez domenę wiążącą substrat (jasnopomarańczowy), domenę wiążącą kofaktor (zielony) oraz C-terminalną domenę oligomeryzacyjną (szary). Dwa regiony tzw. „zawiasów molekularnych" zaznaczono na czerwono. Cząsteczki kofaktora NAD^+ (pomarańczowy) i adenozyny (niebieski) oraz kation Na^+ (żółty) przedstawiono w reprezentacji czaszowej. (B, C) Modele wstęgowe znanych form oligomerycznych SAHaz [20]: ścisłego dimeru AB (B) oraz dimeru dimerów AB-A'B' (C).

W trakcie zmiany konformacji białka z otwartej na zamkniętą tworzy się kanał prowadzący do centrum aktywnego enzymu. Kanał jest otwierany i zamykany przez tzw. „bramkę molekularną" utworzoną przez dwie zachowawcze reszty His i Phe [19],[20] (Rys. 2).

Dodatkowo, reszta His „bramki molekularnej" bezpośrednio oddziałuje z cząsteczką substratu (SAH) lub produktu (Ado) związanego w centrum aktywnym enzymu oraz uczestniczy w jednym z etapów reakcji katalizowanej przez SAHazę [22].
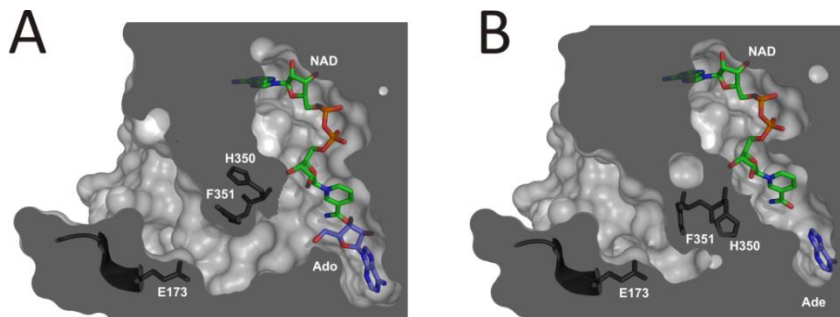
Rysunek 2. W enzymie roślinnym (*Lupinus luteus*) [20] dostęp do centrum aktywnego enzymu regulowany jest przez „bramkę molekularną" utworzoną przez konserwatywną parę reszt His350-Phe351. W kompleksie z adenozyną kanał jest otwarty (A), w kompleksie z adeniną nie ma dostępu do centrum aktywnego enzymu (B). Numeracja odpowiada sekwencji aminokwasowej SAHazy roślinnej.

SAHaza jest kluczowym enzymem regulującym procesy metylacyjne zachodzące w komórkach. Dotyczy to zarówno komórek człowieka, jak i wielu patogennych mikroorganizmów. Selektywne zablokowanie aktywności SAHazy stwarza doskonałą możliwość walki z patogennymi organizmami na poziomie molekularnym, poprzez hamowanie ich kluczowych procesów życiowych. Chemogenomiczne bazy danych wskazują SAHazy jako doskonałe cele przy projektowaniu nowych inhibitorów o potencjalnym znaczeniu medycznym [26]. Użycie inhibitorów SAHaz rozpatrywano w takich schorzeniach jak nowotwory [27], hipercholesterolemia [28], czy w infekcjach wirusowych [29],[30], bakteryjnych [19] i pasożytniczych [18],[31],[32],[33],[34]. Projektowanie inhibitorów SAHaz opiera się na strukturze kieszeni wiążącej substrat, a większość dotychczas poznanych ligandów to analogi adenozyny. Enzymy te z punktu widzenia ewolucji są mocno zachowawcze, a ich centra katalityczne są niemalże identyczne. Znaczne podobieństwo strukturalne praktycznie uniemożliwia znalezienie związków, które blokowałyby SAHazy pochodzące z różnych organizmów, nie wpływając przy tym na aktywność enzymu ludzkiego. Dlatego wysoka cytotoksyczność znanych inhibitorów SAHaz, które wiążą się nieselektywnie w centrum aktywnym enzymu uniemożliwia ich stosowanie w lecznictwie. Badania biochemiczne i strukturalne hydrolaz *S*-adenozylo-L-homocysteiny pochodzenia bakteryjnego są prowadzone od kilku lat na Wydziale Chemii Uniwersytetu w Białymstoku w Laboratorium Biochemii i Biologii

15

Strukturalnej. Mają one na celu znacząco poszerzyć wiedzę biochemiczną i strukturalną na temat tej grupy enzymów, aby móc odpowiedzieć na pytanie, czy możliwe jest zaprojektowanie wysoce selektywnych inhibitorów SAHaz pochodzących z różnych organizmów. Z tego powodu badania prowadzone na Uniwersytecie w Białymstoku koncentrują się na dokładnym wykazaniu różnic biochemicznych i strukturalnych pomiędzy SAHazą ludzką a enzymami pochodzącymi z wybranych organizmów bakteryjnych.

2. Cele naukowe badań

Monotematyczny cykl trzech publikacji naukowych **D1** – **D3** stanowiący podstawę do nadania stopnia doktora dotyczy charakterystyki biochemicznej i strukturalnej bakteryjnych hydrolaz *S*-adenozylo-L-homocysteiny. Moje badania dotyczyły trzech głównych nurtów: (i) nieaktywnej formy rekombinowanej SAHazy z *T. maritima* oraz zagadnień związanych z fałdowaniem białek termofilnych (iTmSAHaza, publikacja **D1**), (ii) wpływu kationów metali jedno- i dwuwartościowych na aktywność SAHazy z *P. aeruginosa* (PaSAHaza, publikacja **D2**) oraz (iii) charakterystyki biochemicznej i strukturalnej SAHazy z *C. hutchinsonii* (ChSAHaza, publikacja **D3**). Cykl publikacji **D1** – **D3** dotyczy następujących aspektów związanych z badaniami hydrolaz *S*-adenozylo-L-homocysteiny:

1. Charakterystyka biochemiczna rekombinowanej termofilnej SAHazy z *T. maritima* uzyskanej w formie nieaktywnej (iTmSAHaza) oraz wyjaśnienie mechanizmu termoaktywacji tego niepoprawnie ufałdowanego białka (publikacja **D1**).

2. Identyfikacja oraz wyjaśnienie roli kationów metali alkalicznych oraz cynku w aktywności i inhibicji SAHaz, głównie w oparciu o badania natywnej PaSAHazy i jej muteiny Gln65Ala, ale również ChSAHazy (publikacje **D2** i **D3**).

3. Charakterystyka strukturalna zamkniętej formy ChSAHazy w kompleksie z adenozyną, kofaktorem i jonem Na^+ oraz analiza upakowania cząsteczek kompleksu ChSAHaza-ligandy w sieci krystalicznej wykazująca ciekawy przypadek kombinacji symetrii krystalograficznej oraz translacyjnej symetrii niekrystalograficznej (ang. *translational non-crystallographic symmetry, tNCS*, publikacja **D3**).

3. Metodyka badań

Realizacja założonych celów badawczych wymagała zastosowania przeze mnie szeregu metod z pogranicza biologii molekularnej, biochemii oraz biokrystalografii. Podstawową metodą badawczą stosowaną w ramach moich badań była charakterystyka biochemiczna trzech SAHaz, wzbogacona o rentgenowską analizę strukturalną enzymu z *C. hutchinsonii*.

3.1. Opracowanie systemu klonowania i ekspresji rekombinowanych SAHaz

W ramach moich badań etap ten dotyczył natywnego enzymu pochodzącego z *C. hutchinsonii* (publikacja **D3**) oraz muteiny PaSAHazy Gln65Ala (publikacja **D2**). W przypadku natywnej PaSAHazy i enzymu z *T. maritima* etap ten został uprzednio wykonany przez dr hab. Krzysztofa Brzezińskiego. Opracowanie systemu ekspresyjnego rekombinowanej ChSAHazy rozpoczęłam od amplifikacji sekwencji kodującej z wykorzystaniem reakcji PCR (ang. *Polymerase Chain Reaction*), katalizowanej przez komercyjnie dostępną polimerazę DNA z *Thermococcus kodakaraensis*. Jako matrycę wykorzystałam komercyjnie dostępne genomowe DNA wyizolowane z *C. hutchinsonii* (szczep ATCC 33406). Wklonowanie do wektora ekspresyjnego pMCSG57 wykonałam w oparciu o technikę LIC (ang. *Ligation Independent Cloning*) [35]. Mutant PaSAHazy Gln65Ala wygenerowałam techniką klonowania PIPE (ang. *Polymerase Incomplete Primer Extension*) [36] z wykorzystaniem plazmidu pMCSG57, który zawierał sekwencję kodującą natywną PaSAHazę. Poprawność wszystkich klonów potwierdziłam poprzez sekwencjonowanie. Wszystkie ekspresje w skali preparatywnej prowadziłam z wykorzystaniem komórek *Eschericha coli* (szczep BL21-CodonPlus(DE3)®-RIPL) w pożywce Terrific-Broth lub Luria-Broth z dodatkiem ampicyliny i chloramfenikolu. Po indukcji ekspresji przez izopropylo-β-D-1-tiogalaktopiranozyd hodowlę prowadziłam przez 15 - 20 godzin w temperaturze 291 K, którą następnie zwirowałam, a osad bakteryjny zamrażałam w ciekłym azocie.

3.2. Oczyszczanie rekombinowanych białek

System ekspresji rekombinowanych SAHaz oparty był na dwóch plazmidach, pMCSG9 (SAHaza z *T. maritima*) oraz pMCSG57 (SAHaza z *P. aeruginosa*

i *C. hutchinsonii*). Oba systemy pozwoliły na ekspresję białka w fuzji ze znacznikiem histydynowym zlokalizowanym na N-końcu rekombinowanych SAHaz, z możliwością usunięcia znacznika w rekombinowanym białku poprzez selektywne trawienie proteazą TEV (ang. *Tobacco Etch Virus*). Pozwoliło to na opracowanie procedury oczyszczania SAHaz opartej na dwuetapowej chromatografii powinowactwa na kolumnie chromatograficznej ze związanymi jonami Ni^{2+} (ang. *Immobilized Metal Affinity Chromatography, IMAC*) wraz z zastosowaniem proteazy TEV, również znakowanej znacznikiem histydynowym. W efekcie, po drugim etapie IMAC uzyskano preparat białkowy o wysokiej czystości. W trakcie ekspresji rekombinowanych SAHaz w komórkach *E. coli* uzyskuje się preparat białkowy o niskim stopniu homogenności, zarówno chemicznym jak i konformacyjnym (nieselektywne wiązanie kofaktora w formie utlenionej i zredukowanej oraz wiązanie adenozyny obecnej w cytoplazmie bakterii). W konsekwencji otrzymuje się preparat białkowy o znacznie obniżonej aktywności katalitycznej (enzym wymaga obecności kofaktora w formie utlenionej, NAD^+). Dodatkowo, białko występuje w dwóch konformacjach: zamkniętej (kompleks z adenozyną) i otwartej (brak związanego liganda w centrum aktywnym), co skutecznie uniemożliwia krystalizację SAHaz oraz wpływa negatywnie na aktywność katalityczną. Dlatego kolejnym etapem oczyszczania było wymywanie i wymiana ligandów [37]. Białko było najpierw kilkukrotnie wytrącane roztworem $(NH_4)_2SO_4$ o pH 3,3, tak aby uzyskać formę apo. Następnie białko inkubowano z utlenioną formą kofaktora NAD^+, uzyskując w pełni aktywny i konformacyjnie jednorodny kompleks $SAHaza-NAD^+$ w formie otwartej. Tak uzyskany preparat doczyszczano z wykorzystaniem filtracji żelowej.

W każdym przypadku przedstawiona powyżej standardowa procedura oczyszczania SAHaz wymagała pewnych modyfikacji:

1. W trakcie badań wykazałam, że etap wymywania i wymiany ligandów może zostać pominięty w trakcie oczyszczania SAHazy z *T. maritima* (publikacja **D1**).
2. Oczyszczony preparat PaSAHazy wykazywał bardzo niską aktywność katalityczną. W trakcie równolegle prowadzonych badań wykazano, że PaSAHaza bardzo mocno koordynuje jony Zn^{2+} w regionie centrum aktywnego enzymu, w konsekwencji inaktywując enzym. Próby wymycia tego kationu z wykorzystaniem EDTA nie

powiodły się. Ostatecznie zdecydowałam się na zastosowanie *N,N,N′,N′*-tetrakis(pirydyn-2-ylometylo)etano-1,2-diaminy (TPEN), która bardzo silnie chelatuje jony cynku. Zabieg ten okazał się skuteczny, dzięki czemu uzyskałam preparat białkowy o bardzo wysokiej aktywności enzymatycznej (publikacja **D2**). Sposób otrzymania muteiny PaSAHazy Gln65Ala (publikacja **D2**) zaproponowałam w oparciu o system ekspresji opracowany dla natywnej PaSAHazy oraz zoptymalizowaną procedurę oczyszczania enzymu. Etapy związane z uzyskaniem muteiny PaSAHazy Gln65Ala zostały wykonane przeze mnie oraz dr Barbarę Imiołczyk, w trakcie stażu naukowego, który odbyłam w Instytucie Chemii Bioorganicznej PAN w 2017 roku.

3. W trakcie oczyszczania ChSAHazy zaobserwowałam znaczną niestabilność białka, która przejawiała się jego strąceniem i dezaktywacją. Próby oczyszczania białka w 277 K, jak również znaczne przyspieszenie procesu oczyszczania, nie przyniosły pożądanego efektu. Ostatecznie wykazałam, że ChSAHaza ma tendencję do nagłego wytrącania się z roztworu o stężeniu powyżej 8 mg/mL. Zmodyfikowałam procedurę oczyszczania enzymu w taki sposób, aby na każdym etapie stężenie białka nie przekroczyło wartości krytycznej (publikacja **D3**).

3.3. Biochemiczna charakterystyka rekombinowanych SAHaz

Charakterystyka stanów oligomerycznych białek

Analizując stany oligomeryczne charakteryzowanych SAHaz wykorzystywałam trzy podstawowe metody. Pierwszą z nich była filtracja żelowa, którą stosowałam również jako ostatni etap oczyszczania rekombinowanych enzymów (publikacje **D1** – **D3**). Dodatkowo, w trakcie zatężania białka metodą ultrafiltracji, stosowałam membrany ze średnią wielkością porów odpowiadających makromolekule globularnej o masie cząsteczkowej około 100 kDa (publikacje **D1** – **D3**). Dokładniejszą charakterystykę wielkości cząsteczek przeprowadzałam metodą dynamicznego rozpraszania światła (ang. *Dynamic Light Scattering, DLS*). Zastosowanie metody DLS pozwoliło mi na pomiar wielkości cząsteczek białka w zależności od jego stężenia oraz w różnych temperaturach (publikacja **D1**).

Badanie aktywności enzymatycznej i wpływu inhibitorów

Aktywność hydrolityczną (publikacja **D2** i **D3**) natywnej formy PaSAHazy i ChSAHazy, muteiny PaSAHazy Gln65Ala oraz wpływ kationów litowców i Zn^{2+} na aktywność PaSAHazy wyznaczałam spektrofotometrycznie z wykorzystaniem testu opartego na odczynniku Ellmana (DTNB, 5,5′-disulfanodiylobis(kwas 2-nitrobenzoesowy)) [38],[39]. Metoda ta opiera się na ilościowym oznaczaniu tworzącej się L-homocysteiny w trakcie reakcji hydrolizy SAH. W przypadku natywnej PaSAHazy, aktywność hydrolityczną badałam w obecności różnych jonów metali alkalicznych (Li^+, Na^+, K^+, Rb^+, Cs^+) lub przy ich braku. Pomiary aktywności hydrolitycznej muteiny PaSAHazy Gln65Ala oraz ChSAHazy przeprowadziłam jedynie w obecności jonów K^+. Dla każdej z analizowanych reakcji enzymatycznych wyznaczyłam podstawowe parametry kinetyczne: (i) stałą Michaelisa-Menten (K_M), (ii) maksymalną szybkość reakcji (V_{max}) oraz (iii) stałą katalityczną (liczbę obrotów, k_{cat}). Hamujący wpływ jonów Zn^{2+} na aktywność PaSAHazy opisałam poprzez wyznaczenie parametru IC_{50} oraz stałej inhibicji K_i. Dodatkowo, opracowałam metodę pozwalającą na ocenę wpływu jonów Zn^{2+} na stabilizację konformacji zamkniętej białka. Metoda oparta jest na konkurencyjnym wiązaniu adenozyny (substrat/produkt) i 2′-deoksyadenozyny (2′-dAdo). 2′-dAdo jest silnym inhibitorem SAHaz, a jego związanie w centrum aktywnym enzymu inicjuje jego rozkład do adeniny oraz redukcję kofaktora. Stan utlenienia kofaktora (NAD^+/NADH) monitorowałam spektrofluorymetrycznie.

W przypadku badania aktywności syntetycznej SAHazy z *T. maritima* (publikacja **D1**) opracowałam metodę pozwalającą na zastosowanie wysokosprawnej chromatografii cieczowej HPLC do oznaczania SAH powstającego w trakcie reakcji enzymatycznej w obecności Ado i Hcy. Aktywność syntetyczną analizowałam w temperaturach 298 i 358 K. Pomiary te wykonałam wspólnie z dr hab. Edytą Nalewajko-Sieliwoniuk.

Ustalenie stanu utlenienia kofaktora w centrum aktywnym enzymu

W trakcie ekspresji SAHazy w komórkach *E. coli* enzym wiąże kofaktor nikotynoamidoadeninowy niezależnie od jego stanu utlenienia. W ramach badań dotyczących termofilnej SAHazy (publikacja **D1**) oraz PaSAHazy (publikacja **D2**) stosunek

NAD^{+}/NADH w preparacie białkowym wyznaczałam spektrofluorymetrycznie w oparciu o metodę opisaną przez Yuana i współpracowników [37].

3.4. Krystalizacja rekombinowanej SAHazy z *C. hutchinsoni* oraz pomiary dyfrakcyjne na uzyskanych kryształach

Przed rozpoczęciem prób krystalizacji rekombinowany enzym inkubowałam z adenozyną. Kryształy kompleksu ChSAHazy z ligandami uzyskałam w temperaturze 292 K metodą dyfuzji par w kropli wiszącej w kilku warunkach eksperymentalnych dostępnych w komercyjnym zestawie *Structure Screen 1* (Molecular Dimensions). Wstępne badanie jakości uzyskanych monokryształów przeprowadziłam w temperaturze 100 K z wykorzystaniem dyfraktometru rentgenowskiego z miedziowym źródłem promieniowania rentgenowskiego. Takie podejście pozwoliło mi wybrać najlepszy warunek wstępny do krystalizacji białka (oparty na Li_2SO_4 i PEG 8000), jak również dobrać odpowiedni krioprotektant (PEG 400). Wstępny warunek krystalizacyjny następnie optymalizowałam zmieniając stężenia białka i objętość kropli krystalizacyjnej. Docelowe dane dyfrakcyjne o rozdzielczości 2.09 Å zarejestrowałam z wykorzystaniem promieniowania synchrotronowego w ośrodku HZB BESSY w Berlinie z wykorzystaniem linii pomiarowej BL14.1. Uzyskane dane dyfrakcyjne opracowałam z wykorzystaniem pakietu *XDSAPP* [40],[41]. Niemodyfikowane obrazy dyfrakcyjne zdeponowałam w repozytorium RepOD przy Interdyscyplinarnym Centrum Modelowania Matematycznego i Komputerowego Uniwersytetu Warszawskiego.

3.5. Rozwiązywanie i udokładnianie struktury krystalicznej SAHazy z *C. hutchinsonii*

Na podstawie uzyskanych danych dyfrakcyjnych, strukturę krystaliczną ChSAHazy w kompleksie z Ado i NAD^{+} rozwiązałam metodą podstawienia cząsteczkowego wykorzystując program *PHASER* [42] z pakietu *CCP4* [43]. Uzyskany model został automatycznie wbudowany w mapę gęstości elektronowej za pomocą programu *ARP/wARP* [44]. Strukturę krystaliczną udokładniłam z wykorzystaniem programu *REFMAC* [45] z zastosowaniem indywidualnych izotropowych atomowych parametrów przemieszczenia (ang. *Atomic Displacement Parameters*, ADP) oraz trzech grup TLS (ang. *Translation/Libration/Screw*) [46] na podjednostkę enzymu opisujących anizotropię

drgań bryły sztywnej. Do wizualizacji i przebudowy modelu używałam programu *COOT* [47]. Końcowy model wraz z czynnikami struktury zdeponowałam w bazie struktur białkowych PDB.

3.6. Analiza modeli krystalograficznych

Obecność kationów Na$^+$ w strukturze ChSAHazy potwierdziłam w oparciu o analizę sfery koordynacji z wykorzystaniem programu *CheckMyMetal* [48] (publikacja **D3**). W celu porównania modeli krystalograficznych aktywnej i nieaktywnej formy SAHazy z *T. maritima* wykorzystałam program *SSM* [49] (publikacja **D1**).

4. Omówienie wyników badań

Artykuł D1

Charakterystyka biochemiczna rekombinowanej SAHazy z T. maritima uzyskanej w formie nieaktywnej oraz wyjaśnienie mechanizmu termoaktywacji niepoprawnie ufałdowanego białka

Brzezinski, K., **Czyrko, J.**, Sliwiak, J., Nalewajko-Sieliwoniuk, E., Jaskolski, M., Nocek, B., Dauter, Z. *S*-adenosyl-L-homocysteine hydrolase from a hyperthermophile (*Thermotoga maritima*) is expressed in *Escherichia coli* in inactive form - Biochemical and structural studies. (2017). *International Journal of Biological Macromolecules* **104**, 584-596.

Optymalizacja procesu oczyszczania oraz charakterystyka biochemiczna iTmSAHazy

Genom termofilnej bakterii *T. maritima* koduje liczne białka ewolucyjnie wywodzące się od archeonów, w tym hydrolazę *S*-adenozylo-L-homocysteiny. Najprawdopodobniej jest to związane z masowym transferem horyzontalnym genów od termofilnych archeonów do bakterii, związanym z adaptacją komórek bakteryjnych do wysokiej temperatury otoczenia [10],[13],[50].

W ramach badań analizowałam aktywność katalityczną rekombinowanego enzymu, który uzyskano i oczyszczono w temperaturze pokojowej (iTmSAHaza). Enzym otrzymano w formie tetramerycznej, jednak nie wykazywał on aktywności hydrolitycznej wobec substratu (SAH), którą monitorowałam z wykorzystaniem testu opartego na DTNB. Z uwagi na to, że białko pochodzi z organizmu termofilnego, postanowiłam sprawdzić jego aktywność w szerszym zakresie temperatur. Jednak używany przeze mnie test nie mógł być

zastosowany w wyższych temperaturach. Dlatego opracowałam inną metodę opartą na chromatografii HPLC, pozwalającą monitorować aktywność enzymatyczną w kierunku syntezy SAH w szerokim zakresie temperatur. W nowych testach monitorowałam w czasie przyrost stężenia SAH dla reakcji prowadzonej w temperaturach 298 i 358 K. Dodatkowo, przeprowadziłam reakcję w temperaturze 298 K z wykorzystaniem preparatu enzymu ogrzanego do temperatury 358 K i ponownie schłodzonego do 298 K. Co ciekawe, w żadnym z warunków nie stwierdziłam obecności SAH (Rys. 3). Brak aktywności w temperaturze 298 K można by wytłumaczyć faktem, że enzym termofilny nie jest aktywny w niższych temperaturach, jednak brak aktywności w temperaturze 358 K wydawał się intrygujący.

Równolegle z prowadzonymi przeze mnie badaniami dr hab. Krzysztof Brzeziński rozwiązał struktury krystaliczne iTmSAHazy w kompleksie z NAD$^+$ oraz NAD$^+$/Ado. Modele struktury częściowo wyjaśniały brak aktywności katalitycznej iTmSAHazy. W ramach tetrameru, dwie podjednostki przyjmują konformację otwartą, co pozwala na związanie substratu. Jednak podjednostki te nie wiążą cząsteczek kofaktora niezbędnego do przeprowadzenia reakcji katalizowanej przez enzym. Kolejne dwie podjednostki, które wiązały cząsteczkę kofaktora przyjmowały konformację zamkniętą, uniemożliwiając przez to związanie cząsteczki substratu w centrum aktywnym. Dodatkowo, w oparciu o pomiary spektrofluorymetryczne wykazałam, że większość cząsteczek kofaktora obecnego w kompleksie iTmSAHazy jest zredukowana, uniemożliwiając przeprowadzenie części etapów reakcji enzymatycznej. Wynik ten zasugerował mi, że z uwagi na zamkniętą konformację podjednostek wiążących kofaktor, jego wymycie i wymiana na formę utlenioną może być nieefektywna. Kolejne oczyszczania, przeprowadzone z pominięciem etapu wytrącania białka zakwaszonym roztworem $(NH_4)_2SO_4$, potwierdziły słuszność mojego założenia. Dlatego w kolejnych badaniach pomijałam etap wymywania i wymiany kofaktora.

Analiza strukturalna iTmSAHazy zasugerowała mi, że przyczyną braku aktywności enzymatycznej, zwłaszcza w wyższej temperaturze może być brak związanego kofaktora w dwóch z czterech podjednostek, jak również dominacja zredukowanej formy kofaktora związanego w dwóch pozostałych podjednostkach. Dlatego kolejne testy aktywności

enzymatycznej przeprowadziłam w obecności 5 mM NAD$^+$. Dwie z reakcji przeprowadziłam w temperaturze 298 K z wykorzystaniem preparatów: (i) oczyszczonego w temperaturze pokojowej oraz (ii) ogrzanego do temperatury 358 K i następnie schłodzonego do temperatury 298 K. W obu reakcjach zaobserwowałam szczątkową aktywność katalityczną. Natomiast dla reakcji przeprowadzonej w temperaturze 358 K aktywność enzymatyczna, oceniona na podstawie wydajności syntezy SAH, była wysoka (Rys. 3).
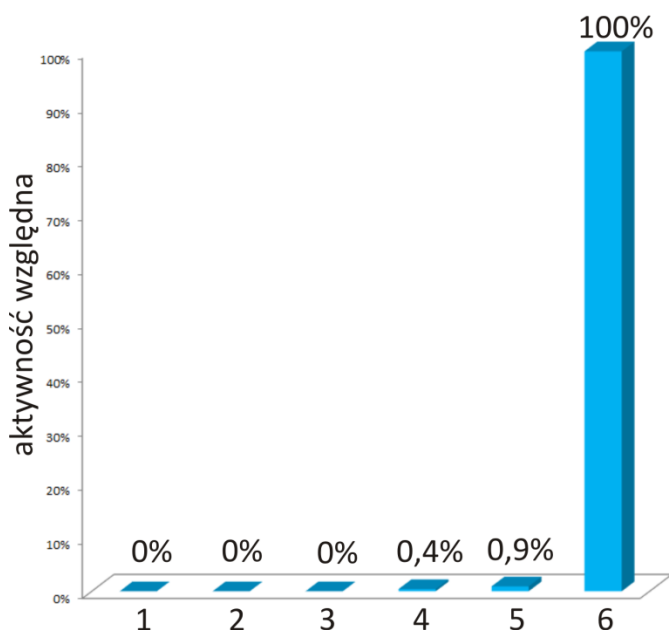

Rysunek 3. Aktywność katalityczna (wyrażona jako przyrost stężenia SAH) rekombinowanej SAHazy z *T. maritima* monitorowana w różnych warunkach. Reakcje 1-3 nie zawierały dodatku NAD$^+$, natomiast reakcje 4-6 zawierały kofaktor w stężeniu końcowym 5 mM. Reakcje prowadzono w temperaturze 298 K (reakcja 1 i 4) oraz w temperaturze 298 K z wykorzystaniem preparatu enzymu ogrzanego do temperatury 358 K i ponownie schłodzonego do 298 K (reakcja 2 i 5) oraz 358 K (reakcja 3 i 6).

Wyjaśnienie mechanizmu termoaktywacji iTmSAHazy

Znaczące różnice w aktywności enzymu obserwowane w temperaturze 298 i 358 K oraz wymóg dodatku kofaktora do mieszaniny reakcyjnej wskazywały, że enzym przyjmuje odmienną, indukowaną podwyższoną temperaturą konformację. Aby to wykazać przeprowadziłam pomiary wielkości cząsteczek białka metodą DLS według trzech różnych scenariuszy: (i) w temperaturze 298 K, (ii) preparat białkowy ogrzany do temperatury 358

K, następnie schłodzony do 298 K oraz (iii) 358 K. Wyniki pomiarów wskazywały na niewielkie, ale powtarzalne różnice w wielkości cząsteczek w zależności od warunków przeprowadzonych eksperymentów (Rys. 4). Dodatkowo, eksperymenty z wykorzystaniem miareczkowania kalorymetrycznego ITC (ang. *Isothermal Titration Microcalorimetry, ITC*), przeprowadzone przez dr Joannę Śliwiak, wykazały ponad dziesięciokrotne (NAD$^+$) lub dwukrotne (Ado) zwiększenie efektywności wiązania liganda w przypadku białka ogrzanego do temperatury 358 K i następnie schłodzonego do temperatury 298 K przed pomiarami ITC. Zarówno wyniki eksperymentów DLS jak i ITC wskazują, że w trakcie termoaktywacji iTmSAHazy dochodzi do zmiany konformacji białka. Wpływa to znacząco na wiązanie cząsteczki kofaktora (NAD$^+$) i substratu/produktu reakcji (Ado). Przejawia się to poprzez zmianę: (i) stechiometrii wiązania ligandów oraz (ii) mechanizmu wiązania ligandów z entalpowego na entropowy.
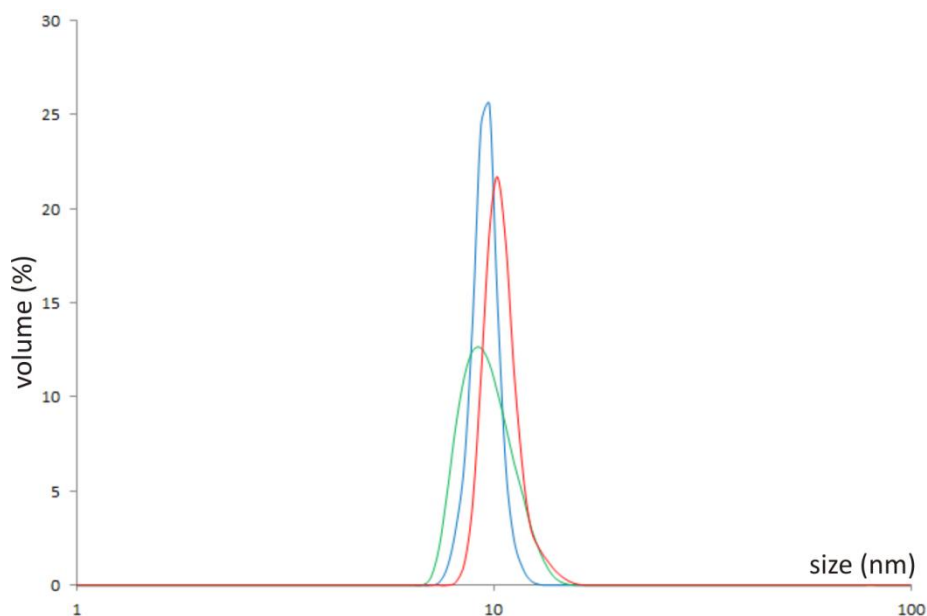
Rysunek 4. Wyniki analizy DLS obrazujące niewielkie różnice wielkości cząsteczek białka w zależności od sposobu przygotowania próbki oraz warunków pomiarowych: (i) preparat nieogrzany, pomiar przeprowadzony w temperaturze 298 K (linia zielona), (ii) preparat ogrzany do temperatury 358 K, następnie schłodzony do 298 K, pomiar przeprowadzony w temperaturze 298 K (linia niebieska) oraz (iii) pomiar przeprowadzony w temperaturze 358 K (linia czerwona).

W międzyczasie Zheng i współpracownicy opublikowali pracę opisującą struktury krystaliczne aktywnej formy SAHazy z *T. maritima* w konformacji otwartej i zamkniętej [23]. Stworzyło to doskonałą możliwość porównania modeli strukturalnych aktywnego

i nieaktywnego białka, co mogłoby wyjaśnić mechanizm termoaktywacji iTmSAHazy na poziomie molekularnym. W tym celu dokonałam serii porównań strukturalnych, zarówno indywidualnych podjednostek tworzących tetramer iTmSAHazy i TmSAHazy w konformacji otwartej i zamkniętej, jak również trzech domen tworzących podjednostkę poszczególnych tetramerów. Znaczne różnice są obserwowane w sposobie organizacji przestrzennej pomiędzy formą aktywną i nieaktywną enzymu, natomiast struktura poszczególnych domen jest bardzo podobna. Wskazuje to, że termoaktywacja iTmSAHazy oparta jest na reorganizacji przestrzennej domen białka i związaniu cząsteczki kofaktora (Rys. 5).
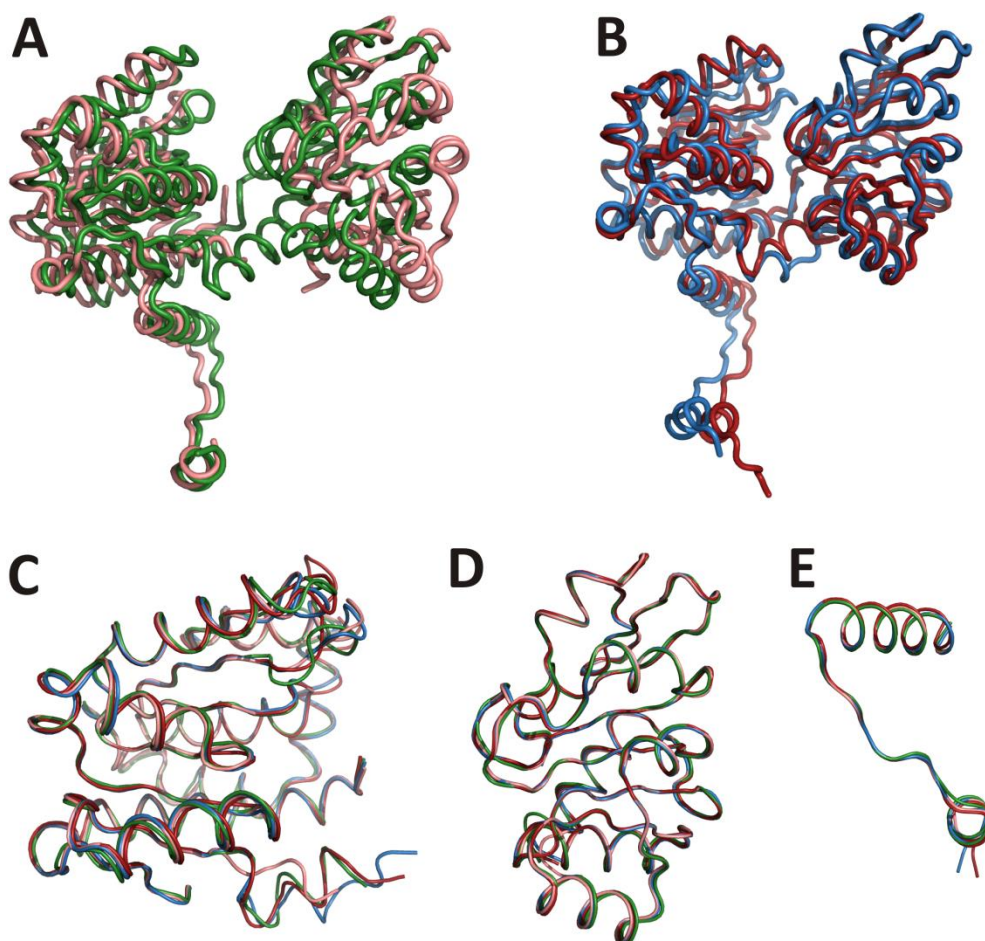
Rysunek 5. Nałożenie podjednostek oraz indywidualnych domen nieaktywnej (iTmSAHaza) i aktywnej (TmSAHaza) SAHazy [23]. Nałożenie podjednostek w (A) konformacji otwartej enzymu nieaktywnego (różowy) i aktywnego (zielony) oraz (B) zamkniętej enzymu nieaktywnego (niebieski) i aktywnego (czerwony) oraz (C) domen wiążących substrat, (D) domen wiążących kofaktor oraz (E) domen C-końcowych.

Artykuł D2

Identyfikacja i wyjaśnienie roli kationów metali alkalicznych oraz cynku w aktywności i inhibicji SAHazy z P. aeruginosa

Czyrko, J., Sliwiak, J., Imiolczyk, B., Gdaniec, Z., Jaskolski, M., Brzezinski, K. Metal-cation regulation of enzyme dynamics is a key factor influencing the activity of *S*-adenosyl-ʟ-homocysteine hydrolase from *Pseudomonas aeruginosa*. (2018). *Scientific Reports* **8**, 11334.

Optymalizacja procedury oczyszczania rekombinowanej PaSAHazy oraz opracowanie systemu klonowania, ekspresji i oczyszczania muteiny PaSAHazy Gln65Ala

Hydrolaza *S*-adenozylo-ʟ-homocysteiny jest jedynym enzymem u *P. aeruginosa* rozkładającym SAH, dlatego jest ona kluczowa dla metabolizmu bakterii. Pierwotnie opracowany system ekspresji i oczyszczania był bardzo wydajny i pozwalał na uzyskanie ponad 100 mg czystego białka (w formie tetramerycznej) z 1 L hodowli bakteryjnej, które następnie wykrystalizowano. Jednak uzyskiwany preparat białkowy wykazywał jedynie szczątkową aktywność enzymatyczną. Sekwencjonowanie plazmidu ekspresyjnego nie wykazało żadnych mutacji w obrębie sekwencji kodującej, a analiza widm masowych nie wskazywała na jakąkolwiek modyfikację kowalencyjną białka. Analiza spektrofluorymetryczna wykazała, że praktycznie cała ilość związanego kofaktora występuje w formie utlenionej, warunkującej aktywność PaSAHazy. W międzyczasie, w oparciu o badania krystalograficzne i rentgenowską spektroskopię fluorescencyjną, dr hab. Krzysztof Brzeziński wykazał, że w regionie centrum aktywnego PaSAHazy, na styku dwóch głównych domen koordynowany jest kation Zn^{2+}, co mogłoby wpływać negatywnie na aktywność katalityczną białka. Podjęte przeze mnie próby usunięcia tego kationu z enzymu przez dializę wobec buforu zawierającego EDTA nie powiodły się, co wskazywało na silne oddziaływanie jonów Zn^{2+} z otoczeniem makromolekularnym. Usunięcie jonów Zn^{2+} powiodło się dopiero podczas dializy wobec buforu z dodatkiem TPEN. Zabieg ten przywrócił pełną aktywność katalityczną rekombinowanego enzymu, co pozwoliło na przeprowadzenie pełnej charakterystyki biochemicznej PaSAHazy. Opracowaną przeze mnie procedurę z wykorzystaniem TPEN z powodzeniem zastosowałam do oczyszczenia muteiny PaSAHazy Gln65Ala.

*Rola kationów metali alkalicznych i cynku w aktywności PaSAHazy*

Badania krystalograficzne formy zamkniętej PaSAHazy wykazały obecność jonu K^+ skoordynowanego w pobliżu miejsca wiązania substratu, w obszarze jednego z dwóch tzw. „zawiasów molekularnych" uczestniczących w reorientacji domen w trakcie cyklu katalitycznego. Co ciekawe, porównanie tego regionu z innymi krystalograficznymi modelami bakteryjnych oraz eukariotycznych SAHaz wiążących jony Na^+, Rb^+ czy NH_4^+ (co wynika jedynie z obecności danego kationu w roztworach krystalizacyjnych), wskazuje na niezmienność geometrii tego obszaru białka, a także na niemal identyczny sposób wiązania nukleozydu (Rys. 6A).
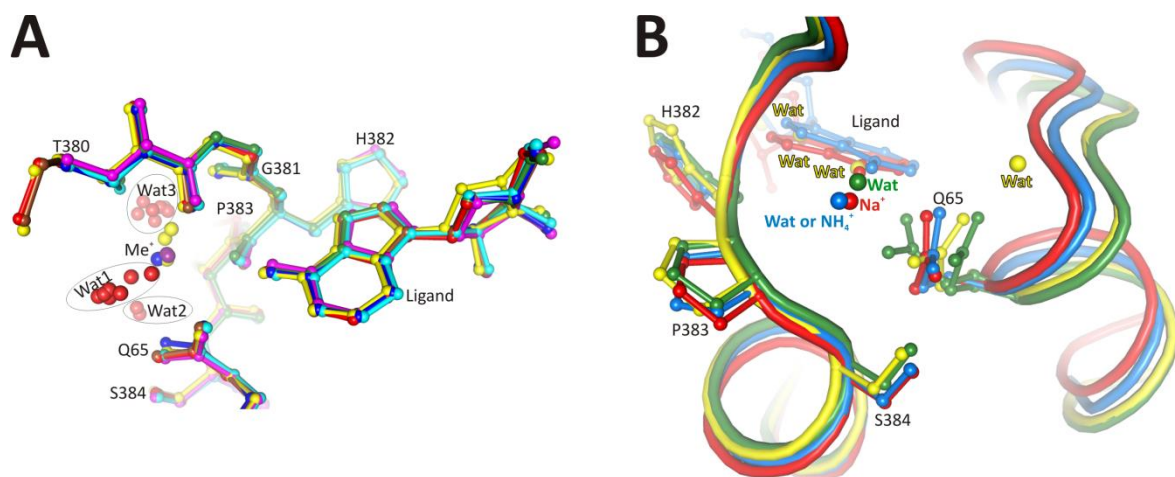
Rys. 6. (A) Porównanie miejsca wiążącego kationy litowców lub jon amonowy wraz z cząsteczką adenozyny - ligandem związanym w kieszeni wiążącej substrat PaSAHazy (jasnoniebieski) z modelem białka ludzkiego [51] (żółty), z zarodźca malarii [18] (niebieski), z *Brucella melitensis* (kod PDB: 3N58; jasnofioletowy), z łubinu żółtego [20] (zielony), z *Bradyrhizobium elkani* [21],[24], z jonem Na^+ (czerwony) lub NH_4^+ (brązowy). Cząsteczki wody (czerwone) oraz kationy (Me^+): K^+ (fioletowy), Na^+ (żółty) oraz NH_4^+ (niebieski) pokazano jako sfery. (B) Porównanie miejsca wiążącego kation w SAHazie w konformacji zamkniętej (czerwony) z modelami enzymów w konformacji półotwartej (niebieski) oraz otwartej (żółty i zielony). Kationy Na^+ i NH_4^+ oraz cząsteczki wody przedstawione są jako sfery. Numeracja reszt aminokwasowych odpowiada sekwencji aminokwasowej PaSAHazy.

Z drugiej strony, badania kinetyki reakcji enzymatycznych przeprowadzone przeze mnie w obecności różnych jonów metali alkalicznych (Li^+, Na^+, K^+, Rb^+ lub Cs^+) wskazują, że enzym osiąga maksymalną aktywność w obecności jonów K^+. W pozostałych przypadkach aktywność katalityczna jest znacznie niższa, a w obecności jonów Rb^+ jest silnie hamowana w sposób niekompetencyjny (Rys. 7A-C). Przeciwstawny wpływ jonu K^+ i Rb^+ na aktywność PaSAHazy był zaskakujący, gdyż oba jony mają zbliżone promienie

jonowe). Wyniki pomiarów ITC (Rys. 7D), przeprowadzonych przez dr Joannę Śliwiak, wskazują natomiast, że wiązanie Ado jest najsilniejsze i porównywalne w obecności obu jonów K^+ i Rb^+. W przypadku pozostałych kationów wiązanie nukleozydu było mniej efektywne. Analiza modeli SAHaz dostępnych w PDB (w formie otwartej i zamkniętej) oraz badania wykonane przez prof. dr hab. Zofię Gdaniec z wykorzystaniem spektroskopii ^{23}Na NMR wskazują, że enzym koordynuje kation dopiero w momencie wiązania liganda w trakcie zmiany konformacji podjednostek z otwartej na zamkniętą. Ma to na celu uporządkowanie i dokładną orientację łańcucha bocznego reszty glutaminy (Gln65) zaangażowanej w wiązanie liganda (Rys. 6B). Badania aktywności katalitycznej oraz ITC muteiny Gln65Ala potwierdzają rolę glutaminy w wiązaniu liganda w kieszeni wiążącej substrat.
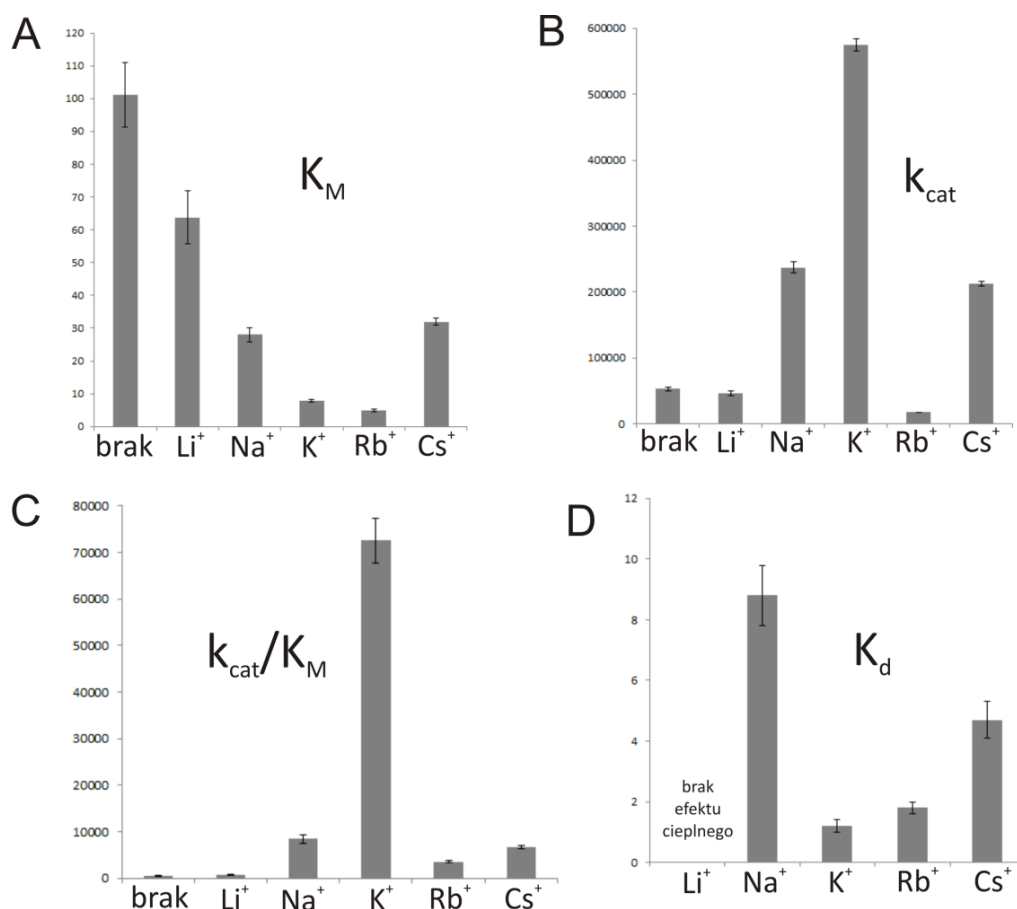

Rysunek 7. Parametry kinetyki reakcji enzymatycznych K_M, k_{cat} oraz k_{cat}/K_M wyznaczonych w obecności jonów metali alkalicznych lub przy ich braku (A-C) oraz stałe dysocjacji kompleksu enzym-adenozyna wyznaczone metodą ITC w obecności poszczególnych kationów litowców (D).

Analiza strukturalna oparta na dostępnych modelach krystalograficznych wskazywała, że zarówno geometria otoczenia makromolekularnego, które uczestniczy w koordynacji kationu oraz sposób wiązania liganda w kieszeni wiążącej substrat są niezależne od wiązanego kationu. Co więcej, niezależnie od typu wiązanego kationu, łańcuch boczny reszty odpowiadającej Gln65 w PaSAHazie jest zawsze uporządkowany i zorientowany w taki sposób, aby mógł on oddziaływać z ligandem związanym w kieszeni wiążącej substrat. Dlatego, w oparciu o analizę strukturalną oraz przeprowadzone eksperymenty nie mogłam wytłumaczyć zróżnicowanego wpływu poszczególnych kationów litowców na aktywność PaSAHazy oraz opisać mechanizmu, według którego odbywa się ta regulacja.

Aby wyjaśnić zróżnicowany wpływ kationów na aktywność PaSAHazy odniosłam się do dynamiki białka w trakcie cyklu katalitycznego, podczas którego białko oscyluje pomiędzy konformacją otwartą i zamkniętą. W oparciu o pomiary anizotropii fluorescencji wykazano, że w przypadku braku substratu w otoczeniu enzym również oscyluje pomiędzy dwiema konformacjami z częstością wynoszącą około $4 \cdot 10^7$ s^{-1} (wartość zmierzona dla SAHazy ludzkiej) [52],[53]. Jednak przy braku substratu w otoczeniu, stan równowagi pomiędzy obiema formami jest mocno przesunięty w kierunku tworzenia się formy otwartej. Z drugiej strony, reakcja hydrolizy SAH jest znacznie wolniejsza w porównaniu z czasem oscylacji pomiędzy dwiema konformacjami. Przykładowo, wartość k_{cat} wyznaczona dla reakcji hydrolizy substratu przez PaSAHazę wynosi około 0,6 s^{-1}. Znacznie większa częstość oscylacji domen w porównaniu do czasu niezbędnego do przeprowadzenia jednego cyklu katalitycznego uniemożliwiałaby zajście reakcji. Dlatego zaproponowałam, że jony K$^+$ zapewniają maksymalną aktywność enzymatyczną poprzez osiągnięcie odpowiednich właściwości dynamicznych białka. W założonym przeze mnie modelu, wiązanie jonu K$^+$ stabilizowałoby kompleks enzym-substrat w konformacji zamkniętej na czas zapewniający zakończenie cyklu katalitycznego. W takim scenariuszu jony o mniejszym promieniem jonowym (Li$^+$ i Na$^+$) lub znacznie większym (Cs$^+$) niż kation K$^+$ słabiej stabilizują kompleks enzym-substrat (Li$^+$, Na$^+$) lub tworzą kompleks z enzymem w sposób mniej efektywny (Cs$^+$), obniżając przez to aktywność enzymu. Ponadto, promień jonowy Rb$^+$ jest tylko nieznacznie większy niż K$^+$ (1,12 i 1,02 Å) [54], co mogłoby za bardzo zwiększyć trwałość kompleksu Rb$^+$, zaburzając synchronizację

oscylacji domen z reakcją enzymatyczną. Moje założenia potwierdziłam eksperymentalnie poprzez pomiar: (i) tempa wymiany Ado na 2′-dAdo w kompleksie PaSAHaza-Ado-kation (K$^+$ lub Rb$^+$) oraz (ii) tempa wiązania 2′-dAdo. Z uwagi na fakt, że wiązanie 2′-dAdo powoduje redukcję NAD$^+$ do NADH, tempo wymiany monitorowałam spektrofluorymetrycznie (przyrost NADH). W pierwszym eksperymencie obserwowałam wolniejsze tempo wymiany ligandów w obecności jonów Rb$^+$ (Rys. 8A), natomiast w drugim wiązanie 2′-dAdo zachodziło nieco efektywniej (Rys. 8B). Stabilizacja kompleksu enzym-substrat zależy od typu skoordynowanego kationu i może być również wykorzystana do hamowania aktywności PaSAHazy nie tylko przez jony Rb$^+$, ale również przez kation Zn^{2+}, który jest skoordynowany w pobliżu „bramki molekularnej" utworzonej przez parę His-Phe. Analiza tempa wymiany Ado na 2′-dAdo wykazuje, że jony Zn^{2+} bardzo silnie hamują aktywność SAHazy poprzez utrzymanie enzymu w nieaktywnej, zamkniętej konformacji (Rys. 8C).
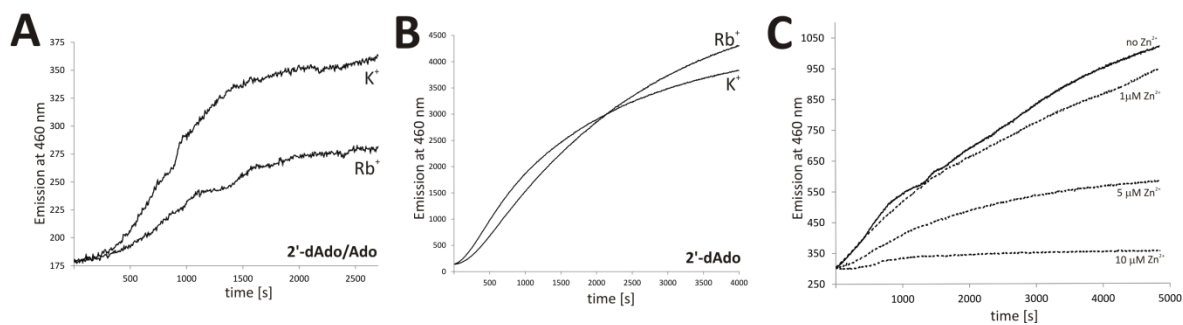
Rysunek 8. Pomiary nieodwracalnej redukcji kofaktora NAD$^+$ wywołanej związaniem 2′-dAdo w trakcie pomiaru: (A) tempa wymiany Ado na 2′-dAdo w kompleksie PaSAHaza-Ado-kation w obecności K$^+$ lub Rb$^+$, (B) tempa wiązania 2′-dAdo w obecności K$^+$ lub Rb$^+$ oraz (C) tempa wymiany Ado na 2′-dAdo przy braku lub w obecności jonów Zn^{2+} w stężeniu 1, 5 lub 10 µM.

Artykuł D3

Charakterystyka biochemiczna i strukturalna SAHazy z C. hutchinsonii oraz upakowanie cząsteczek białka w sieci krystalicznej

Czyrko, J., Jaskolski, M., Brzezinski, K. Crystal structure of *S*-adenosyl-L-homocysteine hydrolase from *Cytophaga hutchinsonii*, a case of combination of crystallographic and non-crystallographic symmetry. (2018). *Croatica Chemica Acta* **91**, 153-162.

Podstawowa charakterystyka biochemiczna

Analiza filogenetyczna hydrolazy *S*-adenozylo-L-homocysteiny wskazuje, że enzym z *C. hutchinsonii* jest bardziej spokrewniony z SAHazami zwierzęcymi, niż homologami bakteryjnymi [10]. Opracowany przeze mnie system ekspresji i oczyszczania rekombinowanej ChSAHazy pozwolił na uzyskanie znacznych ilości (10 mg/L hodowli) czystego i homogennego preparatu na potrzeby badań biochemicznych i strukturalnych. Głównym problemem pojawiającym się na różnych etapach oczyszczania białka było wytrącanie białka z roztworu i jego dezaktywacja. Ustaliłam, że przyczyną tego było zbyt wysokie stężenie białka. Dlatego, w dalszych badaniach unikałam przekraczania stężenia białka powyżej 8 mg/mL. Analiza stanu oligomerycznego wykazała, że w roztworze enzym występuje głównie w formie tetramerycznej o masie cząsteczkowej 192 kDa. Badania kinetyki reakcji hydrolizy SAH przez ChSAHazę pokazują, że wydajność katalityczna jest niższa w porównaniu z innymi SAHazami pochodzenia bakteryjnego, np. PaSAHazą.

Ogólna charakterystyka strukturalna ChSAHazy w konformacji zamkniętej

SAHazy są mocno zachowawczymi enzymami. Dotyczy to zarówno organizacji strukturalnej protomeru jak i reszt tworzących centrum aktywne. Dlatego sposób wiązania takich ligandów jak produkt reakcji (Ado) czy kofaktor (NAD$^+$) jest bardzo podobny zarówno w enzymach eukariotycznych jak i wielu bakteryjnych. Ponadto, w pobliżu miejsca wiązania substratu/produktu reakcji koordynowany jest kation metalu alkalicznego lub jon amonowy. Struktura ChSAHazy została określona dla enzymu w konformacji zamkniętej w kompleksie z Ado, NAD$^+$ i Na$^+$ (Rys. 1A). Protomer ChSAHazy utworzony jest przez dwie duże, wyraźnie rozseparowane domeny, które są odpowiedzialne za wiązanie cząsteczki substratu i kofaktora oraz niewielką C-końcową domenę oligomeryzacyjną przechodzącą z jednej podjednostki białka na drugą, w ramach ścisłego

dimeru. Domena wiążąca substrat i domena wiążąca kofaktor połączone są przez dwa międzydomenowe „zawiasy molekularne" odpowiadające za zmianę konformacji białka. Każda z podjednostek enzymu wiąże jedną cząsteczkę Ado i NAD$^+$ oraz jeden jon Na$^+$ (Rys. 1A).

Oddziaływanie ligandów z otoczeniem makromolekularnym

W wiązaniu cząsteczki Ado uczestniczą reszty aminokwasowe obu głównych domen (Rys. 9A). Pierścień heterocykliczny liganda znajduje się w wąskiej, hydrofobowej szczelinie, której ściany utworzone są przez łańcuchy boczne reszty Leu350 i Met361. Pozwala to na stabilizację pozycji pierścienia purynowego poprzez oddziaływania typu C-H⋯π. Dodatkowo, reszta adeniny oddziałuje z otoczeniem makromolekularnym poprzez kilka interakcji typu polarnego. Atom N6 reszty purynowej (związanej w formie enolowej) jest donorem w dwóch wiązaniach wodorowych z grupą karbonylową reszty His356 oraz amidowym atomem tlenu łańcucha bocznego reszty Gln60. Oddziaływanie z resztą Gln60 jest możliwe dzięki określonej pozycji i orientacji łańcucha bocznego tej reszty. Dzieje się tak dzięki jej równoczesnemu oddziaływaniu (typu kation-dipol) z jonem Na$^+$ skoordynowanym w pobliżu kieszeni wiążącej substrat przez reszty tworzące jeden z „zawiasów molekularnych" (Rys. 9B). Heterocykliczne atomy N1 i N7 oddziałują odpowiednio z hydroksylowym atomem tlenu reszty Thr58 oraz atomem azotu łańcucha głównego reszty His356. Dodatkowo, w wiązaniu adenozyny uczestniczą również trzy grupy hydroksylowe reszty D-rybozy. W oddziaływaniach tych uczestniczą zarówno reszty aminokwasowe domeny wiążącej substrat (His56, Asp134, Glu159, Thr160) oraz domeny wiążącej kofaktor (Lys189, Asp193 i His304). Ostatnia reszta, wraz z Phe305, tworzy również bramkę molekularną, regulującą dostęp do centrum aktywnego z obszaru rozpuszczalnika. W strukturze opisywanego kompleksu ChSAHazy „bramka molekularna" przyjmuje konformację zamkniętą.

Cząsteczka kofaktora znajduje się w szczelinie utworzonej przez dwie podstawowe domeny, a sposób jej wiązania przedstawiłam na Rys. 9C. Podobnie jak to miało miejsce w kieszeni wiążącej substrat, pierścień adeniny jest stabilizowany przez oddziaływania typu C-H⋯π w wąskiej kieszeni hydrofobowej utworzonej przez łańcuchy boczne reszty Ile247 oraz Thr279. W oddziaływaniach polarnych z cząsteczką NAD$^+$ uczestniczą

zarówno reszty aminokwasowe z domeny wiążącej kofaktor (Asn194, Asn227, Glu246, Asn281, Ile302 oraz His304) jak i substrat (Thr160, Thr161 i Thr162). Dodatkowo, w wiązaniu cząsteczki kofaktora uczestniczą reszty Lys429 i Tyr433, obie pochodzące z C-terminalnej domeny oligomeryzacyjnej przechodzącej do kieszeni wiążącej kofaktor z sąsiedniej podjednostki białka.
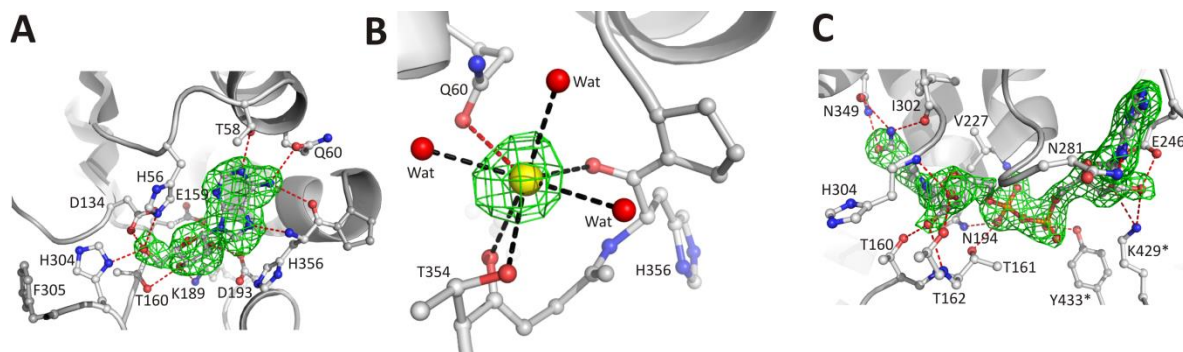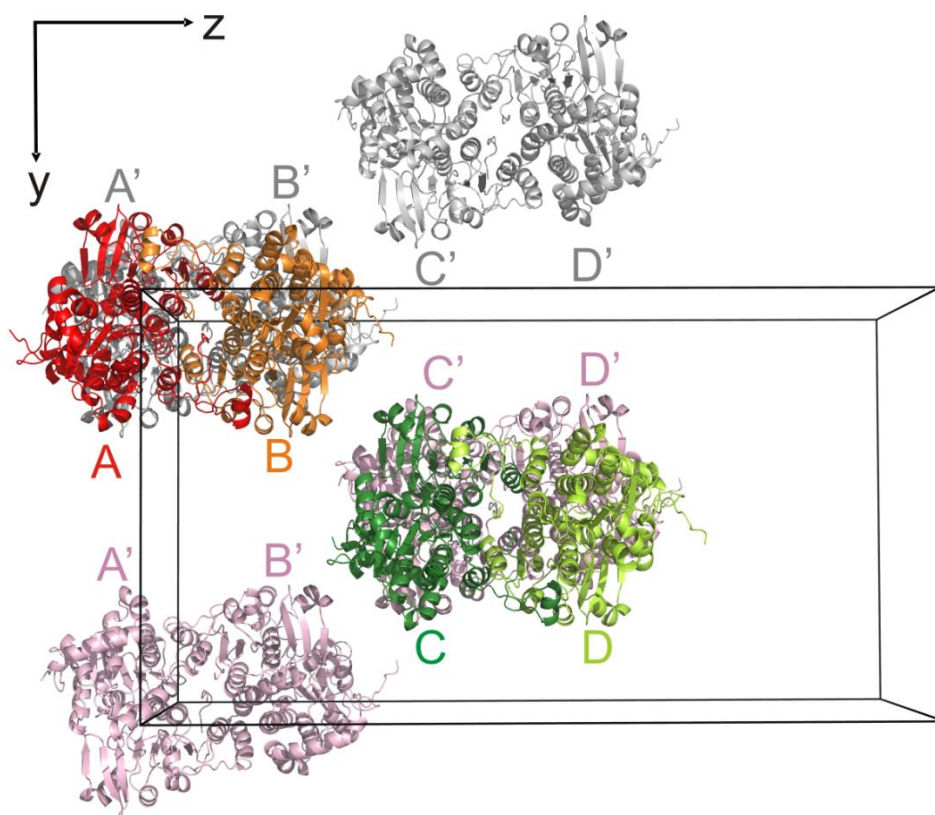

Rysunek 9. Sposób wiązania poszczególnych ligandów oraz kationu metalu alkalicznego w strukturze krystalicznej ChSAHazy: (A) adenozyny, (B) kationu Na$^+$ oraz (C) kofaktora NAD$^+$. Przerywaną czerwoną linią przerywaną zaznaczono potencjalne oddziaływania polarne, natomiast czarną zaznaczono wiązania koordynacyjne wokół kationu Na$^+$. Cząsteczki wody przedstawiono jako czerwone kule. Obecność ligandów stwierdzono na podstawie różnicowej mapy gęstości elektronowej *mF*$_o$-*DF*$_c$ typu OMIT (zielona), obliczonej z pominięciem atomów liganda lub jonu i wyświetlonej przy konturze 2.5σ (adenozyna) lub 3.0σ (Na$^+$ i NAD$^+$).

Rozwiązanie struktury krystalicznej ChSAHazy i analiza upakowania cząsteczek białka w sieci krystalicznej

Analiza zawartości komórki elementarnej kryształu ChSAHazy na podstawie objętości Matthewsa [55] wykazała obecność czterech podjednostek enzymu w części asymetrycznej. Mogłoby to odpowiadać dimerowi dimerów (AB-A'B'), aktywnej formy oligomerycznej ChSAHazy. Jednakże analiza oparta na czynnikach struktury, którą przeprowadziłam w programie *PHASER* wskazywała na obecność symetrii niekrystalograficznej, a długość wektora translacji (wyznaczona w oparciu o funkcję Pattersona) wynosiła około 95 Å. Problem fazowy rozwiązałam metodą podstawienia cząsteczkowego z wykorzystaniem modelu ścisłego dimeru SAHazy ludzkiej [51] (kod PDB: 1LI4) w grupie przestrzennej *P*2$_1$2$_1$2. W części asymetrycznej kryształu obecne są dwa ścisłe dimery enzymu (oznaczone jako AB i CD) powiązane symetrią niekrystalograficzną (Rys. 10). Odległość pomiędzy dimerami AB i CD wynosząca 95 Å

połączona jest z rotacją jednego dimeru względem drugiego o około 1°, co wskazuje na relację typu tNCS pomiędzy dimerami. Oba dimery znajdują się przy dwóch różnych krystalograficznych osiach dwukrotnych równoległych do kierunku *z*, które generują dwa dimery dimerów AB-A'B' oraz CD-C'D' o symetrii 222 (Rys. 10). Co ciekawe, oba dimery, AB i CD różnią się znacznie ruchliwością atomów w sieci krystalicznej, a co za tym idzie - ich uporządkowaniem. Dimer AB jest zdecydowanie bardziej usztywniony – średni parametr ADP to około 32 Å^2 dla atomów Cα wobec prawie 54 Å^2 dla atomów Cα z dimeru CD. Ponadto, w przypadku dimeru CD zdecydowanie więcej łańcuchów bocznych zostało udokładnionych z częściowym obsadzeniem tworzących je atomów (95 wobec 40 w dimerze AB). Wynikało to ze słabo zdefiniowanej gęstości elektronowej dla tych obszarów, co z reguły jest powiązane z mniejszym uporządkowaniem atomów w sieci krystalicznej.

Rysunek 10. Sposób upakowania poszczególnych ścisłych dimerów AB i CD powiązanych niekrystalograficzną symetrią translacyjną obecnych w części asymetrycznej kryształu. Kompletne tetrametry AB-A'B' oraz CD-C'D' generowane w sieci krystalicznej poprzez dwie niezależne krystalograficzne osie dwukrotne, równoległe do kierunku *z*. Symetrycznie równoważne dimery A'B' i C'D' są zaznaczone na szaro i jasnoróżowo. Rysunek przedstawiono w rzucie wzdłuż kierunku *x*.

5. Podsumowanie

Wyniki uzyskane podczas prowadzenia badań przyczyniły się do powstania trzech publikacji **D1 – D3**, stanowiących podstawę do ubiegania się o nadanie stopnia doktora. Obejmują one charakterystykę biochemiczną trzech bakteryjnych hydrolaz *S*-adenozylo-L-homocysteiny pochodzących z *T. maritima*, *P. aeruginosa* oraz *C. hutchinsonii*. Dodatkowo, wykonałam analizę porównawczą modeli formy aktywnej i nieaktywnej SAHazy termofilnej. Ponadto przeprowadziłam badania strukturalne SAHazy z *C. hutchinsonii* w kompleksie z adenozyną i kofaktorem NAD$^+$ wykorzystując metody biokrystalografii. Zaprezentowane badania mają charakter interdyscyplinarny i przedstawiają zagadnienia o charakterze poznawczym oraz metodycznym, co pozwoliło na pełną realizację założonych celów badawczych. Za moje najważniejsze osiągnięcia w cyklu publikacji **D1 – D3** uważam:

1. Opracowanie systemu klonowania, ekspresji oraz procedury oczyszczania natywnej ChSAHazy oraz systemu klonowania muteiny PaSAHazy Gln65Ala. Dodatkowo, zoptymalizowałam procedurę oczyszczania iTmSAHazy i PaSAHazy. W pierwszym przypadku procedura pozwoliła na pominięcie jednego z etapów oczyszczania bez wpływu na wydajność i jakość uzyskanego preparatu. W przypadku białka z *P. aeruginosa* nowa procedura pozwoliła na uzyskanie aktywnego enzymu.

2. Charakterystykę biochemiczną termofilnej SAHazy oraz analizę porównawczą aktywnej (TmSAHaza) i nieaktywnej (iTmSAHaza) formy tego białka. Badania te pozwoliły na określenie podstaw molekularnych związanych z termoaktywacją tego enzymu. W szerszej perspektywie badania te poruszają problematykę procesów dotyczących poprawnego zwijania białek termofilnych. Uzyskane wyniki są podstawą dwóch złożonych wniosków patentowych WP1 i WP2.

3. Wykazanie, że aktywność PaSAHazy ściśle zależy od typu koordynowanego w pobliżu centrum aktywnego enzymu kationu metalu jednowartościowego i jest najwyższa w obecności jonów K$^+$. Poszczególne kationy metali alkalicznych wpływają w określony sposób na dynamikę białka. Częstość oscylacji dwóch głównych domen enzymu jest optymalnie skoordynowana z czasem cyklu katalitycznego w obecności jonów K$^+$.

Mechanizm ten jest prawdopodobnie powszechny wśród wszystkich SAHaz eukariotycznych i wielu pochodzących z bakterii.

4. Wykazanie, że aktywność enzymatyczna PaSAHazy jest bardzo silnie hamowana przez jony cynku. Koordynacja jonu Zn^{2+} zaburza dynamikę białka, stabilizując cząsteczki enzymu w konformacji zamkniętej. Uniemożliwia to zmianę konformacji enzymu na otwartą, co jest konieczne do zakończenia cyklu katalitycznego.

5. Krystalizację, badania dyfrakcyjne, rozwiązanie i udokładnienie struktury krystalicznej ChSAHazy w kompleksie z adenozyną i kofaktorem NAD^+ oraz jonem Na^+. Badania te pozwoliły na charakterystykę strukturalną tego enzymu.

Interdyscyplinarne badania prowadzone w ramach publikacji D1 – D3 zostały wykonane we współpracy naukowej z:

1. Ośrodkiem synchrotronowym BESSY przy Helmholtz Centrum Berlin – w zakresie przeprowadzenia eksperymentów dyfrakcji rentgenowskiej na monokryształach białkowych oraz fluorescencji rentgenowskiej (publikacja **D2** i **D3**).

2. Ośrodkiem synchrotronowym Argonne National Laboratory – w zakresie przeprowadzenia eksperymentów dyfrakcji rentgenowskiej na monokryształach białkowych (publikacja **D1**).

3. Zakładem Krystalografii Instytutu Chemii Bioorganicznej PAN w Poznaniu – w zakresie analizy oddziaływań białko – ligand w oparciu o miareczkowanie kalorymetryczne ITC (publikacja **D1** i **D2**).

4. Zakładem Biomolekularnego NMR Instytutu Chemii Bioorganicznej PAN w Poznaniu – w zakresie analizy oddziaływań białko – jony metali alkalicznych w oparciu o pomiary widm ^{23}Na NMR (publikacja **D2**).

5. Zakładem Chemii Analitycznej Uniwersytetu w Białymstoku – w zakresie analizy aktywności enzymatycznej w oparciu o chromatografię HPLC (publikacja **D1**).

6. Piśmiennictwo

[1] M.C. Weiss, F.L. Sousa, N. Mrnjavac, S. Neukirchen, M. Roettger, S. Nelson-Sathi, W.F. Martin, The physiology and habitat of the last universal common ancestor, Nat. Microbiol. 1 (2016) 16116.

[2] G.L. Cantoni, Biological methylation: selected aspects, Annu. Rev. Biochem. 44 (1975) 435–451.

[3] H.H. Richards, P.K. Chiang, G.L. Cantoni, Adenosylhomocysteine hydrolase. Crystallization of the purified enzyme and its properties, J. Biol. Chem. 253 (1978) 4476–4480.

[4] Y. Hao, J.D. King, S. Huszczynski, D. Kocíncová, J.S. Lam, Five new genes are important for common polysaccharide antigen biosynthesis in *Pseudomonas aeruginosa*, MBio. 4 (2013) e00631-00612.

[5] L.E.P. Dietrich, A. Price-Whelan, A. Petersen, M. Whiteley, D.K. Newman, The phenazine pyocyanin is a terminal signalling factor in the quorum sensing network of *Pseudomonas aeruginosa*, Mol. Microbiol. 61 (2006) 1308–1321.

[6] J. Casadesús, Bacterial DNA Methylation and Methylomes, Adv. Exp. Med. Biol. 945 (2016) 35–61.

[7] J.E. Poulton, V.S. Butt, Purification and properties of *S*-adenosyl-L-methionine: caffeic acid *O*-methyltransferase from leaves of spinach beet (*Beta vulgaris L*), Biochim. Biophys. Acta. 403 (1975) 301–314.

[8] P.K. Chiang, G.L. Cantoni, Perturbation of biochemical transmethylations by 3-deazaadenosine *in vivo*, Biochem. Pharmacol. 28 (1979) 1897–1902.

[9] P.K. Chiang, Biological effects of inhibitors of *S*-adenosylhomocysteine hydrolase, Pharmacol. Ther. 77 (1998) 115–134.

[10] T. Stepkowski, K. Brzezinski, A.B. Legocki, M. Jaskolski, G. Béna, Bayesian phylogenetic analysis reveals two-domain topology of *S*-adenosylhomocysteine hydrolase protein sequences, Mol. Phylogenet. Evol. 34 (2005) 15–28.

[11] G. De La Haba, G.L. Cantoni, The enzymatic synthesis of *S*-adenosyl-L-homocysteine from adenosine and homocysteine, J. Biol. Chem. 234 (1959) 603–608.

[12] J.E. Poulton, V.S. Butt, Purification and properties of *S*-adenosyl-L-homocysteine hydrolase from leaves of spinach beet, Arch. Biochem. Biophys. 172 (1976) 135–142.

[13] K.E. Nelson, R.A. Clayton, S.R. Gill, M.L. Gwinn, R.J. Dodson, D.H. Haft, E.K. Hickey, J.D. Peterson, W.C. Nelson, K.A. Ketchum, L. McDonald, T.R. Utterback, J.A. Malek, K.D. Linher, M.M. Garrett, A.M. Stewart, M.D. Cotton, M.S. Pratt, C.A. Phillips, D. Richardson, J. Heidelberg, G.G. Sutton, R.D. Fleischmann, J.A. Eisen, O. White, S.L. Salzberg, H.O. Smith, J.C. Venter, C.M. Fraser, Evidence for lateral gene transfer between *Archaea* and bacteria from genome sequence of *Thermotoga maritima*, Nature. 399 (1999) 323–329.

[14] G. Xie, D.C. Bruce, J.F. Challacombe, O. Chertkov, J.C. Detter, P. Gilna, C.S. Han, S. Lucas, M. Misra, G.L. Myers, P. Richardson, R. Tapia, N. Thayer, L.S. Thompson, T.S. Brettin, B. Henrissat, D.B. Wilson, M.J. McBride, Genome Sequence of the Cellulolytic Gliding Bacterium *Cytophaga hutchinsonii*, Appl. Environ. Microbiol. 73 (2007) 3536–3546.

[15] C.K. Stover, X.Q. Pham, A.L. Erwin, S.D. Mizoguchi, P. Warrener, M.J. Hickey, F.S.L. Brinkman, W.O. Hufnagle, D.J. Kowalik, M. Lagrou, R.L. Garber, L. Goltry, E. Tolentino, S. Westbrock-Wadman, Y. Yuan, L.L. Brody, S.N. Coulter, K.R. Folger, A. Kas, K. Larbig, R. Lim, K. Smith, D. Spencer, G.K.-S. Wong, Z. Wu, I.T. Paulsen, J. Reizer, M.H. Saier, R.E.W. Hancock, S. Lory, M.V. Olson, Complete genome sequence of *Pseudomonas aeruginosa* PAO1, an opportunistic pathogen, Nature. 406 (2000) 959–964.

[16] M.A. Turner, C.S. Yuan, R.T. Borchardt, M.S. Hershfield, G.D. Smith, P.L. Howell, Structure determination of selenomethionyl *S*-adenosylhomocysteine hydrolase using data at a single wavelength, Nat. Struct. Biol. 5 (1998) 369–376.

[17] Y. Hu, J. Komoto, Y. Huang, T. Gomi, H. Ogawa, Y. Takata, M. Fujioka, F. Takusagawa, Crystal structure of *S*-adenosylhomocysteine hydrolase from rat liver, Biochemistry. 38 (1999) 8323–8333.

[18] N. Tanaka, M. Nakanishi, Y. Kusakabe, K. Shiraiwa, S. Yabe, Y. Ito, Y. Kitade, K.T. Nakamura, Crystal structure of *S*-adenosyl-L-homocysteine hydrolase from the human malaria parasite *Plasmodium falciparum*, J. Mol. Biol. 343 (2004) 1007–1017.

[19] M.C.M. Reddy, G. Kuppan, N.D. Shetty, J.L. Owen, T.R. Ioerger, J.C. Sacchettini, Crystal structures of *Mycobacterium tuberculosis* *S*-adenosyl-L-homocysteine hydrolase in ternary complex with substrate and inhibitors, Protein Sci. 17 (2008) 2134–2144.

[20] K. Brzezinski, Z. Dauter, M. Jaskolski, High-resolution structures of complexes of plant *S*-adenosyl-L-homocysteine hydrolase (*Lupinus luteus*), Acta Crystallogr. D Biol. Crystallogr. 68 (2012) 218–231.

[21] T. Manszewski, K. Singh, B. Imiolczyk, M. Jaskolski, An enzyme captured in two conformational states: crystal structure of *S*-adenosyl-L-homocysteine hydrolase from *Bradyrhizobium elkanii*, Acta Crystallogr. D Biol. Crystallogr. 71 (2015) 2422–2432.

[22] Y. Kusakabe, M. Ishihara, T. Umeda, D. Kuroda, M. Nakanishi, Y. Kitade, H. Gouda, K.T. Nakamura, N. Tanaka, Structural insights into the reaction mechanism of *S*-adenosyl-L-homocysteine hydrolase, Sci. Rep. 5 (2015) 16641.

[23] Y. Zheng, C.-C. Chen, T.-P. Ko, X. Xiao, Y. Yang, C.-H. Huang, G. Qian, W. Shao, R.-T. Guo, Crystal structures of *S*-adenosylhomocysteine hydrolase from the thermophilic bacterium *Thermotoga maritima*, J. Struct. Biol. 190 (2015) 135–142.

[24] T. Manszewski, K. Szpotkowski, M. Jaskolski, Crystallographic and SAXS studies of *S*-adenosyl-L-homocysteine hydrolase from *Bradyrhizobium elkanii*, IUCrJ. 4 (2017) 271–282.

[25] H. Berman, K. Henrick, H. Nakamura, Announcing the worldwide Protein Data Bank, Nat. Struct. Mol. Biol. 10 (2003) 980–980.

[26] F. Agüero, B. Al-Lazikani, M. Aslett, M. Berriman, F.S. Buckner, R.K. Campbell, S. Carmona, I.M. Carruthers, A.W.E. Chan, F. Chen, G.J. Crowther, M.A. Doyle, C. Hertz-Fowler, A.L. Hopkins, G. McAllister, S. Nwaka, J.P. Overington, A. Pain, G.V. Paolini, U. Pieper, S.A. Ralph, A. Riechers, D.S. Roos, A. Sali, D. Shanmugam, T. Suzuki, W.C. Van Voorhis, C.L.M.J. Verlinde, Genomic-scale prioritization of drug targets: the TDR Targets database, Nat. Rev. Drug Discov. 7 (2008) 900–907.

[27] S. Yaginuma, N. Muto, M. Tsujino, Y. Sudate, M. Hayashi, M. Otani, Studies on neplanocin A, new antitumor antibiotic. I. Producing organism, isolation and characterization, J. Antibiot. (Tokyo). 34 (1981) 359–366.

[28] T. Yamada, J. Komoto, K. Lou, A. Ueki, D.H. Hua, K. Sugiyama, Y. Takata, H. Ogawa, F. Takusagawa, Structure and function of eritadenine and its 3-deaza analogues: Potent inhibitors of *S*-adenosylhomocysteine hydrolase and hypocholesterolemic agents, Biochem. Pharmacol. 73 (2007) 981–989.

[29] E. De Clercq, M. Cools, J. Balzarini, V.E. Marquez, D.R. Borcherding, R.T. Borchardt, J.C. Drach, S. Kitaoka, T. Konno, Broad-spectrum antiviral activities of neplanocin A, 3-deazaneplanocin A, and their 5'-nor derivatives., Antimicrob. Agents Chemother. 33 (1989) 1291–1297.

[30] E. De Clercq, The discovery of antiviral agents: Ten different compounds, ten different stories, Med. Res. Rev. 28 (2008) 929–953.

[31] J.M. Bujnicki, S.T. Prigge, D. Caridha, P.K. Chiang, Structure, evolution, and inhibitor interaction of *S*-adenosyl-L-homocysteine hydrolase from *Plasmodium falciparum*, Proteins 52 (2003) 624–632.

[32] N.B. Parker, X. Yang, J. Hanke, K.A. Mason, R.L. Schowen, R.T. Borchardt, D.H. Yin, *Trypanosoma cruzi*: molecular cloning and characterization of the *S*-adenosylhomocysteine hydrolase, Exp. Parasitol. 105 (2003) 149–158.

[33] V. Ctrnáctá, J.M. Fritzler, M. Surinová, I. Hrdý, G. Zhu, F. Stejskal, Efficacy of *S*-adenosylhomocysteine hydrolase inhibitors, D-eritadenine and (*S*)-DHPA, against the growth of *Cryptosporidium parvum in vitro*, Exp. Parasitol. 126 (2010) 113–116.

[34] G.J. Crowther, A.J. Napuli, J.H. Gilligan, K. Gagaring, R. Borboa, C. Francek, Z. Chen, E.F. Dagostino, J.B. Stockmyer, Y. Wang, P.P. Rodenbough, L.J. Castaneda, D.J. Leibly, J. Bhandari, M.H. Gelb, A. Brinker, I.H. Engels, J. Taylor, A.K. Chatterjee, P. Fantauzzi, R.J. Glynne, W.C. Van Voorhis, K.L. Kuhen, Identification of inhibitors for putative malaria drug targets among novel antimalarial compounds, Mol. Biochem. Parasitol. 175 (2011) 21–29.

[35] C. Aslanidis, P.J. de Jong, Ligation-independent cloning of PCR products (LIC-PCR), Nucleic Acids Res. 18 (1990) 6069–6074.

[36] H.E. Klock, E.J. Koesema, M.W. Knuth, S.A. Lesley, Combining the polymerase incomplete primer extension method for cloning and mutagenesis with microscreening to accelerate structural genomics efforts, Proteins. 71 (2008) 982–994.

[37] C.S. Yuan, J. Yeh, S. Liu, R.T. Borchardt, Mechanism of inactivation of *S*-adenosylhomocysteine hydrolase by (*Z*)-4',5'-didehydro-5'-deoxy-5'-fluoroadenosine, J. Biol. Chem. 268 (1993) 17030–17037.

[38] G.L. Ellman, Tissue sulfhydryl groups, Arch. Biochem. Biophys. 82 (1959) 70–77.

[39] C.S. Yuan, D.B. Ault-Riché, R.T. Borchardt, Chemical modification and site-directed mutagenesis of cysteine residues in human placental *S*-adenosylhomocysteine hydrolase, J. Biol. Chem. 271 (1996) 28009–28016.

[40] W. Kabsch, *XDS*, Acta Crystallogr. D Biol. Crystallogr. 66 (2010) 125–132.

[41] K.M. Sparta, M. Krug, U. Heinemann, U. Mueller, M.S. Weiss, *XDSAPP2.0*, J. Appl. Crystallogr. 49 (2016) 1085–1092.

[42] A.J. McCoy, R.W. Grosse-Kunstleve, P.D. Adams, M.D. Winn, L.C. Storoni, R.J. Read, *Phaser* crystallographic software, J. Appl. Crystallogr. 40 (2007) 658–674.

[43] M.D. Winn, C.C. Ballard, K.D. Cowtan, E.J. Dodson, P. Emsley, P.R. Evans, R.M. Keegan, E.B. Krissinel, A.G.W. Leslie, A. McCoy, S.J. McNicholas, G.N. Murshudov, N.S. Pannu, E.A. Potterton, H.R. Powell, R.J. Read, A. Vagin, K.S. Wilson, Overview of the *CCP4* suite and current developments, Acta Crystallogr. D Biol. Crystallogr. 67 (2011) 235–242.

[44] G. Langer, S.X. Cohen, V.S. Lamzin, A. Perrakis, Automated macromolecular model building for X-ray crystallography using *ARP/wARP* version 7, Nat. Protoc. 3 (2008) 1171–1179.

[45] G.N. Murshudov, P. Skubák, A.A. Lebedev, N.S. Pannu, R.A. Steiner, R.A. Nicholls, M.D. Winn, F. Long, A.A. Vagin, *REFMAC* 5 for the refinement of macromolecular crystal structures, Acta Crystallogr. D Biol. Crystallogr. 67 (2011) 355–367.

[46] M.D. Winn, M.N. Isupov, G.N. Murshudov, Use of TLS parameters to model anisotropic displacements in macromolecular refinement, Acta Crystallogr. D Biol. Crystallogr. 57 (2001) 122–133.

[47] P. Emsley, B. Lohkamp, W.G. Scott, K. Cowtan, Features and development of *Coot*, Acta Crystallogr. D Biol. Crystallogr. 66 (2010) 486–501.

[48] H. Zheng, D.R. Cooper, P.J. Porebski, I.G. Shabalin, K.B. Handing, W. Minor, *CheckMyMetal*: a macromolecular metal-binding validation tool. Acta Crystallogr D Struct Biol 73 (2017) 223–233.

[49] E. Krissinel, K. Henrick, Secondary-structure matching (*SSM*), a new tool for fast protein structure alignment in three dimensions, Acta Crystallogr. D Biol. Crystallogr. 60 (2004) 2256–2268.

[50] G. Deckert, P.V. Warren, T. Gaasterland, W.G. Young, A.L. Lenox, D.E. Graham, R. Overbeek, M.A. Snead, M. Keller, M. Aujay, R. Huber, R.A. Feldman, J.M. Short, G.J. Olsen, R.V. Swanson, The complete genome of the hyperthermophilic bacterium *Aquifex aeolicus*, Nature. 392 (1998) 353–358.

[51] X. Yang, Y. Hu, D.H. Yin, M.A. Turner, M. Wang, R.T. Borchardt, P.L. Howell, K. Kuczera, R.L. Schowen, Catalytic strategy of *S*-adenosyl-L-homocysteine hydrolase: transition-state stabilization and the avoidance of abortive reactions, Biochemistry. 42 (2003) 1900–1909.

[52] D. Yin, X. Yang, Y. Hu, K. Kuczera, R.L. Schowen, R.T. Borchardt, T.C. Squier, Substrate binding stabilizes *S*-adenosylhomocysteine hydrolase in a closed conformation, Biochemistry. 39 (2000) 9811–9818.

[53] M. Wang, J.R. Unruh, C.K. Johnson, K. Kuczera, R.L. Schowen, R.T. Borchardt, Effects of ligand binding and oxidation on hinge-bending motions in *S*-adenosyl-L-homocysteine hydrolase, Biochemistry. 45 (2006) 7778–7786.

[54] R.D. Shannon, Revised effective ionic radii and systematic studies of interatomic distances in halides and chalcogenides, Acta Crystallogr. Sect. A. 32 (1976) 751–767.

[55] B.W. Matthews, Solvent content of protein crystals, J. Mol. Biol. 33 (1968) 491–497.

ARTYKUŁY STANOWIĄCE

MONOTEMATYCZNY ZBIÓR PUBLIKACJI
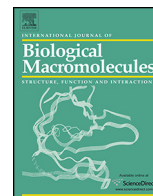
Research paper

S-adenosyl-L-homocysteine hydrolase from a hyperthermophile (Thermotoga maritima) is expressed in Escherichia coli in inactive form – Biochemical and structural studies

Krzysztof Brzezinski [a,*], Justyna Czyrko [a], Joanna Sliwiak [b], Edyta Nalewajko-Sieliwoniuk [a], Mariusz Jaskolski [b,c], Boguslaw Nocek [d], Zbigniew Dauter [e]

[a] Institute of Chemistry, University of Bialystok, Ciolkowskiego 1K, 15-245 Bialystok, Poland
[b] Center for Biocrystallographic Research, Institute of Bioorganic Chemistry, Polish Academy of Sciences, Noskowskiego 12/14, 61-704 Poznan, Poland
[c] Department of Crystallography, Faculty of Chemistry, A. Mickiewicz University, Umultowska 89b, 61-614 Poznan, Poland
[d] Structural Biology Center, Biosciences Division, Argonne National Laboratory, Argonne, IL 60439, USA
[e] Synchrotron Radiation Research Section, MCL, National Cancer Institute, Argonne National Laboratory, Argonne, IL 60439, USA

ARTICLE INFO

ABSTRACT

Thermotoga maritima is a hyperthermophilic bacterium but its genome encodes a number of archaeal proteins including S-adenosyl-L-homocysteine hydrolase (SAHase), which regulates cellular methylation reactions. The question of proper folding and activity of proteins of extremophilic origin is an intriguing problem. When expressed in E.coli and purified (as a homotetramer) at room temperature, the hyperthermophilic SAHase from T.maritima was inactive. ITC study indicated that the protein undergoes heat-induced conformational changes, and enzymatic activity assays demonstrated that these changes are required to attain enzymatic activity. To explain the mechanism of thermal activation, two crystal structures of the inactive form of T. maritima SAHase (iTmSAHase) were determined for an incomplete binary complex with the reduced cofactor (NADH), and in a mixture of binary complexes with NADH and with adenosine. In contrast to active SAHases, in iTmSAHase only two of the four subunits contain a bound cofactor, predominantly in its non-reactive, reduced state. Moreover, the closed-like conformation of the cofactor-containing subunits precludes substrate delivery to the active site. The two other subunits cannot be involved in the enzymatic reaction either; although they have an open-like conformation, they do not contain the cofactor, whose binding site may be occupied by an adenosine molecule. The results suggest that this enzyme, when expressed in mesophilic cells, is arrested in the activity-incompatible conformation revealed by its crystal structures.

© 2017 Elsevier B.V. All rights reserved.

1. Introduction

Most biological transmethylation reactions are catalyzed by methyltransferases that utilize S-adenosyl-L-methionine (SAM) as the methyl group donor [1]. A byproduct of these reactions is S-adenosyl-L-homocysteine (SAH), which is a potent negative-feedback inhibitor of SAM-dependent methyltransferases. Therefore, SAH concentration has to be strictly controlled to ensure proper methylation activity in a living cell [2–4]. In all organisms, this control function is fulfilled by two distinct enzymes, namely methylthioadenosine/S-adenosyl-L-homocysteine nucleosidase (MTAN, EC 3.2.2.9) or/and S-adenosyl-L-homocysteine hydrolase (SAHase, EC 3.3.1.1). MTAN hydrolyzes SAH to adenine and S-ribosyl-L-homocysteine, whereas SAHase catalyzes the reversible hydrolysis of SAH to adenosine (Ado) and L-

homocysteine (Hcy). Depending on the organism, the genomes encode both enzymes or only one of them [5].

Thermotoga maritima is a hyperthermophilic bacterium with optimal growth temperature of 353 K [6], adapted to geothermally heated environment, such as hot springs or hydrothermal vents. Its genome contains two distinct genes involved in SAH metabolism, namely *mtaN* encoding methylthioadenosine/*S*-adenosyl-L-homocysteine nucleosidase and *ahcY* encoding *S*-adenosyl-L-homocysteine hydrolase (TmSAHase) [7]. The former gene encodes a bacterial enzyme with numerous orthologs in *Eubacteria*. On the other hand, *ahcY* is one of many genes of archaeal origin found in the *T. maritima* genome. The acquisition of the archeal-type *ahcY* gene was most likely a consequence of massive lateral gene transfer related to the adaptation to hyperthermophilic environment [5,7].

Insight into SAHase structure and function is based mainly on crystallographic studies reported for several enzymes. The first crystal structures were determined for mammalian SAHases [8,9]. Currently, the Protein Data Bank (PDB) stores models of SAHases from diversified organisms representing eubacteria*Mycobacterium tuberculosis* [10], *Bradyrhizobium elkanii* [11], *Burkholderia pseudomallei* (PDB entry 3GLQ; unpublished), *Brucella melitensis* (3N58; unpublished)], eukaryotic microorganisms [*Plasmodium falciparum* [12], *Trypanosoma brucei* (3H9U, unpublished), *Leishmania major* (3G1U; unpublished), *Cryptosporidium parvum* (5HM8; unpublished)], plants (*Lupinus luteus* [13]), and mammals (*Mus musculus* [14]). Recently, the first crystal structure of SAHase from the hyperthermophilic *Thermotoga maritima* in its active form has been determined and deposited in the PDB in the open (3X2E) and closed (3X2F) conformations, between which the enzyme oscillates during the catalytic cycle [15]. SAHases are oligomeric enzymes, usually active as homotetramers. The only exception are plant SAHases, which form active dimers in solution [13,16,17]. All SAHases require for their activity a tightly but non-covalently bound NAD$^+$ cofactor, which is present in each subunit of the oligomeric protein.

A typical SAHase subunit is comprised of the substrate binding domain (residues 1–175 and 330–369 in TmSAHase numbering), cofactor binding domain (176–369) and a small C-terminal tail (370–404). The substrate and cofactor domains oscillate between two conformational states, known as open and closed, during the catalytic cycle. A channel leading to the active site can be open or shut depending on the conformation of a molecular gate formed by a tandem of His and Phe residues (284–285). In most SAHases, the C-terminal tail is a dimerization domain, mutually swapped between two tightly associated subunits, and participates in cofactor binding of the adjacent subunit. The tetramer is formed by side-by-side association of two intimate dimers. However, this is not the case with TmSAHase, where the C-terminal domain is shorter by eleven residues and therefore cannot be involved in cofactor binding across the intimate dimer [15].

Enzyme samples that are directly isolated form hyperthermophiles are usually properly folded and therefore fully active. A similar situation has been encountered in numerous cases of recombinant hyperthermophilic proteins expressed in mesophilic organisms and purified at room or even lower temperature. However, some exceptions have been reported, where the recombinant enzymes were expressed and purified in an inactive form as a result of improper folding. These include, for instance, D-glyceraldehyde-3-phosphate dehydrogenase from *T. maritima* [18], glutamate dehydrogenase from *Pyrococcus* sp. [19–22], indolepyruvate ferredoxin oxidoreductase from *Pyrococcus kodakaraensis* KOD1 [23], or sulfur oxygenase reductase from *Aquifex aeolicus* [24]. It is of note that most of these examples are enzymes utilizing a redox cofactor during the enzymatic reaction. Usually, the enzyme obtained from a mesophilic expression system can be converted to the active form using heat- or urea-induced activation, which involves changes in

the oligomeric state or structural rearrangements within the same oligomeric form [21].

Here, we present a thermal activation study of an inactive form of *E. coli*-expressed SAHase from *T. maritima* (iTmSAHase). The results of enzymatic assays and isothermal titration calorimetry experiments suggest that the protein might be arrested in an activity-incompatible conformation, and that it can be converted to the catalytically competent enzyme by heat-induced activation. These observations were corroborated by our crystallographic structural characterization of iTmSAHase. This inactive form of TmSAHase was crystallized as an incomplete binary complex with the reduced form of the cofactor, NADH, and as a mixture of binary complexes with NADH and with adenosine, which is a substrate/product of the catalytic reaction. Both crystal structures show that the enzyme cannot be active because of the conformation adopted by the subunits. Moreover, the cofactor is present only in two subunits. Our results also indicate that the cofactor is incorporated into the protein structure during the expression step mainly in its reduced form, which does not support the catalytic reaction.

2. Material and methods

2.1. Cloning, expression, purification and preliminary characterization of the protein

The coding sequence of the *ahcY* gene was amplified by PCR from *T. maritima* MSB8 genomic DNA. The amplicon was cloned into pMCSG9 expression vector using the ligation independent cloning reaction and sequenced. The correct construct was transformed into BL21-CodonPlus(DE3)$^®$-RIPL *E. coli* cells and expressed. 15 mL of LB medium containing 34 µg mL^{-1} chloramphenicol and 100 µg mL^{-1} ampicillin were inoculated and grown overnight at 310 K and the overnight culture was used for inoculation of 1 L of LB medium, which was subsequently cultivated with appropriate antibiotics to an OD$_{600}$ of ∼1.0. The temperature was decreased to 291 K and protein expression was induced with IPTG at a final concentration of 0.3 mM. The cells were harvested 18 h after induction and flash-frozen in liquid nitrogen.

The cell pellet was resuspended in buffer A (20 mM imidazole, 500 mM NaCl, 20 mM Tris·HCl pH 8.0, 10% glycerol) with the addition of 1 mM TCEP·HCl, 1 mM PMSF, 100 µg mL^{-1} lysozyme and 500 units of benzonase. Cells were disrupted by sonication on ice and centrifuged for removal of cell debris. Thermal precipitation, the standard step of purification of proteins from thermophilic organisms, was deliberately omitted in this study. The supernatant was loaded onto a HisTrap column equilibrated with 0.1 M NiSO$_4$. The protein was eluted with a buffer containing 500 mM imidazole, 500 mM NaCl, 20 mM Tris·HCl pH 8.0, 10% glycerol and 1 mM TCEP·HCl. TEV protease was added to the final concentration of 0.1 mg mL^{-1} to remove the His tag and the protein solution was extensively dialyzed against buffer A. After overnight incubation at 292 K, the solution was loaded onto a HisTrap column equilibrated with 0.1 M NiSO$_4$ and the protein was eluted with buffer A, subsequently exchanged for buffer B (100 mM NaCl, 25 mM Tris·HCl pH 8.0) *via* dialysis. The protein solution was concentrated using Amicon Ultra 30 ultracentrifugation filters and loaded onto a Superdex 200 (Pharmacia) gel filtration column pre-equilibrated with buffer B supplemented with 1 mM TCEP·HCl. The protein was eluted with buffer B as a tetramer. Fractions with iTmSAHase were concentrated to 10 mg mL^{-1} by ultracentrifugation and the fresh protein solution was used for crystallization experiments. Protein concentration was estimated by UV absorption measured at 280 nm. The purified protein has the TmSAHase sequence, extended at the N-terminus by a short tripeptide (SNA-) cloning artifact. SDS-PAGE analysis confirmed the size of the expressed protein (∼45 kDa).

Finally, mass spectrometry was used to confirm the size and sequence of the recombinant enzyme.

2.2. SAHase activity assays

Assays for the enzymatic activity in the direction of SAH synthesis were carried out using ACQUITY UPLC® H-Class high performance liquid chromatograph (HPLC) with a photodiode array (PDA) eλ detector (Waters Corp., USA). Chromatographic separations were carried out using an XBridge BEH Shield RP18 column (5 μm, 4.6 mm × 150 mm) with Sentry Guard Cartridge (5 μm, 4.6 mm × 20 mm) (Waters, USA). For elution, a mobile phase containing methanol and water (12:88, v:v) was used. The flow rate was 0.8 mL min^{-1} and the injection volume was 20 μL. All chromatographic separations were performed at 298 K. Under the experimental conditions, the retention times of NAD$^+$, SAH and Ado were 3.9, 4.4 and 6.5 min, respectively. The rate of SAH formation was monitored at 260 nm. The assays were performed in 1 mL volume in a buffer containing 150 mM KCl and 25 mM Tris·HCl pH 8.0, supplemented with 2 mM Ado and 4 mM L-Hcy. As a variable, tests were performed in the absence or presence of 5 mM NAD$^+$. Three different temperature-dependent conditions of the reaction were tested: (i) assays were performed at 298 K and monitored after 2, 6 and 24 h; (ii) iTmSAHase samples were incubated at 358 K for 30 min and subsequently chilled to 298 K prior to the assays conducted at 298 K and monitored after 2, 6 and 24 h; (iii) reactions were performed at 358 K and monitored after 1, 2 and 4 h. As a negative control, reaction mixtures without the addition of the enzyme were used.

2.3. Determination of the oligomeric state in solution

The oligomeric state of the protein in solution was determined as a function of concentration and temperature. Size exclusion chromatography (SEC) was applied to confirm the homotetrameric state in the concentration range from 1 to 10 mg mL^{-1} at a constant, room temperature. The experiments were carried out using a Superdex 200 gel filtration column pre-equilibrated with buffer B and calibrated with a gel filtration standard (BioRad).

Dynamic light scattering (DLS) experiments were performed to establish the oligomeric state of the enzyme at various temperatures but at a constant concentration of 5 mg mL^{-1}. Three scenarios were utilized: (i) unheated protein sample measured at 298 K; (ii) protein sample heated to 358 K for 30 min and then measured at 298 K; and (iii) protein sample heated to 358 K for 30 min and then measured at 358 K. All samples were filtered (0.1 μm) prior to the experiment.

2.4. Isothermal titration calorimetry

ITC measurements were performed at 293 K using a MicroCal iTC200 calorimeter (GE Healthcare). Prior to the titrations, the protein was dialyzed against a buffer containing 100 mM NaCl and 25 mM HEPES·NaOH pH 7.5. Two differently treated protein samples were used for the measurements: (i) protein incubated at 358 K for 30 min and cooled down to 293 K and (ii) unheated protein. Prior to the titrations, the protein concentration was estimated by the Bradford method. The final protein concentration was adjusted to 86 μM or 106 μM. Adenosine, NAD$^+$ and adenosine 5′-monophosphate (AMP) were dissolved in the dialysis buffer to the concentrations of 1.5 mM, 0.5 mM and 1.0 or 1.5 mM, respectively. The ligands were injected to the protein solution (300 μL) in 2 μL aliquots until saturation was observed. The raw ITC data were analyzed with the *ORIGIN* 7.0 software (OriginLab) to obtain the thermodynamic parameters of the complexation reactions: stoichiometry (N), dissociation constant (K$_d$), as well as changes in

enthalpy (ΔH) and entropy (ΔS). For sigmoidal titration curves, the *one set of sites* model was fitted and N was obtained from the experiment. For hyperbolic curves, for which the determination of N is impossible, N was fixed while fitting the same model. All measurements were performed in triplicates.

2.5. Determination of the redox state of the cofactor

The oxidized:reduced ratio of the cofactor in a sample of iTm-SAHase was determined spectrofluorimetrically by excitation at 340 nm and measurement of emission at 460 nm, as described previously [25].

2.6. Crystallization

Initial screening for crystallization conditions was performed with Robotic Sitting Drop Vapor Diffusion setup (Mosquito) using Crystal Screen 1 from Hampton Research. The protein was subjected to crystallization in the absence or presence of adenosine. In the latter case, prior to crystallization trials, a portion of the protein solution in buffer B was incubated overnight at room temperature with 2 mM adenosine. For both samples, initial crystals were obtained from 20 mM CaCl$_2$, 0.1 M sodium acetate pH 4.6 and 30% (v/v) MPD. The conditions were manually refined by adjusting the protein concentration, pH and type of divalent cation. Crystallization drops were mixed from 2 μL of the protein solution (6 mg mL^{-1}) incubated without (crystal 1) or with (crystal 2) adenosine, and 2 μL of the reservoir solution containing 20 mM MgCl$_2$ or CaCl$_2$, 0.1 M sodium acetate, pH 4.6 or 5.3, and 30% (v/v) MPD for crystal 1 or 2, respectively. Diffraction-quality crystals were grown within a few days at 292 K using the hanging-drop vapor-diffusion method.

2.7. X-Ray data collection and processing

X-ray diffraction data were measured at the Advanced Photon Source (ANL, Argonne, IL, USA) SER-CAT 22-BM beamline at 100K using a Mar 225 mm CCD detector. Crystals were fished out directly from the mother liquor and vitrified in liquid nitrogen. Diffraction data extending to 1.90/1.75 Å resolution were obtained from 180/360 images recorded with 1.0°/0.5° oscillation at 200/180 mm crystal-to-detector distance for crystal 1/2, respectively. Indexing and integration of all images was performed in *DENZO* and scaling in *SCALEPACK* from the *HKL2000* package [26]. The crystals are isomorphous, with the monoclinic space group *C*2. The final data sets are characterized in Table 1.

2.8. Structure solution and refinement

2.8.1. iTmSAHase-NADH-adenosine complex

The crystal structure of iTmSAHase was solved by molecular replacement, as implemented in the program *PHASER* [27] from the *CCP4* suite [28]. The substrate- (residues 18–181 and 355–421) and cofactor-binding (182–354) domains of a model of *H. sapiens* SAHase (PDB entry 1LI4) [29] were used as search probes. The correct solution was found in space group *C*2 for two different-conformation subunits in the asymmetric unit. Automatic model building was carried out with the online version of *ARP/wARP* [30]. Isotropic stereochemically-restrained structure-factor refinement was carried out in *REFMAC5* [31] with maximum-likelihood targets and with the inclusion of three TLS groups [32] per protein chain, defined as suggested by the *TLSMD* server [33]. In the final model, one subunit (B) has the cofactor-binding domain occupied by a molecule of the reduced form of the cofactor, NADH, while the other subunit (A) has a molecule of adenosine in the cofactor binding site. The ligands were identified without ambiguity in

Table 1
Crystallographic data and data collection and structure refinement statistics.

Data collection and processing statistics		
Data set	iTmSAHase-NADH	iTmSAHase-NADH-Ado
Beamline	APS SER-CAT 22-BM	
Wavelength (Å)	0.97242	0.97856
Temperature (K)		100
Space group		C2
Cell dimensions (Å,°)		
a	120.4	120.4
b	106.7	105.5
c	85.9	85.5
β	109.2	108.8
Mosaicity (°)	0.27	0.52
Resolution range (Å)	30.0–1.90 (1.93–1.90)[a]	30.0–1.75 (1.81–1.75)[a]
Total/unique reflections	306144/80548	387679/101542
Completeness (%)	99.6 (92.7)	99.9 (100)
Multiplicity	3.8 (3.2)	3.8 (3.8)
$<I/\sigma(I)>$	23.4 (2.1)	21.9 (2.3)
R_{merge}[b]	0.056 (0.505)	0.051 (0.589)
Refinement statistics		
Resolution (Å)	30.0–1.90	30.0–1.75
No. of reflections in		
working/test set	79463/1069	100299/1169
R/R_{free}[c] (%)	16.1/19.7	16.6/18.8
No. of atoms (protein/ligand/water/Cl$^-$)	6198/44/491/2	6215/71/581/2
R.m.s. deviation from ideal		
bond lengths (Å)	0.014	0.015
bond angles (°)	1.595	1.674
Average B factor (Å^2)	40.3	39.5
Ramachandran statistics (%)		
most favored/allowed regions	98/2	99/1
PDB code	5TOV	5TOW

[a] Values in parentheses correspond to the last resolution shell.

[b] $R_{merge} = \Sigma_{hkl}\Sigma_i |I_i(hkl) - <I(hkl)>|/\Sigma_{hkl}\Sigma_i I_i(hkl)$, where $<I(hkl)>$ is the average intensity of reflection hkl.

[c] $R = 100 \cdot \Sigma_{hkl}||F_o(hkl)| - |F_c(hkl)||/\Sigma_{hkl}|F_o(hkl)|$, where F_o and F_c are the observed and calculated structure factors, respectively. R_{free} is calculated analogously for the test reflections, randomly selected and excluded from the refinement.

mF_o-DF_c omit electron density maps phased with the contribution of the protein atoms only. Additionally, 581 water molecules, one molecule of MPD and two chloride anions were identified in the asymmetric unit. Geometrical restraints for the NADH and adenosine molecules were generated using the Grade Web server [34]. Electron density was not defined for some parts of the structure and residues 169–174, 330–334 and 401–404 of chain A, as well as four N-terminal residues (including the artifactual tripeptide) of both chains were not modeled.

2.8.2. iTmSAHase-NADH complex

The iTmSAHase-NADH-adenosine complex model stripped of the adenosine molecule was transferred to the nearly identical unit cell of the iTmSAHase-NADH crystal. The refinement was carried out as for the above crystal structure. The final rounds of refinement included 491 water molecules, in addition to one NADH molecule and two chloride anions. As in the iTmSAHase-NADH-adenosine structure, electron density was not defined for some parts of the structure and residues 172–177, 283–284, 290, 330–334 and 498-404 from chain A, as well as four N-terminal residues from both chains were not modeled.

2.8.3. Final refinement and validation

The *COOT* program [35] was used for manual modeling in electron density maps. Stereochemical quality of the models was assessed using the wwPDB validation pipeline [36]. Final refinement statistics for both crystal structures are reported in Table 1. The atomic coordinates and structure factors have been deposited in the Protein Data Bank with the accession codes 5TOV (iTmSAHase-NADH, incomplete binary complex), and 5TOW (iTmSAHase-NADH-adenosine, a mixture of two binary complexes). Raw diffraction images for both structures were deposited

in the Integrated Resource for Reproducibility in Macromolecular Crystallography (ProteinDiffraction.org) with DOI numbers 10.18430/M35TOV and 10.18430/M35TOW for the 5TOV and 5TOW models, respectively.

2.9. Other software used

The *SSM* algorithm [37] was used for Cα superposition of protein models. Protein-ligand interactions were analyzed with *PDBsum* [38]. Molecular figures were generated in *PyMOL* [39], with mF_o-DF_c and $2mF_o$-DF_c electron density maps calculated in *PHENIX* [40]. Protein domain movements were analyzed with the *DynDom* server [41] using chain A of the native TmSAHase models (PDB IDs 3X2E and 3X2F) and chains A and B of iTmSAHase in the mixture of binary complexes with NADH and adenosine from this work. Interaction-interface areas were calculated with the PDBePISA server [42].

3. Results and discussion

3.1. Evaluation of enzymatic activity

Since the reaction catalyzed by SAHase is reversible and strongly shifted in the direction of SAH synthesis, we used this synthetic direction (spectrophotometric detection of SAH) in our assays of catalytic activity. In all assays conducted at room temperature and at 358 K without the addition of NAD$^+$, no traces of SAH were detected even after 24 h of incubation. Conversely, all tests performed in the presence of the oxidized form of the cofactor, led to SAH synthesis, although the efficiency was highly variable. These activity assays clearly indicate that the addition of NAD$^+$ to the reaction mixture is essential for enzymatic activity. Very high enzymatic activity was observed when the reaction was carried out at

358 K. However, only traces of SAH could be detected even after 24 h for the reactions performed at 298 K using either heated or unheated enzyme in the presence of NAD$^+$. The efficiency of these reactions was very low and the enzymatic activity was at 0.9 and 0.4%, respectively, when compared with the reaction at 358 K.

3.2. Determination of the oligomeric state

iTmSAHase is inactive in solution at room temperature, although, similarly to the native enzyme, it also exists exclusively as a homotetramer, even at concentrations as low as 1 mg mL^{-1} and at a broad range of temperatures, as confirmed by SEC FPLC and DLS experiments (Supplementary materials, Figs. S1A, B). The DLS experiments indicated a small but measurable change of the molecular size of differently heat-treated samples. Similar averaged sizes of 94.5 ± 9.9 Å and 97.0 ± 12.4 Å were established at 298 K for the unheated and heated iTmSAHase samples, respectively. The homotetramer average size increased to 105.3 ± 6.4 Å at 358 K.

3.3. Calorimetric evaluation of heat-induced conformational changes

The ITC isotherms obtained upon NAD$^+$ titration of unheated protein were hyperbolic and the stoichiometry (N) was fixed at 0.25 (calculated for the monomer) while fitting the *one set of sites* model. This indicates that only one subunit out of four could bind NAD$^+$; fixing N at 0.5 was questionable as it resulted in poor fit and the error in K$_d$ determination was close to 100%. For the isotherms obtained for adenosine titrations, N also had to be fixed, while fitting the *one set of sites* model, again because of the hyperbolic shape of the curves. In this case N was fixed at 0.5 (corresponding to ligand binding by two out of four subunits) and not at 1 (which would correspond to ligand binding by all four subunits, as observed in active SAHases). The reason for this choice of N was the same as in the case of the NAD$^+$ isotherms, namely fixing N at 0.75 or 1 resulted in large errors, while assuming N equal to 0.5 resulted in the best fit.

After the heat treatment, an increase of affinity for NAD$^+$ (∼15 times higher) as well as for adenosine (∼2 times higher) is observed. Moreover, binding of NAD$^+$ by heat-treated protein is more specific, as the shape of the isotherm changes from hyperbolic to sigmoidal. Additionally, a decrease of the enthalpy contribution with a simultaneous increase of the entropic contribution to the complexation reactions is observed for both ligands after the heat treatment. These observations suggest that upon heat treatment at 358 K, iTmSAHase undergoes conformational changes that consequently result in stronger and more specific ligand binding, as compared to the treatment at 293 K. For the sigmoidal isotherms obtained upon titrations of the heat-treated protein with NAD$^+$, a *one set of sites* model was fitted and the Hill constant N of 0.26 was estimated experimentally. This stoichiometry could be explained by a situation where only one cofactor molecule is bound to one of the two cofactor-free subunits of the tetramer with a change of enthalpy. Therefore, we suggest that under the experimental conditions used, NAD$^+$ binding by the two cofactor-free subunits of the tetramer is not identical, i.e. that the first ligand must bind with an enthalpy change, while the second one with unmeasurable heat effect.

Since adenosine can be considered to be a fragment of NAD$^+$, the question arises where exactly this nucleoside binds to the protein upon ITC titration of unheated and heated protein. Due to structural mimicry, adenosine could bind in the substrate or cofactor binding sites, or simultaneously in both places. To clarify this point, a titration with adenosine 5′-monophosphate (AMP), a larger fragment of the cofactor, was also performed. Titrations of the unheated and

heated protein with AMP produced similar results as in the case of adenosine. For both isotherms, N was successfully fixed at 0.5 while fitting the *one set of binding sites* model to the hyperbolic titration curves. These observations suggest that adenosine and AMP occupy the same position. Additionally, in both experiments, only two ligand molecules are bound to the protein tetramer. Moreover, our crystallographic results obtained for iTmSAHase incubated with high concentration of adenosine (2 mM) indicate that the nucleoside is bound only in the cofactor binding domain (vide infra). Therefore we suggest that adenosine (and AMP) is bound in the cofactor binding domain during the ITC experiments as well.

The main conclusion from the calorimetric experiments is that there is an increase in the strength and specificity of NAD$^+$ binding after heat treatment, which is an indication of a conformational change. The results of the ITC measurements are summarized in Table 2 and Fig. 1.

3.4. Experimental conditions of ITC analysis

A note is required to discuss the level of compatibility of the crystallographic experiments, based on crystals grown at acidic pH, and the ITC experiments carried out at neutral conditions. Firstly, we note that our numerous attempts to obtain iTmSAHase crystals at neutral or basic pH have been unsuccessful. In fact, under those conditions hardly any precipitate was observed. The only crystals were obtained at pH 4.6 (iTmSAHase-NADH) and 5.3 (iTmSAHase-NADH-Ado). These observations suggested that acidic pH promotes iTmSAHase crystallization by reducing protein solubility. It is of note that although the two crystals of iTmSAHase complexes were obtained at different pH values of sodium acetate (4.6 and 5.3), their structures are nevertheless very similar. This might suggest that pH does not affect the structure significantly, at least in this pH range. We also note that the real pH values in crystallization drops were somehow higher than nominal, mainly as the result of the presence of Tris buffer of pH 8.0 in the protein solution. To test this, we prepared mock solutions imitating the crystallization drop conditions, and their pH values were higher, 5.2 and 5.7, respectively.

We also tried to conduct the ITC analysis at acidic conditions. Unfortunately, such a study was not possible in the pH range between 5 and 6, for two reasons. (i) The solubility of iTmSAHase is much lower at acidic conditions. We tried to dialyze the protein at 4 °C or room temperature against buffers containing MES, sodium citrate or sodium acetate. After dialysis and centrifugation the protein concentration could be increased to 50 μM, but it was too low to detect any ITC heat effect. Additionally, we observed slow but gradual precipitation of the protein in the supernatant with time (in the crystallization drops the protein was additionally stabilized by high MPD content; however, due to its high viscosity MPD cannot be used in ITC titrations). Our further study indicated that iTmSAHase is not denatured at acidic pH, as the protein was dissolved completely when the pH was increased to 7.5. DLS analysis confirmed that the protein is a tetramer in solution. (ii) When acidic solutions (including MES, sodium acetate or citrate) of iTmSAHase for ITC analysis were heated to 85 °C, protein denaturation was observed. It is of note that no denaturation occurred at neutral pH.

Although it was not possible to directly compare the conditions of the crystallographic and biophysical studies, the experiments performed at acidic and neutral pH lead to similar conclusions. The results indicate that only two of four subunits can bind adenosine molecules in the cofactor binding domains. Moreover, the crystal structure of the iTmSAHase-NADH-Ado complex explains why only two of the four subunits can bind adenosine molecules.
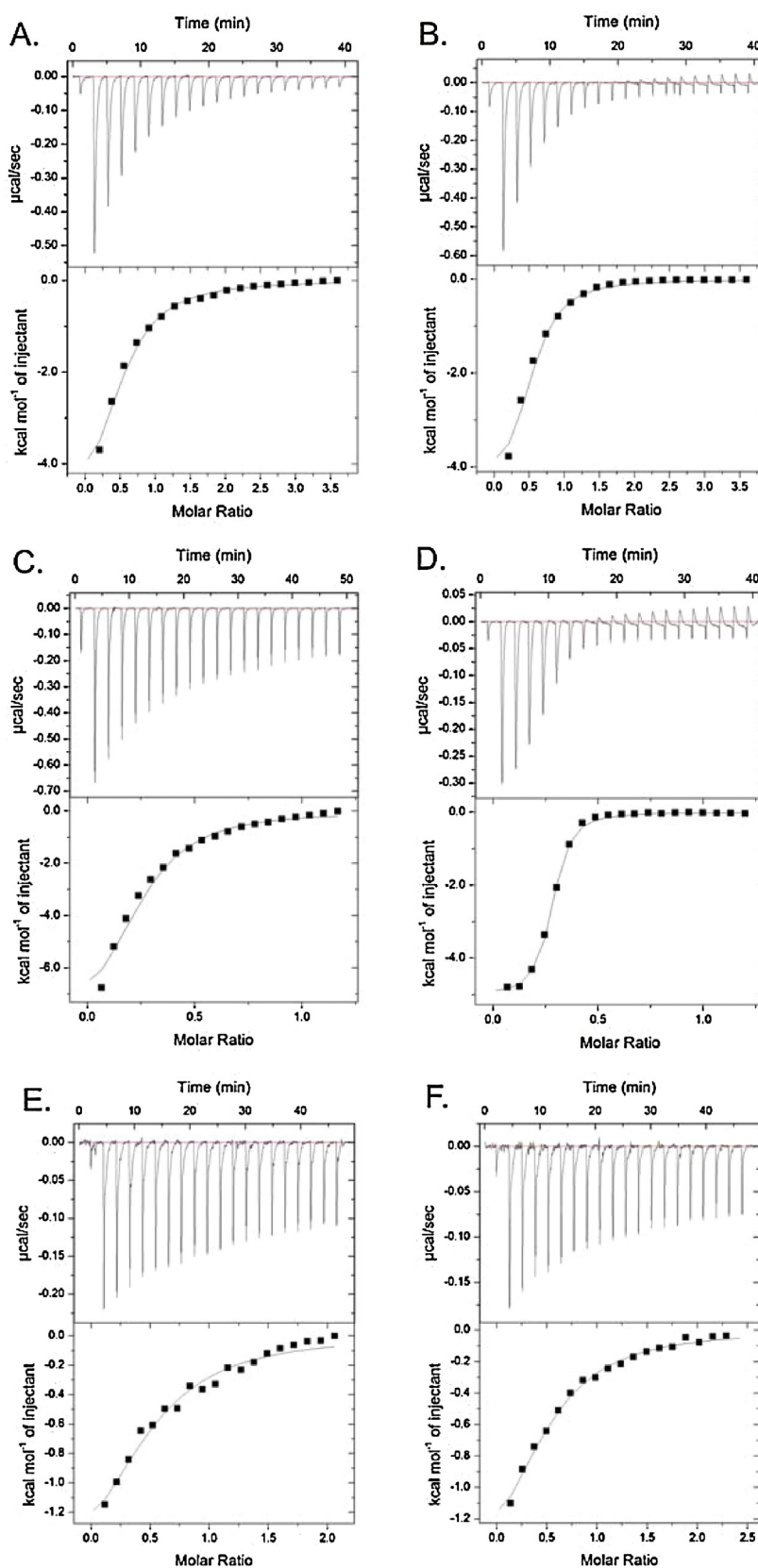
Fig. 1. Calorimetric titration of the protein with adenosine (A, B), NAD⁺ (C, D) and AMP (E, F). Experiments (A), (C) and (E) were conducted using unheated protein (iTmSAHase) whereas in (B), (D) and (F) the protein was preincubated at 358 K (htTmSAHase). The top plot of each panel represents the raw heat data obtained from 20 consecutive 2 μL injections of 1.5 mM (E) or 1.0 mM (F) of AMP, and 1.5 mM adenosine or 0.5 mM NAD⁺ into the sample cell (200 μM) containing 86 μM (A,B,D,F) or 106 μM (C,E) protein. The heat peak areas have been plotted against the molar ratio of adenosine/NAD⁺/AMP added to the protein, creating the binding isotherm at the bottom of each panel. The best fit of the model of *one set of binding sites* is represented by the solid line. All titrations were performed at 293 K.

Table 2
Thermodynamic parameters for interactions of the inactive (iTmSAHase) and heat-treated (htTmSAHase) protein with adenosine (Ado), NAD+ and adenosine 5′-monophosphate (AMP), obtained from ITC titration (protein/titrant).

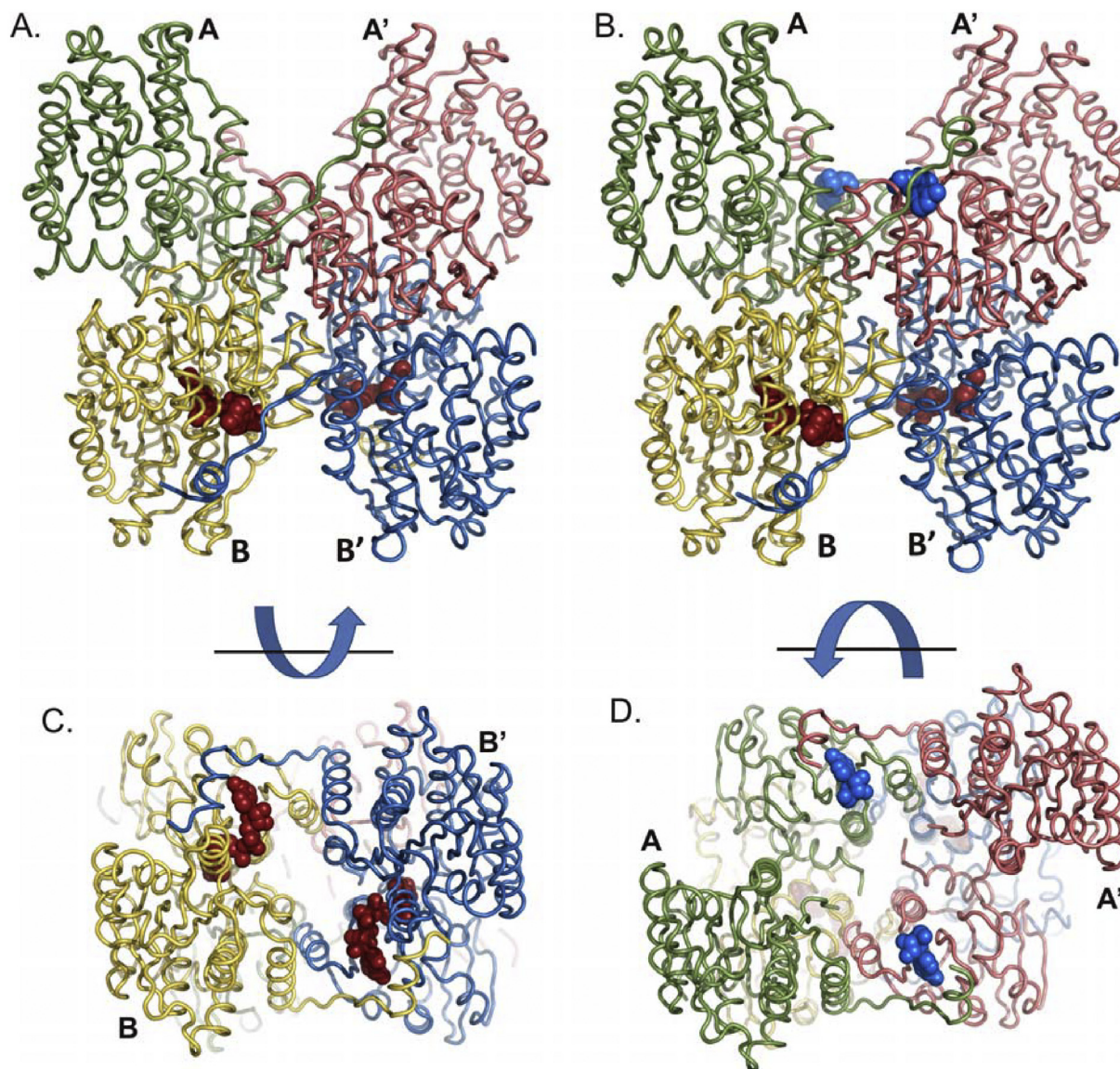|	iTmSAHase/Ado	htTmSAHase/Ado	iTmSAHase/NAD+	htTmSAHase/NAD+	iTmSAHase/AMP	htTmSAHase/AMP
K_d [µM]	19.0 ± 1.5	8.8 ± 1.2	9.4 ± 1.2	0.63 ± 0.04	30.0 ± 3.0	25.0 ± 2.0
N	0.5/fixed	0.5/fixed	0.25/fixed	0.262 ± 0.002	0.5/fixed	0.5/fixed
ΔH [cal/mol]	-5709 ± 157	-4612 ± 160	-8839 ± 362	-5026 ± 54	-1923 ± 88	-1832 ± 44
ΔS [cal/mol/deg]	2.1	7.4	-7.2	11.2	14.1	14.8

Fig. 2. Overall structure of iTmSAHase, described as a dimer of intimate dimers (AA'-BB'). Schematic diagram of the inactive enzyme crystallized as an incomplete binary complex (A) and as a mixture of binary complexes (B) with the ligands, and after 90° rotation presenting a view of subunits BB' in the closed conformation with NADH bound (C), and a view of subunits AA' in the open conformation with adenosine bound (D). The NADH cofactor (red) and adenosine (blue) are shown in space-filling representation. Panels (B), (D) illustrate the iTmSAHase-NADH-Ado complex. In the iTmSAHase-NADH complex (A), (C) the sites filled in iTmSAHase-NADH-Ado with adenosine (blue) are empty. (For interpretation of the references to colour in this figure legend, the reader is referred to the web version of this article.)

3.5. Overall structure of the inactive form of TmSAHase (iTmSAHase)

iTmSAHase crystalizes in space group *C*2 with two subunits (A and B) in the asymmetric unit. Interestingly, these two subunits have different conformation and do not interact with each other to form the intimate SAHase dimer. Crystallographic symmetry generates two intimate dimers from the two subunits, i.e. AA' and BB', and the complete tetramer, composed of two intimate dimers of different conformation, has the form AA'BB' (Fig. 2). The structures of the incomplete binary and mixed binary complexes of iTmSAHase are very similar. The r.m.s. deviation between the two complete tetramers is 0.35 Å over 1560 Cα atoms. Also, the mode of NADH binding in the two structures is nearly identical. Since the crystal structure of the mixture of binary complexes with NADH and Ado was determined at higher resolution (1.75 Å), it will be used for further descriptions unless stated otherwise.

The organization of the iTmSAHase tetramer is different when compared with that observed in all crystal structures of active SAHases. Moreover, the arrangement of the domains within the subunits differs from the typical scheme characteristic of active SAHases. In most cases reported to date, all four subunits of the tetramer uniformly adopt the open conformation in ligand-free from, or the closed conformation when complexed with an active-site ligand. An exception is the crystal structure of SAHase from *Bradyrhizobium elkanii*, where only three subunits bind the serendipitous adenosine ligand and adopt the closed conformation, while the fourth subunit is open [11], or where a mixture of open, closed and intermediate states is possible in different ligand complexes [43].

In the mixed binary complex of iTmSAHase, two subunits (A and A') exist in an open-like conformation and each of them binds one Ado molecule in the cofactor-binding domain if this ligand is added to the protein. Intriguingly, the cofactor-binding site of the subunits in the open-like conformation is not occupied by the cofactor even when the protein samples have been incubated overnight with 5 mM NAD$^+$ (~50 fold molar excess) prior to the last step of FPLC purification (data not shown). The two other subunits (B and B') are in a closed-like conformation and each contains one cofactor molecule in the cofactor binding site, but no ligand in the substrate binding site. The presence of the two cofactor molecules in these two subunits is independent of the purification procedure, which implies that they are incorporated into the complex during protein expression. The tetramer structures, together with the associated ligands are shown in Fig. 2A–D. The Cα traces of the open-like and closed-like subunits deviate by ~4.40 Å, attesting to their significantly different conformation, illustrated in Fig. 3A.

An important consequence of the asymmetric structure of the iTmSAHase tetramer is that there are significant differences between the interface areas and numbers of polar contacts within the interacting subunits. Specifically, the interaction interface area between the two subunits in the open-like conformation (AA') is 1822 Å^2, with 18 polar contacts, whereas for the two subunits in the closed-like conformation (BB') the area is much larger, 2414 Å^2, with 28 polar contacts. The interface area between subunits with different conformation (AB or A'B') is 1376 Å^2 with 29 polar contacts.

Such a quaternary structure of the tetramer explains why the iTmSAHase protein is inactive. The two subunits in the open-like conformation do not contain the cofactor molecule that is essential for the enzymatic reaction. The two other subunits adopt a closed-like conformation, and the entrance (access channel) to the substrate-binding pocked is shut by a molecular gate formed by a pair of highly conserved His284 and Phe285 residues [10,11,13]. In consequence, this conformation precludes any possibility of substrate binding. Moreover, even though the closed-like subunits do contain a cofactor molecule, it is predominantly in the reduced state, as determined spectrofluorimetrically for freshly purified iTmSAHase samples (72 ± 12% of total cofactor content). Therefore, the majority of the bound cofactor molecules are incapable of supporting the key step of the catalytic reaction, i.e. hydride anion abstraction from the C3 atom of the substrate [8,9,44–46].

A detailed comparison indicates additional differences between the subunits in the two states, including their rigidity and completeness of the models. The subunit in the open-like conformation is more flexible, with the mean ADP (atomic displacement parameter) value for main-chain atoms of 40.4 Å^2. The corresponding value for the subunit in the closed-like conformation is lower, 36.4 Å^2. However, rigid and flexible regions map to the same parts of the subunits, as illustrated in Fig. 3B. Additionally, the model of the subunit in the open-like conformation is less complete and some amino acid residues (169–174 and 330–334) of the two hinge regions
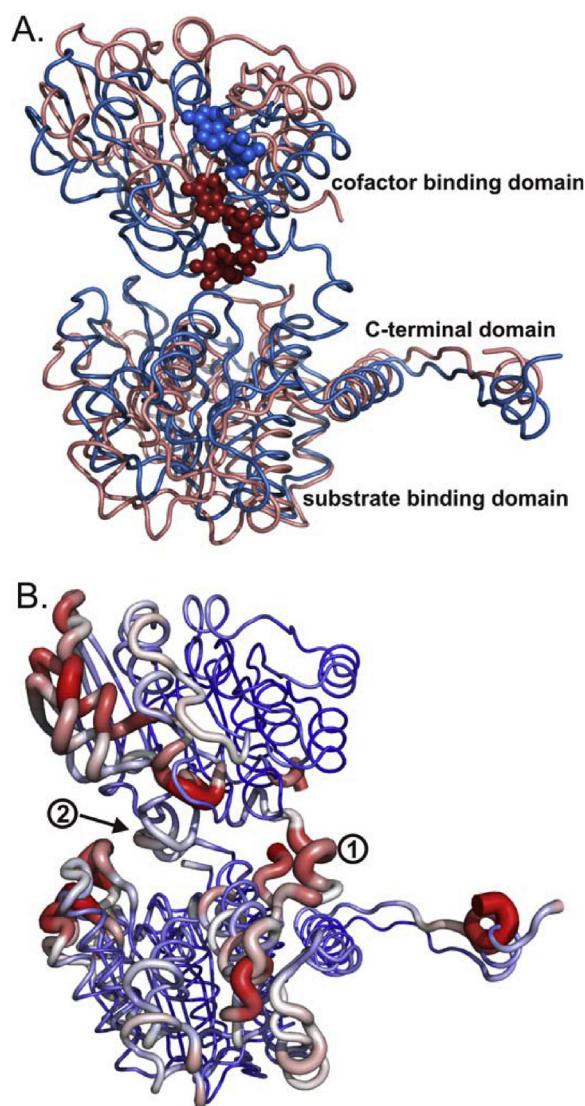

Fig. 3. Overall structure of iTmSAHase subunits. (A) Superposition of the subunits in the closed (blue) and open (salmon) conformation. The cofactor (red) and adenosine (blue) are shown in space-filling representation. (B) Superposition of the closed and open subunits as in (A) but with an indication of main-chain rigidity, as expressed by the ADP values of main-chain atoms, ranging from 20 (blue, thin line) to 80 Å^2 (red, thick line). Encircled numbers indicate the molecular hinges connecting the substrate- and cofactor-binding domains, and involved in domain rearrangement: 1 (residues 162–181) and 2 (residues 327–336). (For interpretation of the references to colour in this figure legend, the reader is referred to the web version of this article.)

linking the substrate and cofactor domains are not defined in the electron density.

A closer inspection of the subunit conformations, as well as detailed comparisons with the structure of the catalytically active protein, clearly indicate that the present subunits cannot be described as having the classical open or closed form. To find out if the structural differences arise from different subunit/domain structure or/and from different domain/subunit orientation, a series of Secondary-Structure Matching (SSM) comparisons of the full subunits as well as of the substrate-, cofactor- and dimerization-domains were performed. The results are illustrated in Fig. 4 and summarized in Table 3. A superposition of the iTmSAHase subunit referred to as "open-like" with the open and closed subunits of the native TmSAHase structure (PDB IDs 3X2E and 3X2F) reveals a poor match, with Cα r.m.s.d. values of 3.42 and 3.82 Å, respectively. A closer match is observed when the iTmSAHase subunit referred
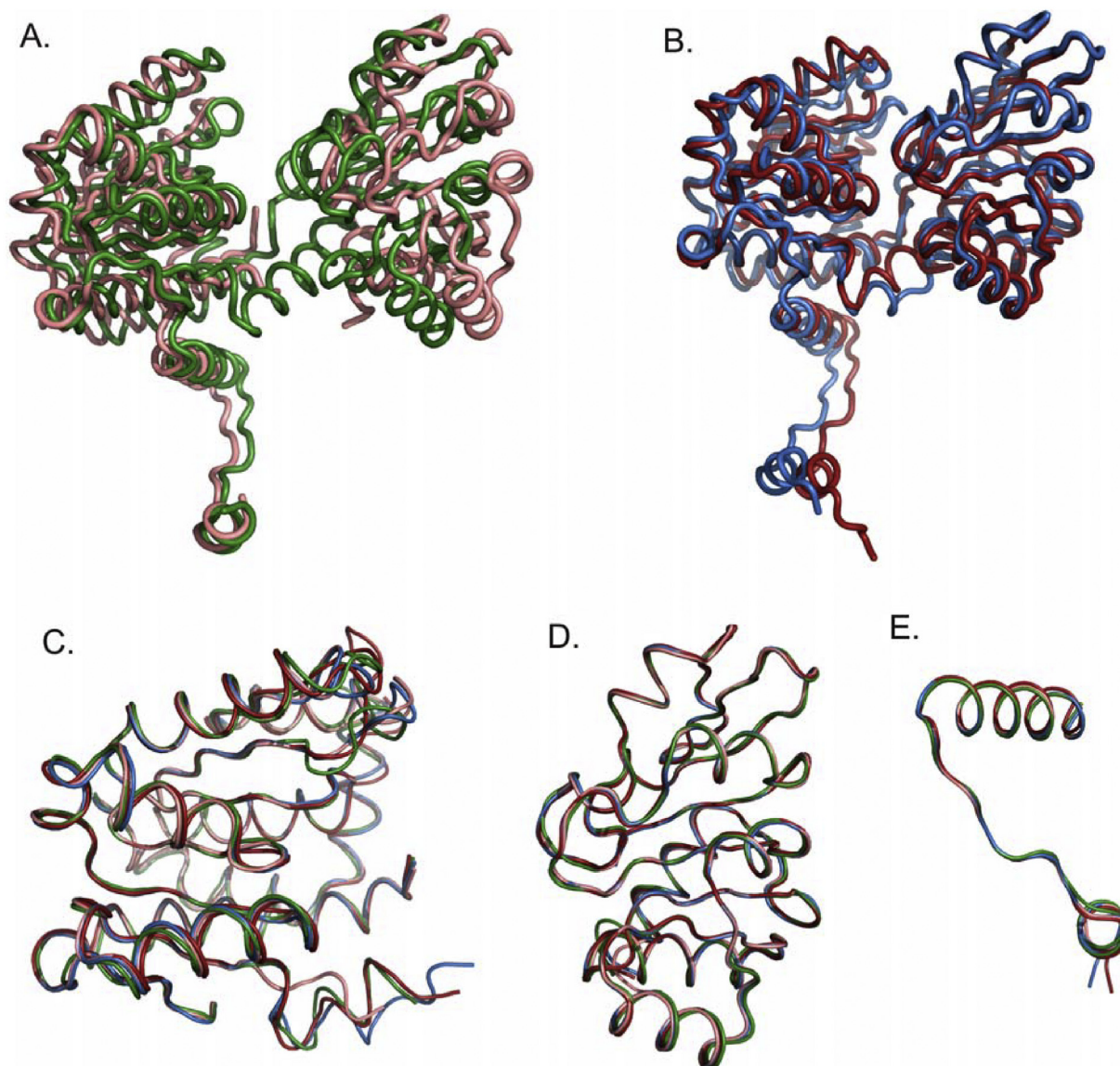
Fig. 4. Superpositions of subunits and individual domains extracted from models of the inactive (present work, mixture of binary complexes) and active (PDB entries 3X2E/3X2F for open/closed conformation, respectively) forms of S-adenosyl-L-homocysteine hydrolase from *T. maritima*. (A) Subunits in the open conformation; (B) subunits in the closed conformation; (C) substrate-binding domains; (D) cofactor-binding domains; (E) C-terminal dimerization domains. The colour code indicates the subunits/domains as follows: salmon, iTmSAHase, open-like conformation; green, TmSAHase, open conformation; blue, iTmSAHase, closed-like conformation; red, TmSAHase, closed conformation. (For interpretation of the references to colour in this figure legend, the reader is referred to the web version of this article.)

Table 3

Secondary-Structure Matching (SSM) comparison of subunits and individual domains of native (TmSAHase) and inactive (iTmSAHase) forms of S-adenosyl-L-homocysteine hydrolase from *T. maritima* in various conformations. The results are presented as r.m.s.d. (N_{align}), where r.m.s.d. is the Cα root-mean-square deviation (Å) between probe and target, and N_{align} is the number of matched residues. SBD is substrate-binding domain (residues 2–175 and 330–369), CBD is cofactor-binding domain (176–329), and CTD is C-terminal domain (370–402). The subunits and domains have been extracted from chain A of the native TmSAHase models in the open (PDB ID 3X2E) and closed (3X2F) conformations, and from chains A and B of iTmSAHase in the binary complexes (this work).

	TmSAHase closed conformation	TmSAHase open conformation
iTmSAHase subunit open-like conformation	3.82 (335)/3.79 (333)	3.42 (359)/3.48 (356)
iTmSAHase subunit closed-like conformation	1.63 (390)/1.56 (391)	2.78 (371)/2.76 (380)
iTmSAHase SBD open-like conformation	0.76 (196)/0.72 (200)	0.62 (193)/0.69 (200)
iTmSAHase SBD closed-like conformation	0.89 (208)/0.91 (208)	0.79 (203)/0.83 (205)
iTmSAHase CBD open-like conformation	0.56 (154)/0.43 (149)	0.44 (150)/0.53 (149)
iTmSAHase CBD closed-like conformation	0.27 (154)/0.26 (154)	0.44 (152)/0.51 (154)
iTmSAHase CTD open-like conformation	0.38 (31)/0.40 (28)	0.40 (31)/0.38 (28)
iTmSAHase CTD closed-like conformation	0.60 (35)/0.63 (35)	0.36 (32)/0.37 (32)

to as "closed-like" is superposed on the open and closed subunits of native TmSAHase, the r.m.s.d. values being 2.78 and 1.63 Å, respectively. Thus, the closest similarity is observed when the

closed subunits are compared. In this comparison, the substrate- and cofactor-binding domains superpose nearly perfectly. However, the relatively high overall r.m.s.d. of 1.63 Å results from

a markedly different orientation of the C-terminal dimerization domains. Superpositions of all corresponding individual domains extracted from the open and closed conformations of the native and inactive TmSAHase models are characterized by low r.m.s.d. values between 0.27 and 0.89 Å. These comparisons indicate that the individual domains of the inactive protein are properly folded, but oriented in an incorrect way. Evidently, this aberrant tertiary structure of domain orientations is linked to the low temperature of the protein expression and purification protocols.

3.6. Analysis of domain movement

As concluded above, the domains of iTmSAHase are properly folded but their spatial arrangement is different from that observed in the native enzyme. To elucidate this behavior, domain movement analysis was performed to compare the inactive and active forms of the protein. In general, the rearrangement is seen as a movement of the cofactor-binding domain towards the substrate-binding domain with a concomitant closure of the gap between these domains. As a consequence, the substrate and the cofactor are brought together to allow the enzymatic reaction to proceed. However, there are significant differences between TmSAHase and iTmSAHase in the mode of "conformational breathing" during the closed-open transition. For the native enzyme, the domain movement can be described as a pure rotation by about 14° around the molecular hinge section. A different situation is observed for the inactive protein, where the rotation angle around the molecular hinge is larger ($\sim$20°) and is coupled with a translation along the rotation axis by $\sim$10 Å. The existence of two modes of reorientation of the cofactor-binding domain is also reflected in differences in the molecular hinge sections. Although the two distinct hinge elements are formed by similar regions of the active and inactive enzyme, they differ slightly in their length and precise location. According to *DynDom* analysis, in iTmSAHase the molecular hinge elements are longer and cover residues 162–181 and 327–336, while in the active enzyme both elements are shorter, 169–182 and 335–336.

3.7. The mode of adenosine binding in the cofactor-binding domain

In the mixed binary complex of iTmSAHase, two subunits in the open-like conformation bind adenosine molecule in the cofactor binding domain (Fig. 5A). The nucleoside occupies a small cavity at the protein surface (Fig. 5C) that is different from the original substrate binding site. In this complex of iTmSAHase, the adenine moiety is docked within the cavity, while the ribose ring is partially exposed to the solvent region. Amino acid residues of the subunit (chain A) in which the ligand is docked participate only indirectly, *via* water molecules, in adenosine binding. Direct hydrogen bonds to the adenosine molecule are provided only by amino acid residues from the cofactor binding domain of the symmetry-related subunit (chain A') within the intimate dimer. In the active form of the enzyme, these residues would be involved in cofactor binding. Specifically, these interactions are formed by side-chain atoms of residues including Glu226 ($O^{\varepsilon2}$...O2'), Lys231 (N^{ζ}...O3'), Asn261 ($N^{\delta2}$...N7) and by the main-chain carbonyl O atom of Ser259 (O...O5'). The adenine ring is sandwiched between the side chains of Val227 and Ser259, accepting C—H$\cdots\pi$ hydrogen bonds. Additionally, three water molecules form hydrogen bonds with the N1 and N6 atoms of the adenine base and the O2'/O3' hydroxyl groups of the ribose moiety. This binding mode of the adenosine molecule is very similar to that observed for the adenosine moiety of the NADH cofactor bound in subunits B and B' of the tetramer (Fig. 5A,B).

The absence of adenosine in the substrate/product binding pocket suggests that the inactive protein has low affinity for adenosine binding in this site. This seems to be the result of different domain organization in iTmSAHase, where the angle between the two principal domains of the subunit in the open-like conformation is larger (Fig. 4A). In consequence, the different domain organization may affect substrate binding and ligand-induced domain rearrangement.

3.8. The mode of NADH binding

Each subunit in the closed-like conformation binds one molecule of the reduced form of the cofactor in the cofactor-binding domain. The closed-like conformation is adopted despite the fact that no substrate/product is bound in the substrate-binding domain. The cofactor binding mode, shown in Fig. 5B, is very similar to that observed in other SAHases, including the active form of *T. maritima* SAHase, where all subunits adopt the canonical closed conformation (PDB entry 3X2F). It is of note that the active form of SAHase from *T. maritima* adopts the closed conformation only in the presence of SAH although the substrate (or products of its hydrolysis) is not defined in the electron density maps [15]. Eight water molecules and amino acid residues from both the cofactor- and substrate-binding domains of iTmSAHase are involved in hydrogen-bonding interactions with the cofactor. These interactions include the side chains of Thr141 ($O^{\gamma1}$...O2N), Thr142 ($O^{\gamma1}$...O3D), Glu226 ($O^{\varepsilon1}$...O2B and $O^{\varepsilon2}$...O3B), Lys231 (N^{ζ}...O3'), Asn261 ($N^{\delta2}$...N7A) and Asn329 ($N^{\delta2}$...O7N and $O^{\delta1}$...N7N), as well as main-chain atoms of residues Cys207, Ala282 and His284. Additionally, the side chains of Val227 and Ser259, which restrict the size of the cofactor-binding cavity, are involved in C—H$\cdots\pi$ interactions with the adenine ring. The nicotinamide moiety of the cofactor is partially disordered and has been modeled with 0.7 partial occupancy. The disorder is coupled to repulsion by one of the alternative side-chain conformations of Cys207. Also, the nicotinamide ring is non-planar, at least in the visible portion, and this buckled structure is a hallmark of its reduced form [47] (Fig. 5D).

To find out if the presence of NADH could be the result of NAD$^+$ reduction in the X-ray beam during data collection, or if there was an earlier reduction event during the protein expression procedure, we determined the NADH:NAD$^+$ ratio in freshly purified protein samples. The results indicate that the NADH fraction significantly predominates over NAD$^+$ ($72 \pm 12\%$ of total cofactor content), thus confirming that the reduced form of the cofactor was present in abundance in the protein preparations prior to the crystallization experiments. Numerous attempts at cofactor exchange in iTmSAHase all failed to yield a homogeneous protein-NAD$^+$ complex [25]. Obviously, this is a consequence of the iTmSAHase structure, where the wrong (i.e. reduced) cofactor is trapped in the cofactor binding domain of a closed-like subunit at an early stage of protein production. In this conformational state, the bound NADH cofactor cannot be removed from the protein and substituted with its oxidized NAD$^+$ form.

3.9. Biochemical and structural implications of thermal activation of iTmSAHase

The active form of TmSAHase was characterized biochemically in two studies before [48,49]. In both those studies, the recombinant enzyme was purified according to a protocol that included thermal precipitation of the cell lysate at 353 K. Additionally, the crystal structure of the active form of TmSAHase has been recently described [15]. In that study, the protein sample was purified with the application of thermal precipitation at the same temperature (353 K). One of the conclusions from those studies is that the activity of the purified enzyme is low or even undetectable, unless the reaction mixture has been supplemented with the cofactor in the correct, oxidized, NAD$^+$ form. Also, crystallization of active TmSAHase required the addition of the NAD$^+$ cofactor to the protein
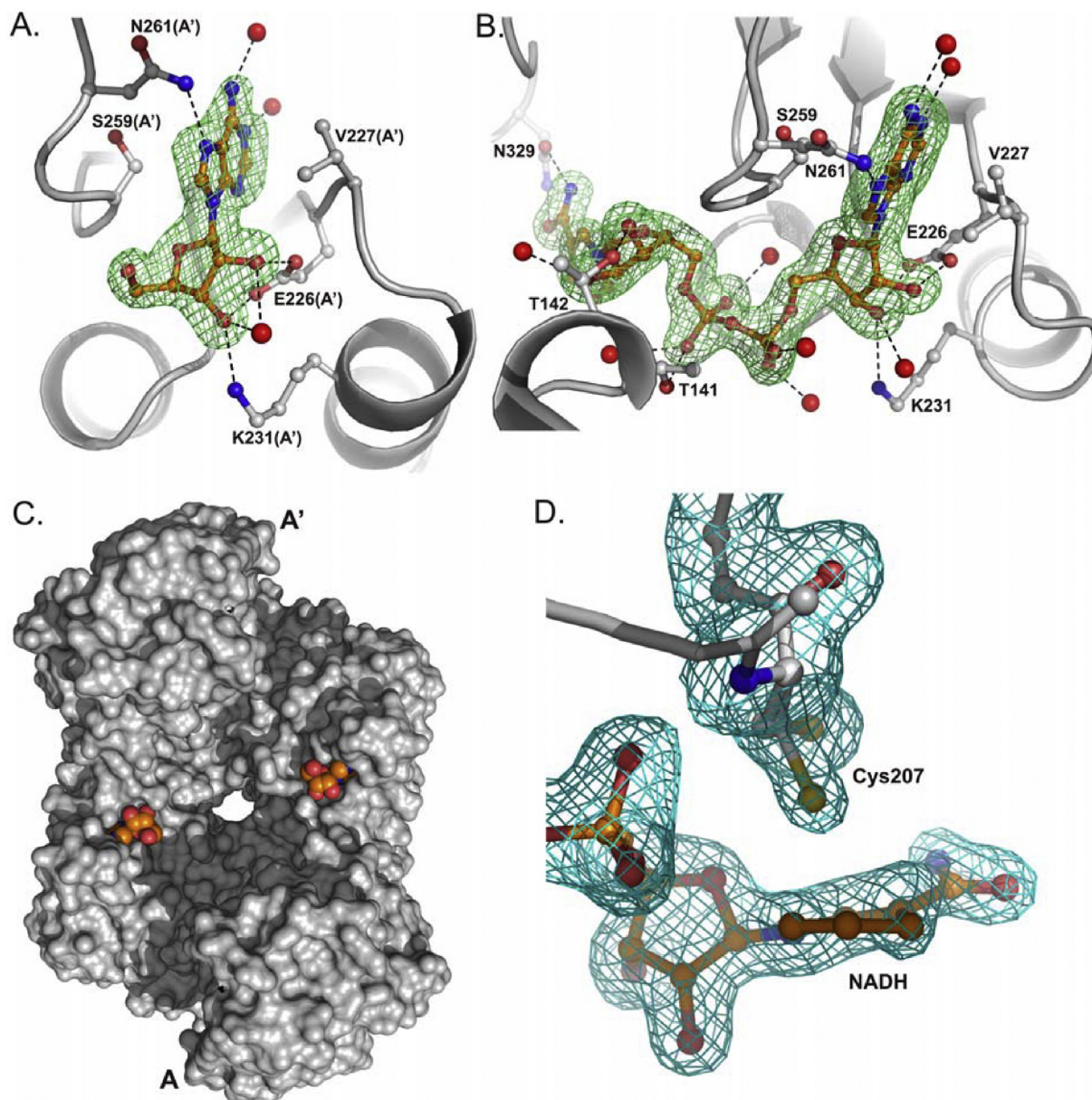
Fig. 5. The mode of adenosine (A) and NADH (B) binding in the cofactor binding site of iTmSAHase. Only side chains involved in polar or hydrophobic interactions and water molecules (red spheres) are shown. Potential hydrogen bonds are indicated by broken lines. The mF_o-DF_c difference electron density map is contoured at 3.0σ. (C) Illustration of adenosine binding in the cofactor binding pocket. The ligand and protein are shown in space-filling and surface representation, respectively. (D) Illustration of the non-planar conformation of the six-membered ring of the nicotinamide moiety of NADH in close proximity of two alternative conformations of Cys207. The $2mF_o$-DF_c electron density map is contoured at 1.0σ. (For interpretation of the references to colour in this figure legend, the reader is referred to the web version of this article.)

solution. The present results provide a rational explanation of those observations.

In the present study, as well as in the previous work, the recombinant enzyme was expressed in the mesophilic *E. coli* at 291–315 K, i.e. well below the temperature required for heat-induced activation of the enzyme. This implies that after the expression step, in all experiments that were not preceded by heat-treatment, the protein existed in its inactive conformation.

Our crystallographic results indicate that the iTmSAHase tetramer binds only two molecules of the cofactor, and that it is predominantly in its reduced form. As demonstrated by our enzymatic assays, no catalytic activity could be detected, not only at room temperature but also at 358 K, without the addition of NAD^+. Although our spectrofluorimetric measurements indicated that iTmSAHase might contain a small fraction of the oxidized cofactor, which in

principle could be involved in the enzymatic reaction, in reality, as demonstrated by the enzymatic assays, this is not the case and evidently other factors are also involved. The most obvious reason is the wrong conformation of the iTmSAHase molecule. In conclusion, the presence of the NAD^+ cofactor in the reaction environment is essential for the restoration of the activity of the enzyme at 358 K. A corollary to this observation might be that all four subunits of the tetrameric enzyme have to bind the correctly oxidized cofactor molecule to attain enzymatic activity.

Our enzymatic activity study revealed that the heat treatment of iTmSAHase at 358 K changes the enzymatic properties significantly. These changes are also reflected in the thermodynamic parameters of NAD^+ and adenosine binding, which are dramatically altered after the heat treatment. Surprisingly, the ITC experiments indicate that the heated enzyme can bind only one instead of two cofac-

tor molecules (in the two formally "empty" subunits). This result is in contrast with the structural studies of enzymatically active SAHases, which bind one cofactor molecule in each subunit. However, it should be stressed that all ITC experiments were performed at 293 K. Similarly, the enzymatic assays in the presence of NAD$^+$ indicate very low (<1%) activity of both heated and unheated samples at 298 K when compared with the heated enzyme tested at 358 K. These results may suggest that the protein heated to 358 K and subsequently cooled down, could exist in other non-native, low-activity conformation(s), but with a higher affinity for the cofactor and the ligand when compared with the unheated protein. This hypothesis is additionally supported by DLS analyses, which indicate some changes in the average size of the homotetramer depending on the heating history and the temperature of the measurements (Fig. S1B).

4. Conclusions

S-adenosyl-L-homocysteine hydrolase from *Thermotoga maritima* was recombinantly expressed in the mesophilic *Escherichia coli* cells and purified as a homotetramer at room temperature. Enzymatic activity study indicated that the enzyme expressed and purified at the room temperature conditions is inactive. Isothermal titration calorimetry experiments revealed that the inactive form of TmSAHase undergoes heat-induced conformational changes and enzymatic activity assays demonstrated that these changes are required to attain enzymatic activity. To elucidate the mechanism of thermal activation, two crystal structures of the inactive form of *T. maritima* SAHase (iTmSAHase) were determined, for a binary complex with the reduced form of the cofactor (NADH), and for a mixture of binary complexes with NADH and a reaction byproduct/substrate (adenosine). The homotetramers in the two structures are very similar and are composed in each case of two subunits in the open conformation and two subunits in the closed conformation. However, the results clearly indicate that the protein has not adopted a structure that is compatible with the catalytically-competent, native enzyme. In contrast to the catalytically active form of SAHase from several sources, in iTmSAHase only two of the four subunits contain a tightly bound cofactor. Additionally, the cofactor exists mainly in its reduced NADH state and, therefore, cannot participate in substrate oxidation, which is a key step of the catalytic cycle. Moreover, the closed-like conformation of the cofactor-containing subunits precludes substrate delivery to the active site. The remaining two subunits cannot be involved in the enzymatic reaction either. Although they have an open-like conformation, they do not contain the cofactor, whose binding site is vulnerable to clogging by an adenosine molecule. The results indicate that the inactive form of the enzyme, iTmSAHase, can be compared to a clockwork that is assembled from more-or-less correct parts, but is functioning incorrectly: its "open"-"closed" transitions are only a poor imitation of the genuine structural transformations required for the catalytic cycle of the active enzyme.

Author contributions

KB designed and performed the experiments, analyzed the data and wrote the manuscript. JC, JS, ENS performed the experiments and analyzed the data. MJ, BN and ZD analyzed the data and wrote the manuscript.

Conflict of interest

None declared.

Appendix A. Supplementary data

Supplementary data associated with this article can be found, in the online version, at http://dx.doi.org/10.1016/j.ijbiomac.2017.06.065.

References

[1] H.H. Richards, P.K. Chiang, G.L. Cantoni, Adenosylhomocysteine hydrolase. Crystallization of the purified enzyme and its properties, J. Biol. Chem. 253 (1978) 4476–4480.
[2] J.E. Poulton, V.S. Butt, Purification and properties of S-adenosyl-L-methionine: caffeic acid O-methyltransferase from leaves of spinach beet (*Beta vulgaris L*), Biochim. Biophys. Acta. 403 (1975) 301–314.
[3] P.K. Chiang, G.L. Cantoni, Perturbation of biochemical transmethylations by 3-deazaadenosine in vivo, Biochem. Pharmacol. 28 (1979) 1897–1902.
[4] P.K. Chiang, Biological effects of inhibitors of S-adenosylhomocysteine hydrolase, Pharmacol. Ther. 77 (1998) 115–134.
[5] T. Stepkowski, K. Brzeziński, A.B. Legocki, M. Jaskólski, G. Béna, Bayesian phylogenetic analysis reveals two-domain topology of S-adenosylhomocysteine hydrolase protein sequences, Mol. Phylogenet. Evol. 34 (2005) 15–28.
[6] R. Huber, T.A. Langworthy, H. König, M. Thomm, C.R. Woese, U.B. Sleytr, K.O. Stetter, *Thermotoga maritima* sp. nov. represents a new genus of unique extremely thermophilic eubacteria growing up to 90 °C, Arch. Microbiol. 144 (1986) 324–333.
[7] K.E. Nelson, R.A. Clayton, S.R. Gill, M.L. Gwinn, R.J. Dodson, D.H. Haft, E.K. Hickey, J.D. Peterson, W.C. Nelson, K.A. Ketchum, L. McDonald, T.R. Utterback, J.A. Malek, K.D. Linher, M.M. Garrett, A.M. Stewart, M.D. Cotton, M.S. Pratt, C.A. Phillips, D. Richardson, J. Heidelberg, G.G. Sutton, R.D. Fleischmann, J.A. Eisen, O. White, S.L. Salzberg, H.O. Smith, J.C. Venter, C.M. Fraser, Evidence for lateral gene transfer between Archaea and bacteria from genome sequence of *Thermotoga maritima*, Nature 399 (1999) 323–329.
[8] M.A. Turner, C.S. Yuan, R.T. Borchardt, M.S. Hershfield, G.D. Smith, P.L. Howell, Structure determination of selenomethionyl S-adenosylhomocysteine hydrolase using data at a single wavelength, Nat. Struct. Biol. 5 (1998) 369–376.
[9] Y. Hu, J. Komoto, Y. Huang, T. Gomi, H. Ogawa, Y. Takata, M. Fujioka, F. Takusagawa, Crystal structure of S-adenosylhomocysteine hydrolase from rat liver, Biochemistry 38 (1999) 8323–8333.
[10] M.C.M. Reddy, G. Kuppan, N.D. Shetty, J.L. Owen, T.R. Ioerger, J.C. Sacchettini, Crystal structures of *Mycobacterium tuberculosis* S-adenosyl-L-homocysteine hydrolase in ternary complex with substrate and inhibitors, Protein Sci. 17 (2008) 2134–2144.
[11] T. Manszewski, K. Singh, B. Imiolczyk, M. Jaskolski, An enzyme captured in two conformational states: crystal structure of S-adenosyl-L-homocysteine hydrolase from *Bradyrhizobium elkanii*, Acta Crystallogr. D Biol. Crystallogr. 71 (2015) 2422–2432.
[12] N. Tanaka, M. Nakanishi, Y. Kusakabe, K. Shiraiwa, S. Yabe, Y. Ito, Y. Kitade, K.T. Nakamura, Crystal structure of S-adenosyl-L-homocysteine hydrolase from the human malaria parasite *Plasmodium falciparum*, J. Mol. Biol. 343 (2004) 1007–1017.
[13] K. Brzezinski, Z. Dauter, M. Jaskolski, High-resolution structures of complexes of plant S-adenosyl-L-homocysteine hydrolase (*Lupinus luteus*), Acta Crystallogr. D Biol. Crystallogr. 68 (2012) 218–231.
[14] Y. Kusakabe, M. Ishihara, T. Umeda, D. Kuroda, M. Nakanishi, Y. Kitade, H. Gouda, K.T. Nakamura, N. Tanaka, Structural insights into the reaction mechanism of S-adenosyl-L-homocysteine hydrolase, Sci. Rep. 5 (2015) 16641.
[15] Y. Zheng, C.-C. Chen, T.-P. Ko, X. Xiao, Y. Yang, C.-H. Huang, G. Qian, W. Shao, R.-T. Guo, Crystal structures of S-adenosylhomocysteine hydrolase from the thermophilic bacterium *Thermotoga maritima*, J. Struct. Biol. 190 (2015) 135–142.

[16] A. Guranowski, J. Pawelkiewicz, Adenosylhomocysteinase from yellow lupin seeds. Purification and properties, Eur. J. Biochem. 80 (1977) 517–523.

[17] K. Brzezinski, G. Bujacz, M. Jaskolski, Purification, crystallization and preliminary crystallographic studies of plant S-adenosyl-L-homocysteine hydrolase (*Lupinus luteus*), Acta Crystallograph. Sect. F Struct. Biol. Cryst. Commun. 64 (2008) 671–673.

[18] V. Schultes, R. Jaenicke, Folding intermediates of hyperthermophilic D-glyceraldehyde-3-phosphate dehydrogenase from *Thermotoga maritima* are trapped at low temperature, FEBS Lett. 290 (1991) 235–238.

[19] J. Diruggiero, F.T. Robb, Expression and in vitro assembly of recombinant glutamate dehydrogenase from the hyperthermophilic archaeon *Pyrococcus furiosus*, Appl. Environ. Microbiol. 61 (1995) 159–164.

[20] S. Goda, M. Kojima, Y. Nishikawa, C. Kujo, R. Kawakami, S. Kuramitsu, H. Sakuraba, Y. Hiragi, T. Ohshima, Intersubunit interaction induced by subunit rearrangement is essential for the catalytic activity of the hyperthermophilic glutamate dehydrogenase from *Pyrobaculum islandicum* †, Biochemistry 44 (2005) 15304–15313.

[21] T. Ohshima, Structural characteristics of active and inactive glutamate dehydrogenases from the hyperthermophile *Pyrobaculum islandicum*, Biosci. Biotechnol. Biochem. 76 (2012) 1601–1610.

[22] R.N. Abd Rahman, S. Fujiwara, M. Takagi, S. Kanaya, T. Imanaka, Effect of heat treatment on proper oligomeric structure formation of thermostable glutamate dehydrogenase from a hyperthermophilic archaeon, Biochem. Biophys. Res. Commun. 241 (1997) 646–652.

[23] M.A. Siddiqui, S. Fujiwara, M. Takagi, T. Imanaka, In vitro heat effect on heterooligomeric subunit assembly of thermostable indolepyruvate ferredoxin oxidoreductase, FEBS Lett. 434 (1998) 372–376.

[24] N. Pelletier, G. Leroy, M. Guiral, M.-T. Giudici-Orticoni, C. Aubert, First characterisation of the active oligomer form of sulfur oxygenase reductase from the bacterium *Aquifex aeolicus*, Extremophiles 12 (2008) 205–215.

[25] C.S. Yuan, J. Yeh, S. Liu, R.T. Borchardt, Mechanism of inactivation of S-adenosylhomocysteine hydrolase by (Z)-4',5'-didehydro-5'-deoxy-5'-fluoroadenosine, J. Biol. Chem. 268 (1993) 17030–17037.

[26] Z. Otwinowski, W. Minor, Processing of X-ray diffraction data collected in oscillation mode, Methods Enzymol. 276 (1997) 307–326.

[27] A.J. McCoy, R.W. Grosse-Kunstleve, P.D. Adams, M.D. Winn, L.C. Storoni, R.J. Read, Phaser crystallographic software, J. Appl. Crystallogr. 40 (2007) 658–674.

[28] M.D. Winn, C.C. Ballard, K.D. Cowtan, E.J. Dodson, P. Emsley, P.R. Evans, R.M. Keegan, E.B. Krissinel, A.G.W. Leslie, A. McCoy, S.J. McNicholas, G.N. Murshudov, N.S. Pannu, E.A. Potterton, H.R. Powell, R.J. Read, A. Vagin, K.S. Wilson, Overview of the CCP4 suite and current developments, Acta Crystallogr. D Biol. Crystallogr. 67 (2011) 235–242.

[29] X. Yang, Y. Hu, D.H. Yin, M.A. Turner, M. Wang, R.T. Borchardt, P.L. Howell, K. Kuczera, R.L. Schowen, Catalytic strategy of S-adenosyl-L-homocysteine hydrolase: transition-state stabilization and the avoidance of abortive reactions, Biochemistry 42 (2003) 1900–1909.

[30] G. Langer, S.X. Cohen, V.S. Lamzin, A. Perrakis, Automated macromolecular model building for X-ray crystallography using ARP/wARP version 7, Nat. Protoc. 3 (2008) 1171–1179.

[31] G.N. Murshudov, P. Skubák, A.A. Lebedev, N.S. Pannu, R.A. Steiner, R.A. Nicholls, M.D. Winn, F. Long, A.A. Vagin, REFMAC 5 for the refinement of macromolecular crystal structures, Acta Crystallogr. D Biol. Crystallogr. 67 (2011) 355–367.

[32] M.D. Winn, M.N. Isupov, G.N. Murshudov, Use of TLS parameters to model anisotropic displacements in macromolecular refinement, Acta Crystallogr. D Biol. Crystallogr. 57 (2001) 122–133.

[33] J. Painter, E.A. Merritt, TLSMD web server for the generation of multi-group TLS models, J. Appl. Crystallogr. 39 (2006) 109–111.

[34] O.S. Smart, T.O. Womack, A. Sharff, C. Flensburg, P. Keller, W. Paciorek, C. Vonrhein, G. Bricogne, grade, version 1.1.02, 2011. http://www.globalphasing.com.

[35] P. Emsley, B. Lohkamp, W.G. Scott, K. Cowtan, Features and development of Coot, Acta Crystallogr. D Biol. Crystallogr. 66 (2010) 486–501.

[36] H. Berman, K. Henrick, H. Nakamura, Announcing the worldwide protein data bank, Nat. Struct. Biol. 10 (2003) 980-980.

[37] E. Krissinel, K. Henrick, Secondary-structure matching (SSM), a new tool for fast protein structure alignment in three dimensions, Acta Crystallogr. D Biol. Crystallogr. 60 (2004) 2256–2268.

[38] T.A.P. de Beer, K. Berka, J.M. Thornton, R.A. Laskowski, PDBsum additions, Nucleic Acids Res. 42 (2014) D292–296.

[39] L.L.C. Schrödinger, The PyMOL Molecular Graphics System, Version 1.8, 2015.

[40] P.D. Adams, P.V. Afonine, G. Bunkóczi, V.B. Chen, I.W. Davis, N. Echols, J.J. Headd, L.-W. Hung, G.J. Kapral, R.W. Grosse-Kunstleve, A.J. McCoy, N.W. Moriarty, R. Oeffner, R.J. Read, D.C. Richardson, J.S. Richardson, T.C. Terwilliger, P.H. Zwart, *PHENIX*: a comprehensive Python-based system for macromolecular structure solution, Acta Crystallogr. D Biol. Crystallogr. 66 (2010) 213–221.

[41] S. Hayward, H.J.C. Berendsen, Systematic analysis of domain motions in proteins from conformational change: new results on citrate synthase and T4 lysozyme, Proteins Struct. Funct. Genet. 30 (1998) 144–154.

[42] E. Krissinel, K. Henrick, Inference of macromolecular assemblies from crystalline state, J. Mol. Biol. 372 (2007) 774–797.

[43] T. Manszewski, K. Szpotkowski, M. Jaskolski, Crystallographic and SAXS studies on S-adenosyl-L-homocysteine hydrolase from *Bradyrhizobium elkanii*, IUCrJ 4 (2017) 271–282.

[44] J.L. Palmer, R.H. Abeles, The mechanism of action of S-adenosylhomocysteinase, J. Biol. Chem. 254 (1979) 1217–1226.

[45] J. Komoto, Y. Huang, T. Gomi, H. Ogawa, Y. Takata, M. Fujioka, F. Takusagawa, Effects of site-directed mutagenesis on structure and function of recombinant rat liver S-adenosylhomocysteine hydrolase. Crystal structure of D244E mutant enzyme, J. Biol. Chem. 275 (2000) 32147–32156.

[46] Y. Takata, T. Yamada, Y. Huang, J. Komoto, T. Gomi, H. Ogawa, M. Fujioka, F. Takusagawa, Catalytic mechanism of S-adenosylhomocysteine hydrolase. site-directed mutagenesis of asp-130, Lys-185 Asp-189, and Asn-190, J. Biol. Chem. 277 (2002) 22670–22676.

[47] R. Meijers, R.J. Morris, H.W. Adolph, A. Merli, V.S. Lamzin, E.S. Cedergren-Zeppezauer, On the enzymatic activation of NADH, J. Biol. Chem. 276 (2001) 9316–9321.

[48] J.D. Lozada-Ramírez, A. Sánchez-Ferrer, F. García-Carmona, Recombinant S-Adenosylhomocysteine hydrolase from *Thermotoga maritima*: cloning, overexpression, characterization, and thermal purification studies, Appl. Biochem. Biotechnol. 170 (2013) 639–653.

[49] G. Qian, C. Chen, R. Zhou, Y. He, W. Shao, A thermostable S-adenosylhomocysteine hydrolase from Thermotoga maritima: Properties and its application on S-adenosylhomocysteine production with enzymatic cofactor regeneration, Enzyme Microb. Technol. 64-65 (2014) 33–37.

Electronic Supplementary Information for

S-adenosyl-L-homocysteine hydrolase from a hyperthermophile (*Thermotoga maritima*) is expressed in *Escherichia coli* in inactive form – Biochemical and structural studies

Krzysztof Brzezinski[a,*], Justyna Czyrko[a], Joanna Sliwiak[b], Edyta Nalewajko-Sieliwoniuk[a], Mariusz Jaskolski [b,c], Boguslaw Nocek[d], Zbigniew Dauter[e]

[a] Institute of Chemistry, University of Bialystok, Ciolkowskiego 1K, 15-245 Bialystok, Poland

[b] Center for Biocrystallographic Research, Institute of Bioorganic Chemistry, Polish Academy of Sciences, Noskowskiego 12/14, 61-704 Poznan, Poland

[c] Department of Crystallography, Faculty of Chemistry, A. Mickiewicz University, Umultowska 89b, 61-614 Poznan, Poland

[d] Structural Biology Center, Biosciences Division, Argonne National Laboratory, Argonne, IL 60439, USA

[e] Synchrotron Radiation Research Section, MCL, National Cancer Institute, Argonne National Laboratory, Argonne, IL 60439, USA

*To whom correspondence should be addressed,
email: k.brzezinski@uwb.edu.pl
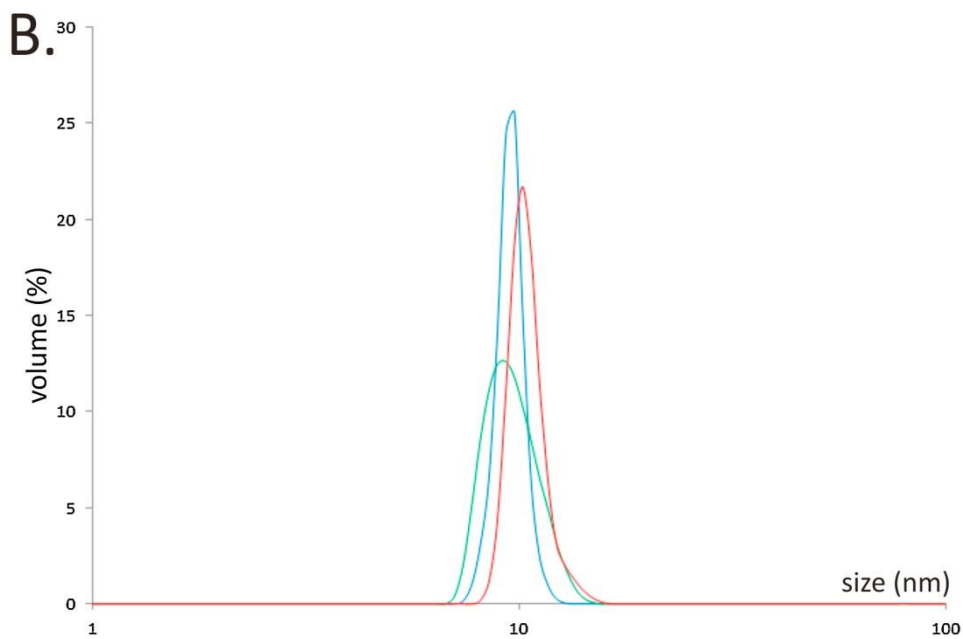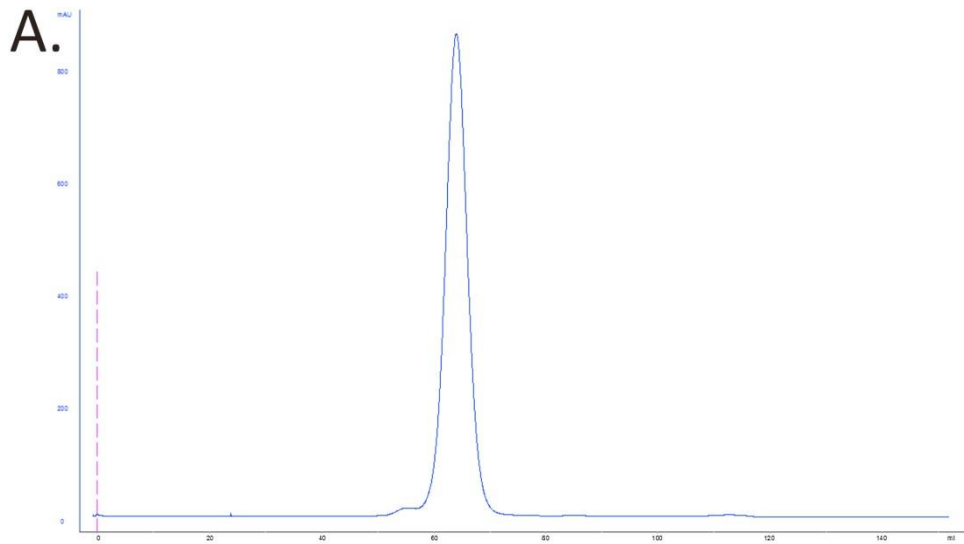
Fig. S1. (A) Size-exclusion chromatographic separation of iTmSAHase shows a distinct peak corresponding to a homotetrameric protein with a molecular mass of about 180 kDa. (B) Dynamic light scattering (DLS) curves presented as particle size (nm) distribution by volume for: (i) unheated protein sample measured at 298 K (blue line), (ii) protein sample heated at 358 K for 30 min and then measured at 298 K (green), and (iii) protein sample heated at 358 K for 30 min and then measured at 358 K (red).

SCIENTIFIC REPORTS

OPEN

Metal-cation regulation of enzyme dynamics is a key factor influencing the activity of *S*-adenosyl-L-homocysteine hydrolase from *Pseudomonas aeruginosa*

Justyna Czyrko[1], Joanna Sliwiak[2], Barbara Imiolczyk[2], Zofia Gdaniec[3], Mariusz Jaskolski[2,4] & Krzysztof Brzezinski [ID][1]

S-adenosyl-L-homocysteine hydrolase from *Pseudomonas aeruginosa* (PaSAHase) coordinates one K^+ ion and one Zn^{2+} ion in the substrate binding area. The cations affect the enzymatic activity and substrate binding but the molecular mechanisms of their action are unknown. Enzymatic and isothermal titration calorimetry studies demonstrated that the K^+ ions stimulate the highest activity and strongest ligand binding in comparison to other alkali cations, while the Zn^{2+} ions inhibit the enzyme activity. PaSAHase was crystallized in the presence of adenine nucleosides and K^+ or Rb^+ ions. The crystal structures show that the alkali ion is coordinated in close proximity of the purine ring and a ^{23}Na NMR study showed that the monovalent cation coordination site is formed upon ligand binding. The cation, bound in the area of a molecular hinge, orders and accurately positions the amide group of Q65 residue to allow its interaction with the ligand. Moreover, binding of potassium is required to enable unique dynamic properties of the enzyme that ensure its maximum catalytic activity. The Zn^{2+} ion is bound in the area of a molecular gate that regulates access to the active site. Zn^{2+} coordination switches the gate to a shut state and arrests the enzyme in its closed, inactive conformation.

S-adenosyl-L-methionine (SAM) is a ubiquitous methyl group donor in methylation reactions of a wide range of acceptors including small and macromolecules[1]. The SAM-dependent reactions generate equimolar amounts of *S*-adenosyl-L-homocysteine (SAH), which is a strong inhibitor of SAM-dependent methyltransferases and needs to be removed to keep the metabolic processes going. By hydrolyzing SAH to adenosine (Ado) and L-homocysteine (Hcy), the enzyme SAHase (SAH hydrolase) serves as an important regulator of SAM-dependent methylation through the control of the SAM:SAH ratio, and is an indicator of the biological methylation activity of the cell[2–4]. SAHase inhibition or dysfunction leads to the accumulation of SAH in the cell and arrest of all crucial SAM-dependent processes. Apart from SAH hydrolysis, which is catalyzed in both directions, the enzyme also splits 2′-deoxyadenosine, which is an irreversible inhibitor of SAHases[5]. SAHase inactivation by 2′-deoxyadenosine proceeds *via* the formation of an unstable 3′-keto-2′-deoxyadenosine in an NAD^+-dependent process that is very similar to the first step of the main SAH breakdown reaction. The subsequent and sponta-neous cleavage of the N-glycosidic bond leads to the elimination of a modified sugar moiety, while the adenine molecule stays bound in the active site of the enzyme[6]. The reduced cofactor (NADH) is not regenerated in the 2-deoxyadenosine reaction, stalling the enzyme in the inactive form.

SAHases are usually active as homotetramers[7–15]. The protomer has a three-domain fold, with two promi-nent domains, the substrate- and cofactor-binding domains, separated by a deep crevice. A small C-terminal dimerization domain locks two subunits into a homodimer by quaternary complementation of the cofactor

[1]Laboratory of Biochemistry and Structural Biology, Institute of Chemistry, University of Bialystok, Bialystok, Poland. [2]Center for Biocrystallographic Research, Institute of Bioorganic Chemistry, Polish Academy of Sciences, Poznan, Poland. [3]Laboratory of Biomolecular NMR, Institute of Bioorganic Chemistry, Polish Academy of Sciences, Poznan, Poland. [4]Department of Crystallography, Faculty of Chemistry, A. Mickiewicz University, Poznan, Poland. Correspondence and requests for materials should be addressed to K.B. (email: k.brzezinski@uwb.edu.pl)

binding site, where a tightly but non-covalently bound nicotinamide adenine dinucleotide (NAD$^+$) is found in its oxidized form. During the catalytic SAHase cycle, the cofactor is first reduced upon abstraction of a hydride anion from the C3′ atom of the sugar moiety. To complete the cycle, the NAD$^+$ cofactor is regenerated through Michael-type addition of a water molecule[16]. The latter step is not part of the irreversible inactivation of the enzyme by 2′-deoxyadenosine, in which case the cofactor is trapped in its non-reactive, reduced state[5,6]. The enzyme undergoes a significant open-closed conformational transformation upon substrate or inhibitor binding. A comparison of the enzyme conformation in the open and in the closed forms reveals that the interdomain crevice is constricted upon substrate or inhibitor binding. The accessibility of the active site from the solvent region is regulated by a molecular gate formed by a conserved pair of His-Phe residues[6,10,11]. Depending on the conformational state of the gate, the channel leading to the active site can be open or shut. The structures of SAHases from various species were determined mainly for the enzymes in the closed conformation, in the presence of adenosine (Ado) or its analogs. In most of those structures, various monovalent cations were found in a coordinating loop located in close proximity of the substrate binding site. However, the ions do not interact with the ligand directly. The type of the coordinated ion strongly depends on the crystallization conditions, which included NH$_4^+$, Na$^+$ or K$^+$ cations. Only a few SAHase structures correspond to the open form[8,11], which is correlated with the absence of an active-site ligand, as well as of a monovalent cation in the substrate binding region. This suggests that the cation is coordinated upon a conformational transformation of the enzyme during the catalytic cycle. However, it is still unclear which monovalent cation is utilized by the enzyme under physiological conditions and what role it serves in the catalytic process. Additionally, it has been suggested that SAHase activity could be regulated by some divalent cations, e.g., copper[17]. However, so far none of the previously determined SAHase structures contained any metal cations other than the monovalent ones[6,7,9–11,14,15,18,19].

Pseudomonas aeruginosa has natural resistance to many antibiotics and disinfectants and is responsible for numerous infections. Therefore, defining new molecular targets for the treatment of *P. aeruginosa* infections is of high medical priority. The purpose of the present study has been to define the catalytic role of the monovalent cations and to explain the molecular mechanism of *P. aeruginosa* SAHase (PaSAHase) inhibition by zinc ions. By combining X-ray crystallography with enzyme kinetics and ITC studies, as well as with ^{23}Na NMR spectroscopy, we were able to elucidate the effect of the monovalent cations on ligand binding, and to explain that the enzyme is most efficient in the presence of potassium. Also, we confirmed the presence of zinc ions by X-ray fluorescence and explained how Zn^{2+} binding blocks a molecular gate, leading to a complete inhibition of enzymatic activity.

Results

Overall structure of PaSAHase.
We present four crystal structures of PaSAHase/ligand/ion(s) complexes at resolutions of 1.35 to 1.75 Å (Supplementary Information Table S1). Two complexes of Zn^{2+}-containing PaSAHase were crystallized in the presence of K$^+$ ions and adenosine (Ado/K$^+$/Zn^{2+}), or an inhibitor, 2′-deoxyadenosine (2′-dAdo/K$^+$Zn^{2+}). Additionally, the latter ligand as well as 3′-deoxyadenosine (non-metabolized adenosine analog) were used for crystallization of zinc-free enzyme in the presence of Rb$^+$ (2′-dAdo/Rb$^+$) or K$^+$ (3′-dAdo/K$^+$) cations. In the Zn^{2+}-containing complexes, the divalent cation site is not fully occupied. Despite the very low activity of the enzyme in the presence of Zn^{2+} cations, 2′-deoxyadenosine undergoes catalytic cleavage at the N-glycosidic bond during incubation with the enzyme or during crystallization[6]. Therefore, only adenine is found in the active site of PaSAHase crystallized in the presence of 2′-deoxyadenosine and K$^+$ or Rb$^+$ cations. It is of note, that the absence of sugar moiety does not change the spatial arrangement of the active site when compared to the complexes with nucleosides. This results from the presence of a phosphate anion from a crystallization buffer, which mimics the positions of the oxygen atoms of the ribose moiety. A similar effect was noted previously[6,19], when four water molecules, superposable with the oxygen atoms of the sugar moiety, were observed close to the adenine molecule. The four water molecules, as well as the phosphate anion are involved in a hydrogen bond network that is very similar to that observed in nucleoside complexes. The presence of water molecules or a phosphate ion depends only on the crystallization conditions. Thus, the anion is not required for adenine binding and to stabilize the closed conformation of the protein. Moreover, the molecule that binds directly to the enzyme is 2′-deoxyadenosine, which is then slowly decomposed to adenine and a sugar moiety[5]. It should be noted that SAHase enzymatic activity assays are carried out in phosphate buffer, as this anion has no inhibitory effect on SAHase activity[20–22].

The binding modes of adenine and its nucleosides in the active site of PaSAHase are similar to those observed in other SAHase models of various origin[6,7,9–11,14,15,18,19,23,24], as shown in Fig. 1a–d. The polar interactions in the active site of the enzyme in all four complexes are presented in Supplementary Information (Table S2). It is of note that in the presented PaSAHase complexes, adenine or its nucleosides are trapped in the active site, as the H323-F324 molecular gate is shut (Fig. 1e).

PaSAHase forms a homotetramer in solution. The complexes crystallize in two different forms, either as a tetramer or as a dimer from which the complete homotetramer is generated by crystallographic symmetry. All the tetramers are very similar, with r.m.s. deviations of their Cα superpositions ranging from 0.08–0.35 Å. A multiple sequence alignment of amino acid sequences of different SAHases (Fig. 2a) reveals a lineage-specific insertion segments in PaSAHase, located in the substrate (inserted residues 414–419) and cofactor (inserted residues 270–280 and 353–359) binding domains on the surface of the enzyme (Fig. 2b,c).

The monovalent cation near the active site of PaSAHase.
In all presented PaSAHase complexes, the four subunits exist in the closed conformation and each of them binds an adenine nucleoside or adenine, as well as an alkali metal cation, K$^+$ or Rb$^+$, in the substrate binding area (Fig. 3a). The K$^+$/Rb$^+$ cations are bound in the monovalent cation coordinating loop (T380-S384) in close proximity of the purine ring of the ligand, but they do not interact with the ligand directly. Additionally, using anomalous dispersion, one non-specific Rb$^+$ site per PaSAHase tetramer was found as a crystallization artifact in the rubidium complex. The metal coordination
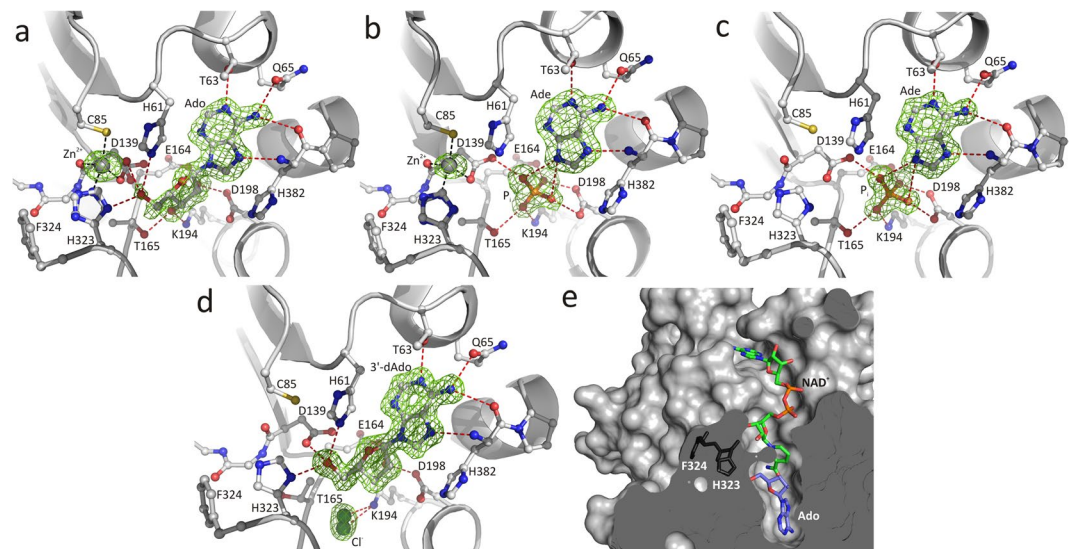
Figure 1. The mode of ligand binding in the substrate binding site of PaSAHase crystallized in the presence of: (**a**) adenosine, K$^+$ and Zn^{2+} ions; (**b**) 2′-deoxyadenosine, K$^+$ and Zn^{2+} ions; (**c**) 2′-deoxyadenosine and Rb$^+$ ions; (**d**) 3′-deoxyadenosine and K$^+$ ions. Possible hydrogen (red) and coordination (black) bonds are indicated by dash lines. Zn^{2+} and Cl$^-$ ions are represented by gray and green spheres, respectively. The mF_o-DF_c difference electron density OMIT maps are contoured at 3.0σ. (**e**) The accessibility of the active site from the solvent region depends on the state of the molecular gate formed by H323-F324. In all four complexes (here illustrated by subunit A of the Ado/K$^+$/Zn^{2+} complex) the channel is shut and the ligand molecule is trapped in the substrate-binding site.

loop is part of one of the two hinge regions linking the substrate- and cofactor-domains that are involved in substrate-induced domain movements[8,23,24]. The coordination sphere of the K$^+$/Rb$^+$ cations is a slightly distorted pentagonal bipyramid (Supplementary Information Table S3) formed by two main-chain carbonyl oxygen atoms (T380 and H382) and the side-chain oxygen atoms of T380 and a highly conserved Q65 residue involved in ligand binding. Three water molecules complete the coordination sphere. A very similar coordination geometry of the K$^+$ cation was observed in the crystal structure of SAHase from *Brucella melitensis* (PDB ID: 3N58, unpublished). Other SAHase models deposited in the PDB bind NH$_4^+$ or Na$^+$ cations at this position. Moreover, in numerous PDB models this position is marked as a water molecule, while in fact it is an alkali metal cation, most likely Na$^+$, coordinated by at least five oxygen atoms. Despite the presence of different monovalent cations, the conformation of the coordinating loop and of the Q65 residue is not affected to any significant degree; likewise, the position of the ligand molecule is very similar in all analyzed models (Fig. 3b). The presence of cations other than potassium is usually reflected in a different arrangement of the coordination sphere (Supplementary Information Table S4). Most importantly, the amide oxygen of the highly conserved Q65 residue interacts with NH$_4^+$ or Na$^+$ ions indirectly, *via* a water molecule[6,10,11], with one notable exception (PDB ID: 5M5K) where the glutamine side chain is involved in direct sodium coordination[19].

Effect of monovalent cations on PaSAHase activity. The crystal structures of SAHases available so far contain NH$_4^+$, Na$^+$ or K$^+$ ions near the substrate binding site, depending on the composition of the purification and crystallization media. The obvious candidate for the monovalent cation involved in the enzymatic activity of SAHase under physiological conditions is potassium, which is the major cation of all living cells and is also a common metal cation bound to cellular proteins[25]. Within this project, enzyme kinetics and isothermal titration calorimetry (ITC) studies were conducted in the presence or absence of alkali cations to investigate their influence on the enzymatic activity and ligand binding of PaSAHase. (Tables 1, 2 and Fig. 4). In the kinetic experiments, the highest activity was observed in the presence of K$^+$ cations. The catalytic rate (k_{cat}) of the reaction in the presence of K$^+$ is 0.575 ± 0.009 s^{-1} and is 2–11 times higher when compared to the rates measured in the presence of other alkali ions or without them. In the case of Rb$^+$, the drop of k_{cat} is almost 33-fold. Moreover, for most of the reactions, the substrate affinity (K_M) is 3–12 times higher in the presence of potassium. The notable exception is the reaction in the presence of Rb$^+$, where the measured substrate affinity is slightly higher than for potassium. Finally, the catalytic proficiency index k_{cat}/K_m is one to over two orders of magnitude higher in the presence of potassium than for other ions. These findings clearly demonstrate that the enzyme attains its maximum catalytic activity when the K$^+$ cation is bound. On the other hand, Rb$^+$ acts as noncompetitive inhibitor.

Also the ITC experiments indicate the importance of K$^+$ cations for ligand (adenosine) binding. During the titrations conducted in the absence of any alkali metals or the presence of Li$^+$ ions, the heat effect was immeasurably small. For the experiments conducted in the presence of Na$^+$, K$^+$, Rb$^+$ and Cs$^+$ ions, the stoichiometry of adenosine binding to the enzyme is one ligand molecule per subunit. The optimal cation for PaSAHase-Ado binding is K$^+$, as the ligand binding is mostly enthalpy driven and the binding constant K$_d$ of 1.2 ± 0.2 μM is the lowest in the presence of potassium. Adenosine binding is only slightly weaker in the presence of Rb$^+$. However,
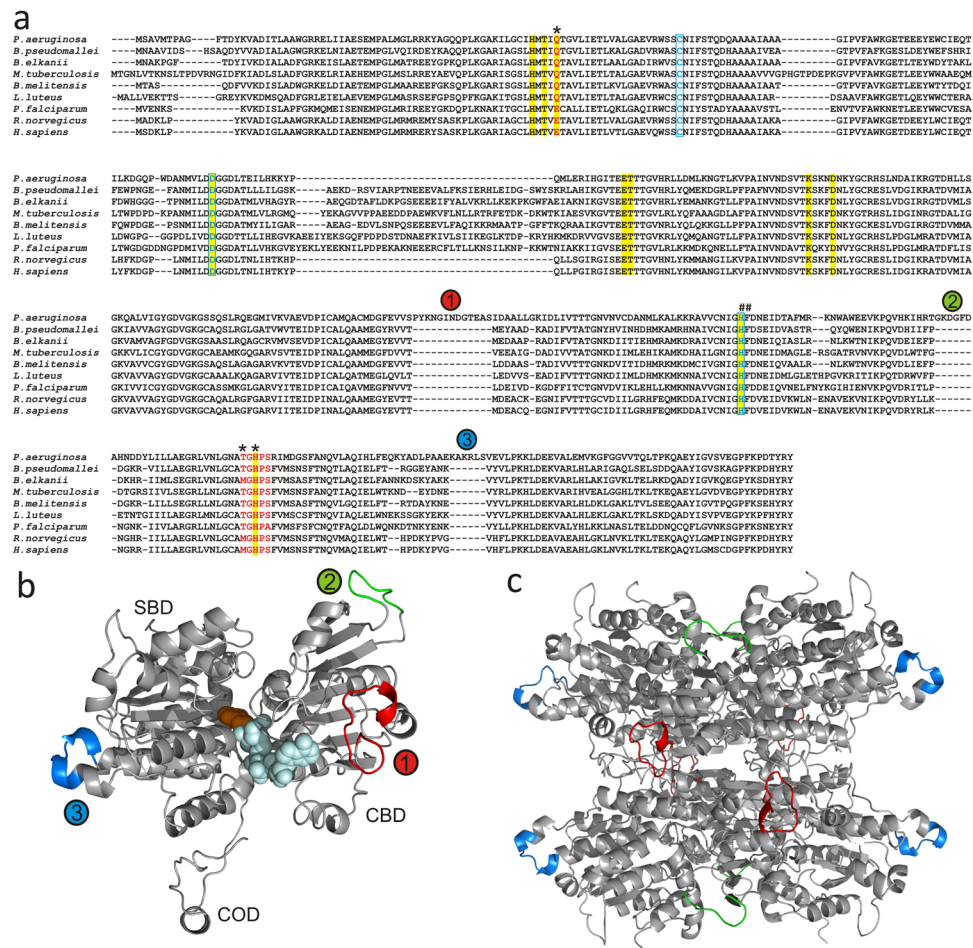
Figure 2. (**a**) Multiple sequence alignment of selected SAHases. Amino acid residues marked in red are in the monovalent ion binding region and the asterisks indicate residues directly involved in metal coordination. A tandem of His-Phe residues (marked with #) form a molecular gate that regulates the accessibility of the active site from the solvent region. Residues involved in substrate binding are highlighted in yellow. Residues involved in the coordination of Zn^{2+} ions are marked in blue and boxed. Circled numbers relate to lineage-specific insertions located in the cofactor- (1,2) and substrate-binding (3) domains of PaSAHase. (**b,c**) Overall structure of PaSAHase. (**b**) The structure of PaSAHase subunit with color-coded specific insertions located in the cofactor-binding domain (CBD), residues 270–280 (1) and 353–359 (2) shown in red and green, respectively, and in the substrate binding domain (SBD), residues 414–419 (3) shown in blue; COD is small C-terminal oligomerization domain. The NAD^+ cofactor (pale blue) and adenosine (orange) are in space-filling representation. (**c**) A ribbon diagram of the active tetrameric form of PaSAHase, with the insertions marked by color as in (**b**).

the use of Na^+ or Cs^+ cations resulted in a significant decrease of binding specificity and increase of entropy contribution (Table 2).

Formation of the monovalent cation binding site. The majority of the crystallographic models of SAHases in the PDB present the enzyme in the closed conformation with a ligand and a monovalent cation bound in the substrate binding region. A few structures present a situation where one or all four subunits of the tetrameric enzyme do not bind a ligand and, therefore, adopt the open conformation[8,11]. In one case, a subunit does contain a ligand (3′-deoxyadenosine) but is found in a semi-open conformation, intermediate between the open and closed states[19]. Those models were derived from crystals that were grown in the presence of NH_4^+, Na^+ or K^+ cations. Inspection of the subunits that are in the open conformation reveals that there is no monovalent cation bound near the substrate binding site, although the metal coordination loop has the same conformation as in the subunits with the closed conformation (Fig. 3c). Also, a very similar loop conformation is observed for the subunit in the semi-open state, however, an undifferentiated water molecule/ammonium ion is located in the position of the monovalent cation. The major structural difference between the closed/semi-open and open states concerns the conformation of Q65 (PaSAHase numbering). In the open state this residue is located far away from the metal binding loop and its side chain is disordered in at least two conformations. Thus, the crystallographic models suggest that the coordination of the monovalent cation does not occur until
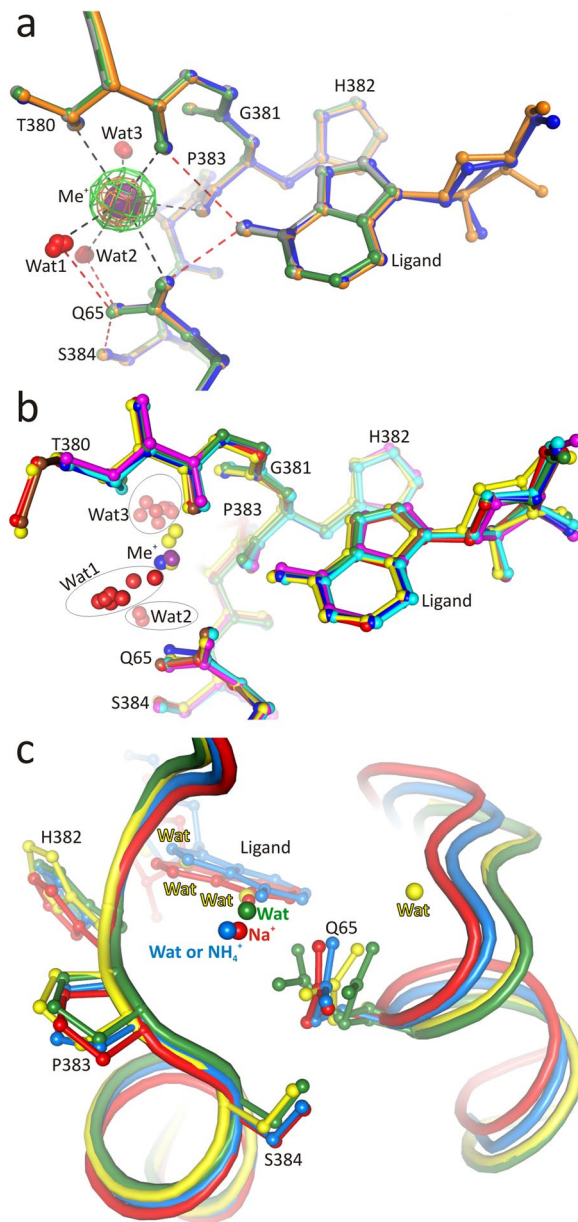
Figure 3. Superpositions of the monovalent cation coordination site and the ligand bound in the substrate binding site of SAHase models. (**a**) Superposition of PaSAHase complex models, Ado/K$^+$/Zn^{2+} (orange), 2′-dAdo/K$^+$/Zn^{2+} (gray), 3′-dAdo/K$^+$ (blue), and 2′-dAdo/Rb$^+$ (green). The red and purple spheres indicate water molecules and monovalent cations, respectively. The difference mF_o-DF_c OMIT map (green) for the potassium cation (Ado/K$^+$/Zn^{2+}) and anomalous difference map for the Rb$^+$ cation (orange) are contoured at 3.0σ and 25.0σ, respectively. Possible coordination (black) and hydrogen (red) bonds are indicated by dash lines. (**b**) Superposition of the monovalent cation coordination region of PaSAHase (cyan) with models of the enzymes from *Homo sapiens* (yellow, PDB entry 1LI4), *Plasmodium falciparum* (blue, 1V8B), *Brucella melitensis* (magenta, 3N58), *Lupinus luteus* (green, 3OND), *Bradyrhizobium elkanii* complexed with Na$^+$ (red, 5M5K), and NH$_4^+$ (brown, 4LVC). The Cα superpositions are based on chains A of the models. Potassium (purple), sodium (yellow) and ammonium (blue) cations, as well as water molecules (red) are represented as spheres. Three water clusters, which correspond to three (Wat1-Wat3) water molecules involved in potassium coordination, are encircled. (**c**) Superposition of the monovalent cation coordination region of the enzyme in the closed conformation (red, *B. elkanii*, PDB entry 5M5K, chain A) with models of the enzyme in semi-open conformation (blue, *B. elkanii*, 5M5K, chain D) and open conformation (green, *B. elkanii*, 4LVC, chain D; and yellow, *B. melitensis*, 3N58, chain B). Sodium and ammonium ions, as well as water molecules are represented by spheres. Residue numbers correspond to PaSAHase sequence.

a conformational transformation upon ligand binding in the active site has taken place. This postulate was confirmed by two other experiments. (i) No effect other than K$^+$ dilution heat was observed during the isothermal

Enzyme/ Alkali cation	V_{max} [μM·s^{-1}]	k_{cat} [s^{-1}]	K_M [μM]	k_{cat}/K_M [M^{-1}·s^{-1}]
WT/none	$(16.9\pm0.9).10^{-3}$	$(52.9\pm3.0).10^{-3}$	101.1 ± 9.9	523 ± 81
WT/Li$^+$	$(14.9\pm1.1).10^{-3}$	$(46.6\pm3.3).10^{-3}$	63.8 ± 8.0	731 ± 143
WT/Na$^+$	$(76.0\pm2.6).10^{-3}$	$(237.3\pm8.0).10^{-3}$	28.0 ± 2.2	8467 ± 940
WT/K$^+$	$(184.0\pm2.1).10^{-3}$	$(575.0\pm9.0).10^{-3}$	7.9 ± 0.4	72502 ± 4858
WT/Rb$^+$	$(5.6\pm0.1).10^{-3}$	$(17.5\pm0.3).10^{-3}$	4.9 ± 0.3	3568 ± 237
WT/Cs$^+$	$(68.2\pm1.1).10^{-3}$	$(213.1\pm3.4).10^{-3}$	32.0 ± 1.1	6668 ± 333
Q65A/K$^+$	$(44.7\pm1.5).10^{-3}$	$(140.0\pm4.7).10^{-3}$	26.2 ± 2.6	5322 ± 358

Table 1. Kinetic parameters characterizing the enzymatic activity of wild type (WT) and Q65A PaSAHase in the absence or presence of alkali metal cations. The values were obtained as averages of two replicates, $\pm$ represents standard error of the mean (SEM) values.

Parameter	WT/Na$^+$	WT/K$^+$	WT/Rb$^+$	WT/Cs$^+$	Q65A/K$^+$
N	0.97 ± 0.02	0.80 ± 0.01	0.84 ± 0.01	0.94 ± 0.02	0.236 ± 0.004
K_d [μM]	8.8 ± 1.0	1.2 ± 0.2	1.8 ± 0.2	4.7 ± 0.6	7.3 ± 0.4
ΔH [cal/mol]	-3891 ± 114	-9665 ± 237	-8935 ± 137	-4174 ± 115	-7447 ± 167
ΔS [cal/mol/°]	9.8	-5.9	-4.2	10.1	2.0

Table 2. Thermodynamic parameters obtained from ITC titrations of wild type (WT) and Q65A PaSAHase with adenosine in the presence of monovalent cations. The parameters obtained from sigmoidal curve fitting are given with $\pm$ standard deviations as follows: stoichiometry (N), dissociation constant (K_d), changes in enthalpy (ΔH) and entropy (ΔS).

titration of a ligand- and alkali-metal-free PaSAHase with K$^+$ ions. This result suggests that the cation does not bind specifically to the enzyme in its open (i.e., ligand-free) conformation. (ii) In ^{23}Na NMR spectra recorded for either adenosine or PaSAHase in the presence of 5 mM NaCl, only one peak is observed with a chemical shift as for NaCl itself (Supplementary Information Fig. S1a). This shows that, in general, the environment of the sodium nuclei is the same in all three samples. The NMR results are in agreement with the isothermal titration data and confirm that monovalent cations (at least Na$^+$) do not bind specifically to the open form of the protein. The observed broadening of the ^{23}Na resonance in the sample containing PaSAHase indicates that non-specific Na$^+$-protein interactions cannot be excluded. The situation is changed when the spectra are recorded for samples containing both the enzyme and the adenosine ligand in the presence of Na$^+$ ions. In this scenario, PaSAHase should adopt the closed conformation enforced by adenosine binding, allowing the cation to be coordinated near the ligand, as indicated by the crystallographic results. In agreement with this scenario, a small but meaningful shift is observed in the ^{23}Na NMR spectrum of PaSAHase/adenosine/^{23}Na$^+$. This effect increases with a decrease of the Na$^+$:PaSAHase ratio (Supplementary Information Fig. S1b) owing to the increased proportion of protein-coordinated Na$^+$ ions in the sample and a concomitant contribution of the bound form to the position of the ^{23}Na signal, which is the weighted average of two signals in fast exchange, derived from the nuclei of protein-coordinated and unbound/hydrated Na$^+$ ions.

In view of all the above observations, the emerging course of events is that the K$^+$ ion coordination site is formed only upon ligand binding, when the enzyme changes its conformation from the open to the closed state. This site is composed of the highly conserved Q65 residue as well as of the loop region T380-S384 that links the substrate- and cofactor-binding domains, with T380 and H382 involved in direct cation coordination. Interestingly, the conformation of the loop does not change significantly during this transformation (Fig. 3c). The situation at the Q65 residue is drastically different. In the open form of the enzyme, the Q65 residue is far from the loop region and its side chain is disordered. Upon ligand binding, Q65 moves close to the coordination loop as the result of the movement of the substrate-binding domain towards the cofactor-binding domain, so that its side chain can directly coordinate the potassium cation. In addition, metal coordination stabilizes and orders the side chain of Q65. With the Oε atom coordinated to the metal cation, the amide group of Q65 is now adequately oriented for the formation of an Oε…N hydrogen bond with the exoamino group of the adenine moiety of the ligand. The importance of Q65 in ligand binding and enzymatic activity of PaSAHase is reflected in our mutagenesis study. In the presence of K$^+$ ions, the Q65A mutant is over four times less active and the K_M value increases over three times compared to the wild type enzyme. The catalytic proficiency index k_{cat}/K_m is over one order of magnitude lower. ITC titrations also confirmed the importance of the Q65 residue for the catalytic cycle. During the titrations of the Q65A mutant with adenosine in the presence of K$^+$, the stoichiometry of adenosine binding to the enzyme is ~0.25, indicating that, on average, three substrate binding sites of the tetramer remain empty. Finally, more than six-fold drop of adenosine affinity is observed in comparison to native PaSAHase. The kinetic and thermodynamic measurements are presented in Fig. 4 and in Tables 1 and 2.

The highly conserved glutamine residue and its rare substitutions. Phylogenetic analyses of SAHase sequences indicate that the enzymes diverged into two major groups during their evolution[26]. The first group comprises enzymes from bacterial and eukaryotic organisms while the second is formed by archaeal
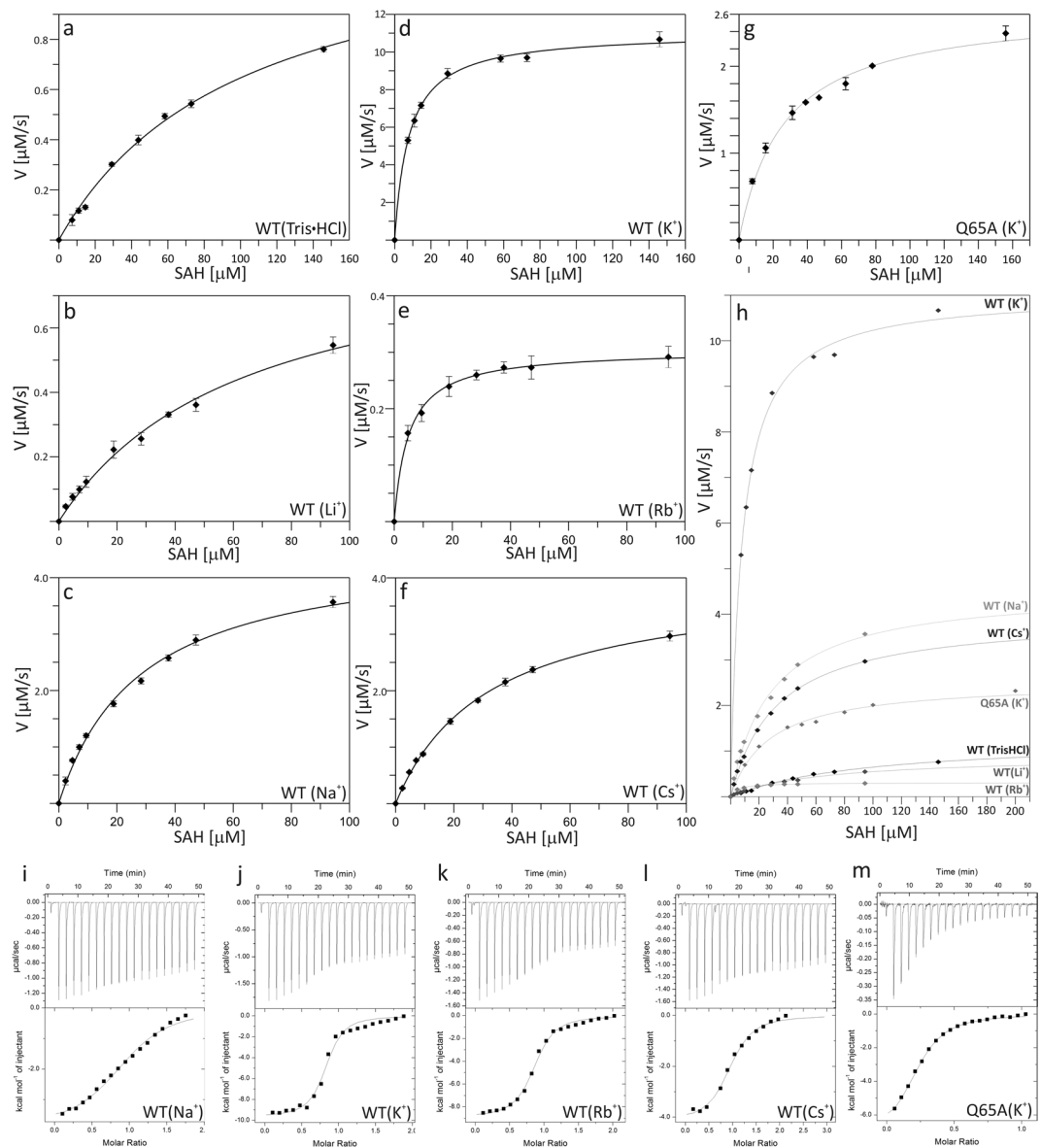
Figure 4. Influence of monovalent cation type and Q65A mutation on enzyme activity and ligand binding. Kinetic analysis of wild-type PaSAHase (**a**–**f**) and its Q65A mutant (**g**) were conducted in the presence of 100 mM Tris·HCl (**a**), Li$^+$ (**b**), Na$^+$ (**c**), K$^+$ (d and g), Rb$^+$ (**e**) or Cs$^+$ (**f**) cations. The activity was determined using variable concentrations of S-adenosyl-ʟ-homocysteine (SAH). In panel (h) all the kinetic curves are presented on common scale to emphasize the differences in enzymatic activities. Calorimetric titrations of PaSAHase with adenosine were conducted in the presence of 100 mM alkali cations: Na$^+$ (**i**), K$^+$ (**j**), Rb$^+$ (**k**), and Cs$^+$ (**l**) and its Q65A mutant in the presence of K$^+$ ions (m). The top plot of each panel represents the raw heat data obtained from consecutive injections of adenosine into the sample cell containing the protein. The heat peak areas have been plotted against the molar ratio of adenosine added to the enzyme, creating the binding isotherm at the bottom of each panel. The best fit of the model of one set of binding sites is represented by the solid line. All titrations were performed at 293 K.

SAHases. The consequences of this divergent evolution are also visible at the structural level. In particular, the mode of adenine ring binding in the substrate domain is different in SAHases from different species. The Q65 residue is highly conserved among bacterial and eukaryotic sequences (Fig. 2a). Phylogenetic analyses suggest that the primordial residue that interacted with the adenine amine group was indeed glutamine. Among eukaryotic SAHases, only in mammalian (e.g., human) and some protozoan (e.g., the pathogenic strains of *Plasmodium*, *Cryptosporidium*, *Theileria* and *Naegleria*) enzymes this glutamine residue is substituted by glutamate. It is of note that these protozoan pathogens are obligate intracellular parasites of humans and other animals with the same substitution. This might suggest co-evolution (but not horizontal gene transfer, as these sequences belong to distant branches of the phylogenetic tree) of the host-pathogen pair with the further implication that the presence of glutamate instead of glutamine at this position is a relatively new evolutionary feature in the first group of

SAHases. The crystal structures of several mammalian and protozoan SAHases that carry the Gln→Glu substitution were solved in the presence of Na$^+$ or NH$_4^+$ cations[9,14,27]. With this substitution, the glutamate carboxylic oxygen can interact directly, or indirectly *via* a water molecule, with the Na$^+$ cation, analogously to the amide oxygen of the glutamine side chain (Supplementary Information Table S4). However, the alkali metal cation is still required for the glutamate side chain ordering. Among SAHases from the second, archaeal group, this position can be occupied either by glutamine, glutamate, or sometimes by a lysine residue. In the latter case the lysine amino group would have to be unprotonated in order to act as an acceptor of the hydrogen bond from the exoamino group of adenine. Moreover, a monovalent cation cannot be involved in the positioning of the lysine side chain. Indeed, the structure of archaeal-type SAHase from *Thermotoga maritima* crystallized in the presence of the SAH substrate does not contain any metal cation in the substrate binding region[12].

Potassium cations ensure the highest activity through the regulation of enzyme dynamics.
The crystallographic studies of SAHases show that the enzymes can exist in at least two distinct conformations, i.e., in the open (ligand-free) and closed (ligand-bound) state. On the other hand, measurements of fluorescence anisotropy (conducted for enzymes with a covalently attached fluorescence probe) in solution revealed that the domain oscillations occur also in substrate-free SAHase[24,28]. These results indicated that the enzyme exists in an equilibrium of the open and closed states, shifted in the direction of the of the substrate-free open form. The frequency of the oscillations was estimated[28] at ~4 × 10^7 s^{-1}. This value exceeds by several orders of magnitude the diffusional-encounter frequency of the enzyme[27], and by 4–8 orders of magnitude the catalytic rates (k$_{cat}$) of SAHases from various sources[29]. Confrontation of these numbers could give the impression that the probability of binding of the substrate and its conversion to products, which ultimately need to be released, is very low. However, in structural studies, binding of the substrate induces the enzyme to change its conformational from the open to the closed state. It is essential that the enzyme should not be frozen in the closed state, but stayed in it only as long as is required for the catalytic reaction to complete, and then proceeded to the open conformation for product release and binding of another substrate molecule. At this point the exact role of the K$^+$ ions in the enzymatic activity cannot be fully explained. The cation/ligand binding regions are not affected structurally by the type of the coordinated monovalent cation, but obviously there are significant cation-dependent differences in the thermodynamics of the ligand binding and enzyme kinetics.

To evaluate this puzzling effect of alkali cations on SAHase activity, two experiments were performed, using 2′-deoxyadenosine, an inhibitor that is involved in the irreversible reduction of the NAD$^+$ cofactor to NADH during the chemical conversion of the inhibitor to adenine and a sugar residue[5,6]. In the first experiment, PaSAHase was incubated in the presence of 2′-deoxyadenosine in a buffer containing Rb$^+$ or K$^+$ ions. In the second experiment, the enzyme was first incubated with adenosine in the presence of Rb$^+$ or K$^+$ and subsequently 2′-deoxyadenosine was added. In both experiments, the rate of NADH formation was monitored spectrofluorimetrically (Fig. 5a,b). In the first experiment at its initial stage, the rate of NADH formation was only slightly higher for the reaction conducted in the presence of K$^+$, however, the intensity of fluorescence emission reached a plateau faster in the presence Rb$^+$ ions, indicating that in the time course the SAHase$_{closed}$-Ligand-Rb$^+$ complex forms more easily and/or the ligand is bound more tightly. In the second experiment, the rate of NADH formation was significantly lower in the presence of Rb$^+$. Moreover, in the presence of Rb$^+$ the fluorescence emission plateau was reached at lower intensity, indicating lower content of the reduced form of the cofactor. This result clearly indicates that the SAHase$_{closed}$-Ligand-Rb$^+$ complex is more stable than SAHase$_{closed}$-Ligand-K$^+$, as the exchange of the bound adenosine to 2′-deoxyadenosine is hampered in the complex containing the Rb$^+$ ions.

The above experiments strongly suggest that for the explanation of the role of potassium in the catalytic activity of SAHase, one should consider the stability of the enzyme-ligand-cation complex (SAHase$_{closed}$-Ligand-Me$^+$). Assuming the same ligand (e.g., adenosine) is bound in the active site, the stability of such a complex would depend only on the metal cation. Coordination of the alkali ion by protein and water oxygen atoms can be treated as a hydration-like process, involving ion-dipole interactions. From the thermodynamic point of view, a decrease in the absolute value of the enthalpy of ion hydration is correlated with the increase of the ionic radius and indicates stronger ion-dipole interactions with smaller ions. However, this is not the case in the SAHase$_{closed}$-Ligand-Me$^+$ complex, where the coordination region is rigid with very similar, cation-independent conformation found in different SAHase models (Fig. 3b). The cation is involved in the formation of a network of polar contacts including the coordinating loop (residues T380-S384, part of the molecular hinge), the side chain of Q65, the substrate/ligand, and several water molecules (Fig. 3a). The ion coordination region is involved in ligand binding and seems to be ideally suited to coordinate K$^+$ and Rb$^+$, the two ions tested that have similar ionic radii (1.46 vs 1.56 Å, coordination number VII)[30]. This conclusion is confirmed by the ITC study, which revealed that binding of the adenosine ligand is very similar and most efficient in the presence of these two cations. On the other hand, their influence on enzyme activity is completely opposite. The ionic radius of Rb$^+$ is slightly larger than K$^+$ and, therefore, it should form a more stable SAHase$_{closed}$-Ligand-Me$^+$ complex, as the contribution of the coordination bond to the protein/water O–Rb$^+$ interaction is higher than for the complex with K$^+$. In consequence, dissociation of the SAHase$_{closed}$-Ligand-Rb$^+$ complex is more difficult and the enzyme is arrested in its closed state. In this scenario, the Rb$^+$ ions inhibit the enzyme activity in a noncompetetive manner. In the SAHase$_{closed}$-Ligand-K$^+$ complex, the contribution of the coordination bond to metal binding is lower, resulting in a less stable complex. In the presence of K$^+$ ions the complex stability seems to be ideally tuned, as the maximum catalytic activity of the enzyme is observed. The complex is stable enough to keep the enzyme in the closed state for the time required to complete the enzymatic reaction and, therefore, the catalytic cycle can be completed by changing the enzyme conformation from closed to open.

Ligand binding and enzymatic activity are impeded when other alkali cations are used. This could be explained by the lower stability of the SAHase$_{closed}$-Ligand-Me$^+$ complexes. Similar enzymatic activity and adenosine binding constants are observed in the presence of Na$^+$ and Cs$^+$ ions. The ionic radius of Cs$^+$ (1.67 Å, coordination
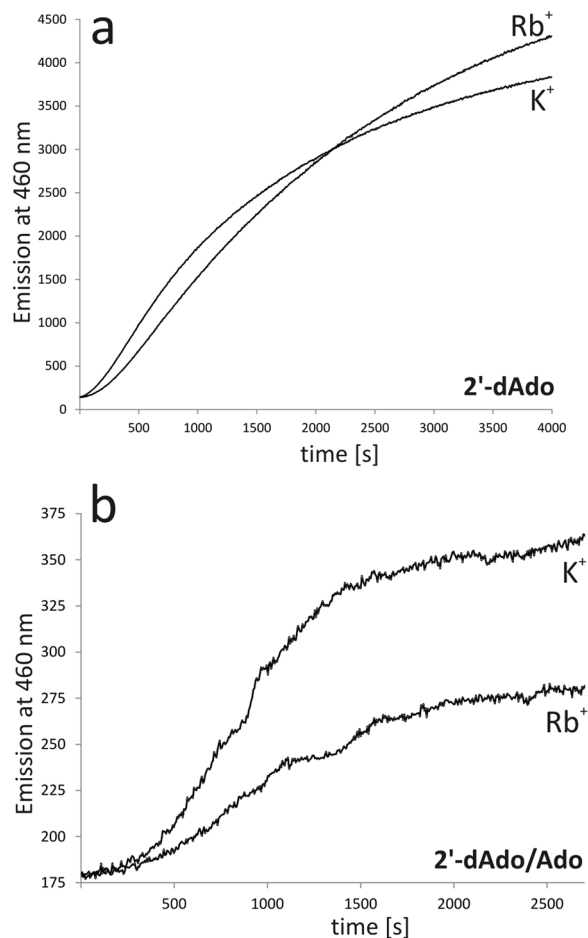
Figure 5. (**a**) Time course of PaSAHase inactivation by 2′-deoxyadenosine (2′-dAdo) in the presence of K$^+$ or Rb$^+$ ions. (**b**) Time course of inactivation of PaSAHase incubated with adenosine (Ado) by 2′-deoxyadenosine in the presence of K$^+$ or Rb$^+$ ions. Irreversible formation of the reduced form of the cofactor (NADH) was monitored spectrofluorimetrically after the addition of the competitive inhibitor 2′-deoxyadenosine.

number VI) is larger than of other alkali ions and thus it should destabilize the complex. Another possible explanation is that Cs$^+$, because of its size, does not fully occupy the available binding sites. The ionic radius of Na$^+$ is significantly smaller (1.02 or 1.12 Å, coordination number VI or VII, respectively) than of K$^+$. Therefore, the stability of the SAHase$_{closed}$-Ligand-Na$^+$ complex is lower, as the ionic contribution to Na$^+$ coordination is higher than in complexes containing Rb$^+$ or K$^+$ ions. Additionally, numerous sodium-containing SAHase models indicate that the distance between the Na$^+$ ion and the amide Oε atom of Q65 is too long and that this Na$^+$–Q65 amide (which is still ordered) interaction should be considered as purely ionic; this would further reduce the stability of the complex. In consequence, complexes containing Cs$^+$ or Na$^+$ are not stable enough to support a high rate of the catalyzed reaction. Even lower (but comparable) activities are observed for the reactions carried out in the presence of Li$^+$ (0.76 Å, coordination number VI) or in the absence of any alkali metal. Moreover, no heat effect was detected during the adenosine binding ITC experiment in in the presence of Li$^+$. As proposed above, binding of the monovalent cation does not take place when the enzyme is in the open conformation, but occurs only after the conformational open-closed change that allows Q65 to approach the cation. Therefore, the possibility of the formation of an SAHase$_{closed}$-Ligand-Li$^+$ complex is questionable and the results may suggest that the Li$^+$ ion is too small to be coordinated and, therefore, is unable to order the side chain of Q65.

Zn^{2+} is a potent inhibitor of PaSAHase. The Zn^{2+} cation was incorporated into recombinant PaSAHase during expression and co-purifies with the enzyme. It was identified in two crystal structures of the enzyme and its presence was additionally confirmed by X-ray fluorescence spectroscopy (Supplementary Information Fig. S2). It should be noted that this is the first report of a divalent cation identification in any SAHase structure. Co-purification of Zn^{2+} with PaSAHase indicates that the enzyme has a very high affinity for this cation. First of all, the recombinant protein was purified using affinity chromatography with Ni^{2+} ions, which are chemically very similar to Zn^{2+}. However, no nickel ions were detected in the protein sample using XRF. Secondly, although the total intracellular Zn^{2+} concentration is in the millimolar range, it is as low as pico- to femtomolar for free zinc ions[31–34]. In *E. coli* cells the concentration of free zinc ions has been established as ~20 pM[35]. Our enzymatic assays revealed that recombinant PaSAHase has only residual activity. Efficient removal of the Zn^{2+} ions (and of any metal ions for that matter) using TPEN restored the enzymatic activity, which shows that the zinc ions inhibit
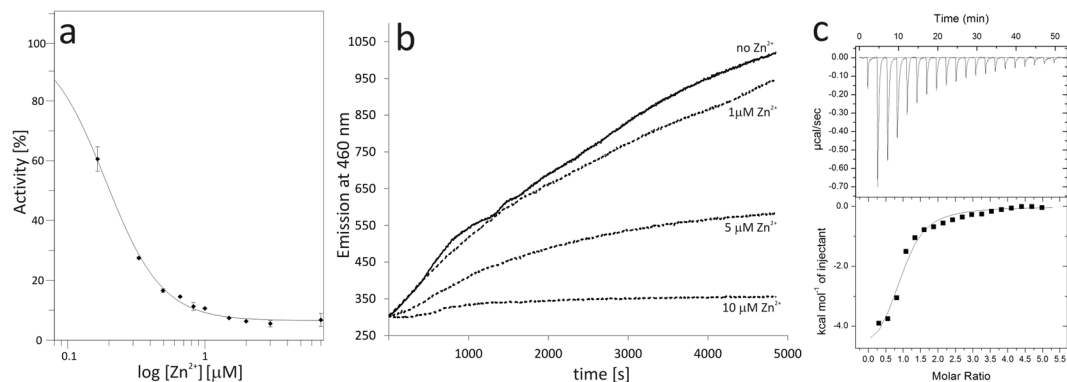
Figure 6. PaSAHase-Zn^{2+} interactions. (**a**) Inhibition of PaSAHase by Zn^{2+} ions. The wild-type Zn^{2+} form of the enzyme was incubated with different concentrations of Zn^{2+} ranging from 0.165 to 20 μM (shown on log scale). The enzymatic activity was followed in the hydrolytic direction by monitoring homocysteine formation *via* its reaction with 5,5′-dithiobis(2-nitrobenzoic acid). For a sample without Zn^{2+} the activity was 100%. (**b**) Time course of inactivation of PaSAHase by 2′-deoxyadenosine. PaSAHase (15 μM) was incubated with adenosine and Zn^{2+} or without the divalent cation. Irreversible formation of the reduced (and, therefore, inactive) form of the cofactor (NADH) was monitored spectrofluorimetrically after the addition of the competitive inhibitor 2′-deoxyadenosine. (**c**) Calorimetric titration (at 293 K) of PaSAHase with Zn^{2+} ions in the presence of 100 mM K$^+$ ions. The top plot of the panel represents the raw heat data obtained from consecutive injections of a solution containing 2 mM Zn^{2+} ions into the sample cell containing 45 μM enzyme. The heat peak areas have been plotted against the molar ratio of Zn^{2+} ions added to the enzyme, creating the binding isotherm at the bottom of the panel. The best fit of the model of one set of binding sites is represented by the solid line.

the activity of PaSAHase. Specifically, our kinetics studies based on PaSAHase inactivation (Fig. 6a) revealed that a tightly bound Zn^{2+} cation acts as a very strong noncompetitive inhibitor with an inhibitory constant K$_i$ as low as 15 nM. Furthermore, the enzymatic study indicated that Zn^{2+} locks the enzyme-ligand complex in the closed conformation. This assay was performed analogously to the tests for the stability of the SAHase$_{closed}$-Ligand-Me$^+$ complexes that utilized 2′-deoxyadenosine. In the Zn^{2+} case, PaSAHase was first incubated in the presence of K$^+$ ions with adenosine and Zn^{2+} ions at various concentrations, and subsequently, 2′-deoxyadenosine was added. The rate of NADH formation was monitored spectrofluorimetrically (Fig. 6b). The highest rate was observed for the reaction without any addition of Zn^{2+} and gradually decreased with increasing Zn^{2+} concentration. These results clearly indicate that the Zn^{2+} ions arrest the enzyme in the closed conformation stymieing the exchange of adenosine to 2′-deoxyadenosine.

Our crystal structures help to elucidate this puzzling behavior by showing that there is a tetrahedral zinc binding site, formed by three highly conserved amino acid residues involving S (Cys85), N (His323), and two O (Asp139) ligand atoms, located in the active site, where - together with the H323-F324 molecular gate - the divalent cation shuts access to the active site of the enzyme. Moreover, the Zn^{2+} cation is located at the interface between the two principal domains and is coordinated by three ligands from the substrate-binding domain (C85 Sγ, D139 O and D139 Oδ1) and one ligand from the cofactor-binding domain (H323 Nε1), thus further stabilizing the SAHase$_{closed}$-Ligand-K$^+$ complex. The zinc binding sites are not fully occupied and, therefore, the side chain of H323 from the molecular gate is modeled in two states, differing in ~180° flip of the imidazole ring. In both conformations the molecular gate remains shut. The rotation of the H323 side chain in the Zn^{2+} complex is necessary for the formation of the coordination bond. The second rotamer interacts *via* the H323 Nδ1 atom with the O5′ atom of adenosine. The dual conformation of H323 is correlated with a similar disorder of the adenosine O5′ atom. The details of the zinc ion coordination are included in Fig. 1a,b and Supplementary Information (Table S5).

The mechanism of PaSAHase inactivation by zinc cations is different from that proposed for the inhibition of human placental SAHase activity by Cu^{2+} ions[17]. The latter study revealed that binding of copper cations affects protein-NAD$^+$ interactions. In turn, the cofactor is released from the enzyme and the catalytic cycle cannot proceed anymore. The inhibition constants of zinc (~15 nM) and copper (~25 nM)[17] ions are very low and similar. It was suggested that the copper-SAHase interactions may have biological significance, e.g., in the regulation of cellular methylation reactions or copper metabolism[36–40]. Contrary to that speculation, so far there is no literature evidences on any biological cross-talk between SAHase and zinc ions. However, since the total intracellular zinc concentration is in the range of millimolar, such an interaction with PaSAHase cannot be excluded.

PaSAHase-Zn^{2+} interactions were also tested by ITC experiments (Fig. 6c). Upon titration in the presence of K$^+$ cations, the stoichiometry of protein:Zn^{2+} binding is around one zinc cation (0.90 ± 0.06) per one subunit with the apparent binding constant K$_d$ of 12.7 ± 2.9 μM. The ITC results are in agreement with the crystallographic models of PaSAHase which also indicate the presence of only one Zn^{2+} site per subunit.

Discussion

Monovalent cations are known to activate numerous enzymes but the mechanisms of their action could be different. Two types of activation have been proposed[41]. Activation is defined as type I for the enzymatic reactions where the cation interacts directly with a substrate to facilitate its binding (type Ia) or hydrolysis (type Ib). Frequently, a monovalent cation is utilized during the catalytic cycle in synergy with an additional divalent cation, e.g., Mg^{2+}, Mn^{2+} or Zn^{2+} [42–46]. A characteristic feature of enzymes activated by type I mechanism is a strong preference for a particular monovalent cation to ensure the highest catalytic activity[43,47–50]. This preference is usually related to a specific spatial arrangement of the active site or to the occurrence of optimal ionic interactions with a substrate provided by a particular monovalent cation[41]. On the other hand, the type of monovalent cation is not so strict for enzymes activated by type II mechanism. A striking feature of type II activation is that the monovalent cation does not interact with the substrate directly. The mechanism of type II activation is based on structural changes upon the monovalent cation binding, which could occur at various (e.g., local or/and global) level(s). Therefore, the detailed mechanism of this activation might be difficult to fully explain. For instance, binding of monovalent ion(s) could induce conformational changes within the whole subunit, the active site, or allosteric sites, and this in turn could facilitate substrate binding[51–58]. Additionally, other effects could also be observed, for instance, stabilization of the quaternary structure[53], shifting of the equilibrium between the active and inactive conformers, or rigidifying of the enzyme structure and increasing protein thermal stability[57–59].

S-adenosyl-ʟ-homocysteine hydrolase obviously does not fall in the type I category as the monovalent cation does not interact with the ligand directly. It is true that the activity of PaSAHase depends on the cation type with a strong preference for K^+, but the activation seems to be more similar to the situation defined for the type II mechanism. In SAHases, the monovalent cation participates in the ordering and proper orientation of Q65, the key residue involved in ligand binding. On the other hand, Q65 behaves similarly in the presence of different monovalent cations. Moreover, the conformation of the cation binding site in different SAHases is almost identical despite the presence of various monovalent cations, including NH_4^+, Na^+, K^+, or Rb^+. Therefore, the strong preference of SAHases for K^+ cannot be explained at the structural level alone. Our results strongly support the hypothesis that the role of the K^+ ion is not restricted to fixing the orientation of the Q65 side chain. Instead, we propose that SAHases are activated by a special variant of type II mechanism, based on tuning of the enzyme dynamics (domain movement), which depends on the type of the coordinated cation. K^+, but not other alkali cations, enables unique dynamic properties of the enzyme to ensure its maximum activity. The K^+ ion stabilizes the enzyme-substrate complex in the closed conformation for a time interval required to complete the catalytic cycle. Stabilization of the closed state is achieved by (i) rigidifying the hinge region involved in substrate-induced domain reorientation and/or (ii) formation of additional polar contacts at the interface between the substrate- and cofactor-binding domains. The influence of metal cations on the enzyme dynamics can be exploited for enzyme inhibition. For example, the Rb^+ cation is an inhibitor occupying the potassium site at the interdomain hinge. On the other hand, the potent inhibitory effect of Zn^{2+} is based on binding at the molecular gate and arresting the enzyme in the closed conformation.

Methods

Cloning, expression and purification of PaSAHase and Q65A mutein. The coding sequence of the *ahcY* gene was amplified by PCR from *P. aeruginosa* PAO1 genomic DNA. The amplicon was cloned into pMCSG57 expression vector using the ligation independent cloning reaction. The construct was used for Q65A mutant generation via PIPE[60] cloning with the following primers: 5′-ATCGCGACCGGCGTGCTGATCGAGACCCTGGTC and 5′-GGTCGCGATGGTCATGTGGATGCAACCGAGGAT. The sequence of both constructs was confirmed by sequencing. The constructs carrying the coding sequence of the wild type PaSAHase or its Q65A mutant were transformed into BL21-CodonPlus(DE3)®-RIPL *E. coli* cells and expressed. 10 mL of LB medium containing 34 µg·mL⁻¹ chloramphenicol and 100 µg·mL⁻¹ ampicillin were inoculated and grown overnight at 310 K and the culture was used for inoculation of 1 L of LB medium, which was subsequently cultivated with appropriate antibiotics to an OD_{600} of 0.8. The temperature was decreased to 291 K and protein expression was induced with IPTG at a final concentration of 0.35 mM. The cells were harvested 20 hours after induction and flash-frozen in liquid nitrogen.

The purification procedure was the same for the wild type enzyme and Q65A mutein. The cell pellet was resuspended in buffer A (20 mM imidazole, 500 mM NaCl, 20 mM Tris·HCl pH 8.0, 10% glycerol) with the addition of 1 mM TCEP·HCl (to enhance enzyme stability) and 100 µg·mL⁻¹ lysozyme. Cells were disrupted by sonication on ice and centrifuged for removal of debris. The supernatant was loaded onto a HisTrap column equilibrated with 0.05 M $NiSO_4$. The protein was eluted with a buffer containing 300 mM imidazole, 500 mM NaCl, 20 mM Tris·HCl pH 8.0, 10% glycerol, and 1 mM TCEP·HCl. TEV protease was added at the final concentration of 0.1 mg·mL⁻¹ and the protein solution was extensively dialyzed against buffer A. After overnight incubation at 277 K, the solution was loaded onto a HisTrap column equilibrated with 0.05 M $NiSO_4$ and the protein was eluted with buffer A, subsequently exchanged for buffer B (100 mM KCl, 25 mM Tris·HCl pH 8.0, 1 mM TCEP·HCl) *via* dialysis. Next, a modified procedure of Yuan *et al.*[20] was used for the preparation of the apo form of the enzyme. Briefly, a solution containing 5 mg of recombinant PaSAHase dissolved in 5 mL of buffer B was gradually mixed with 10 mL of saturated solution of $(NH_4)_2SO_4$ at pH 3.3, and then stored for 10 min on ice. The mixture was centrifuged and the precipitate was dissolved in 5 mL of buffer C (100 mM KCl, 25 mM Tris·HCl pH 8.0). The enzyme was precipitated again as above and the pellet was washed with saturated neutral solution of $(NH_4)_2SO_4$. Finally, the precipitated apo PaSAHase was dissolved in 2 mL of buffer C and subsequently NAD^+ was added to a final concentration of 2 mM. After 30 minutes of incubation on ice, the mixture was loaded onto a Superdex 200 (Pharmacia) gel filtration column pre-equilibrated with buffer D (100 mM KCl, 25 mM HEPES·KOH pH 7.5, 1 mM TCEP·HCl). The protein was eluted with buffer D as a tetramer. Fractions with PaSAHase were concentrated to 20 mg·mL⁻¹ by ultracentrifugation and the fresh protein solution was used for initial activity study,

X-ray fluorescence experiments, and crystallization of Zn^{2+}-containing PaSAHase complexes. For other studies, the purification procedure was modified by introduction of an additional step required to efficiently remove the Zn^{2+} ions by a strong chelator. Briefly, the gel filtration step was preceded with an extensive dialysis of the sample in buffer C supplemented with 50 μM *N,N,N′,N′*-tetrakis(2-pyridinylmethyl)−1,2-ethanediamine (TPEN). The subsequent purification steps were unchanged.

Both purified proteins are extended at the N-terminus by a short tripeptide (SNA-) cloning artifact. SDS-PAGE analysis confirmed the size of the expressed proteins (~53 kDa). Finally, mass spectrometry was used to confirm the size and sequence of the wild type enzyme.

Assays for SAHase activity and inhibition.   Assays for PaSAHase activity in the hydrolytic direction were carried out spectrophotometrically and the rate of L-homocysteine (Hcy) formation was measured by monitoring its reaction with 5,5′-dithiobis(2-nitrobenzoic acid) (DTNB)[21]. Assays were performed in 3 mL volume in a buffer containing 100 mM MeCl (where Me^+ corresponds to Li^+, Na^+, K^+, Rb^+, or Cs^+ ion) and 25 mM HEPES·MeOH pH 7.5, or a buffer containing 100 mM Tris·HCl pH 7.5. For the Q65A mutein, the experiments were conducted in a buffer containing 100 mM KCl and 25 mM HEPES·KOH pH 7.5. The buffers were supplemented with six units of adenosine deaminase, 100 μM DTNB, and 0.32 μM of PaSAHase or its mutein. The reaction was initiated by the addition of *S*-adenosyl-L-homocysteine (SAH) at a final concentration from 2.5 to 200 μM. The conversion of Hcy to Hcy-TNB was carried out at 293 K. The reaction progress was measured for one minute and monitored at 412 nm using a U-3900H spectrophotometer (Hitachi). Initial velocity parameters were estimated from the linear region of the recorded curve.

For the inhibition study, PaSAHase (0.35 μM) in a buffer containing 100 mM KCl and 25 mM Tris·HCl pH 7.5 was incubated with Zn^{2+} at different concentrations, ranging from 0.165 to 20 μM. The reaction was initiated by the addition of SAH at a final concentration of 85 μM. The enzymatic activity was followed in the hydrolytic direction by monitoring homocysteine formation *via* its reaction with DNTB to determine the IC_{50} constant. For the sample without the addition of Zn^{2+} ions, 100% activity was assigned. All measurements were performed in duplicates. The experimental data were analyzed with the *GraFit* 7.0 software (Erithacus) to obtain the kinetic parameters of the enzymatic reactions: substrate affinity (K_M), activity (V_{max}), as well as catalytic rate (k_{cat}) or IC_{50} value for inhibition. The IC_{50}-to-K_i converter[61] was applied to calculate the inhibition constant (K_i) for Zn^{2+} ions using the noncompetitive model of inhibition.

Isothermal titration calorimetry.   ITC measurements were performed at 293 K using a MicroCal iTC200 calorimeter (GE Healthcare). For the adenosine binding studies, the wild type protein was dialyzed against a buffer containing 100 mM MeCl and 25 mM HEPES·MeOH pH 7.5, or an alkali-cation-free buffer containing 100 mM Tris·HCl pH 7.5. The experiment for the Q65A mutein was conducted in a buffer containing 100 mM KCl and 25 mM HEPES·KOH pH 7.5. The final protein concentrations were in the range of 100–120 μM. Adenosine was dissolved in the dialysis buffers to the concentrations of 0.6 to 1.0 mM. The K^+ ion binding study was conducted in 50 mM Tris·HCl pH 7.5 at PaSAHase concentration of 70 μM. The protein was titrated with 1 mM KCl in 50 mM Tris·HCl pH 7.5. The Zn^{2+} ion binding study was conducted in a buffer containing 100 mM KCl and 50 mM Tris·HCl pH 7.5 at PaSAHase concentration of 45 μM. The protein was titrated with 2 mM $ZnCl_2$. In all ITC experiments the ligand was injected to the protein solution (300 μL) in 2 μL aliquots until saturation was observed. The protein concentrations were estimated by the Bradford method and are presented for a single PaSAHase subunit. The raw ITC data were analyzed with the *ORIGIN* 7.0 software (OriginLab) to obtain the thermodynamic parameters of the complexation reactions: stoichiometry (N), dissociation constant (K_d), as well as changes in enthalpy (ΔH) and entropy (ΔS). For sigmoidal titration curves, the *one set of sites* model was fitted and N was obtained from the experiment. For hyperbolic curves, for which the determination of N is impossible, N was fixed while fitting the same model. All measurements were performed in duplicates.

Time course of PaSAHase inactivation by 2′-deoxyadenosine.   The measurements were performed at 293 K using an F-7000 spectrofluorotometer (Hitachi) in the volume of 1 mL. Irreversible formation of the reduced form of the cofactor (NADH) was monitored spectrofluorometrically by excitation at 340 nm and measurement of emission at 460 nm, as described previously[20]. The influence of K^+ and Rb^+ ions on the time-dependent inactivation of the enzyme was carried out for 15 μM PaSAHase in a buffer containing 100 mM KCl or RbCl, 25 mM HEPES·KOH or HEPES·RbOH pH 7.5, and 1 mM TCEP·HCl. In the first experiment, the reaction was initiated by the addition of 2′-deoxyadenosine to the final concentration of 5 mM. In the second experiment, the enzyme was incubated for 2 hours with 100 μM adenosine and subsequently 2′-deoxyadenosine was added at a final concentration of 200 μM. After one minute the reaction was monitored for 4000 seconds (first experiment) or until the intensity of fluorescence emission reached a plateau (second experiment). An analogous experiment was carried out to analyze the influence of Zn^{2+} cations on the enzyme. Herein, 15 μM PaSAHase in a buffer containing 100 mM KCl and 25 mM HEPES·KOH was incubated for 2 hours with adenosine (200 μM) and $ZnCl_2$ (1, 5 or 10 μM) or without the divalent cation. The cofactor conversion reaction was initiated by the addition of 2′-deoxyadenosine to the final concentration of 5 mM and after one minute was monitored for 5000 seconds.

X-ray fluorescence spectroscopy.   Freshly purified PaSAHase in buffer C from the batch not treated with Zn^{2+} chelator was suspended in a cryoloop with the diameter of 1.0 mm and vitrified in liquid nitrogen prior to X-ray fluorescence detection. Initial X-ray fluorescence spectrum for the energy range from 8000 to 11500 eV was recorded at BESSY beamline 14.1 using Amptek X-123 SDD X-ray spectrometer. Maximum of emission related to the presence of zinc ions was observed in the energy range from 9600–9700 eV (Supplementary Fig. 2).

²³Na NMR Spectroscopy.   ²³Na NMR spectra were measured on a BRUKER Avance 500 MHz spectrometer (5 mm BBFO BB-¹⁹F/¹H Z-gradient probe). Six samples were prepared in 50 mM Tris·HCl pH 7.5, which contained: (1) 5 mM NaCl, (2) 5 mM NaCl + 1 mM Ado, (3) 5 mM NaCl + 0.3 mM PaSAHase, (4) 0.3 mM PaSAHase + 5 mM NaCl + 1 mM Ado, (5) 0.3 mM PaSAHase + 0.6 mM NaCl + 1 mM Ado, (6) 0.3 mM PaSAHase + 0.3 mM NaCl + 1 mM Ado. ²³Na NMR chemical shifts are given in ppm relative to 5 mM NaCl in 50 mM Tris·HCl pH 7.5.

Crystallization and X-ray data collection.   Protein solution in a buffer containing 100 mM KCl or RbCl, 25 mM HEPES·KOH or HEPES·RbOH pH 7.5, and 1 mM TCEP·HCl was incubated overnight with 2 mM of adenosine (Ado/K⁺/Zn²⁺), 2′-deoxyadenosine (2′-dAdo/K⁺/Zn²⁺ or 2′-dAdo/Rb⁺), or 3′-deoxyadenosine (3′-dAdo/K⁺) at 277 K. Crystallization drops were mixed from 2 μL of the protein solution (10 mg·mL⁻¹ measured spectrofotometrically at 280 nm) and 2 μL of the reservoir solution containing 20% (w/v) PEG8000 and 50 mM KH_2PO_4 (Ado/K⁺/Zn²⁺ and 2′-dAdo/K⁺/Zn²⁺), or 20% (w/v) PEG8000 and 50 mM RbH_2PO_4 (2′-dAdo/Rb⁺), or 15% (w/v) PEG8000, 50 mM KH_2PO_4 and 20% (v/v) glycerol (3′-dAdo/K⁺). Diffraction-quality crystals were grown within a few days at 292 K using the hanging-drop vapor-diffusion method. X-Ray diffraction data were measured at BESSY beamlines 14.1, 14.2, 14.3 or APS beamline SER-CAT 22-ID. Crystals of the 3′-dAdo/K⁺ complex were fished out directly from mother liquor and vitrified in liquid nitrogen. Other crystals were soaked for a few seconds in the reservoir solution supplemented with 20% (v/v) glycerol and vitrified in liquid nitrogen prior to X-ray data collection. The diffraction data extend to 1.35 Å (3′-dAdo/K⁺), 1.45 Å (2′-dAdo/Rb⁺), 1.60 Å (Ado/K⁺/Zn²⁺), or 1.75 Å (2′-dAdo/K⁺/Zn²⁺) resolution. Indexing and integration of the diffraction images was performed in the *HKL3000* package[62] (2′-dAdo/K⁺/Zn²⁺ and 3′-dAdo/K⁺) or *XDSAPP* graphical interface[63] of the *XDS* package[64] (Ado/K⁺/Zn²⁺ and 2′-dAdo/Rb⁺). The intensity data were scaled in *HKL3000* or *XDS*. The final data sets are characterized in Supplementary Table S1.

Structure solution, refinement and validation.   The crystal structure of PaSAHase in the 3′-dAdo/K⁺ complex was solved by molecular replacement, as implemented in the program *PHASER*[65] from the *CCP4* suite[66] using a subunit of *H. sapiens* SAHase[27] as the search model (PDB entry 1LI4, chain A). The correct solution was found in space group *C*2 with two subunits in the asymmetric unit, from which crystallographic symmetry generates the complete PaSAHase homotetramer. The other three crystal structures were solved by molecular replacement using *PHASER* and a subunit from the 3′-dAdo/K⁺ solution as a search probe. The correct solutions were found in space group *C*2 with four subunits in the asymmetric unit forming the PaSAHase tetramer. For all four complexes, automatic model building was carried out with the online version of *ARP/wARP*[67]. Anisotropic (3′-dAdo/K⁺, 2′-dAdo/Rb⁺) or isotropic (Ado/K⁺/Zn²⁺, 2′-dAdo/K⁺/Zn²⁺) stereochemically-restrained structure-factor refinement was carried out in *REFMAC5*[68] with maximum-likelihood targets and with the inclusion of three TLS groups[69] (Ado/K⁺/Zn²⁺ and 2′-dAdo/K⁺/Zn²⁺) per protein chain, as suggested by the *TLSMD* server[70]. The ligands were identified without ambiguity in mF_o-DF_c omit electron density maps phased with the contribution of the protein atoms only. The occupancy of the zinc ions was adjusted manually to satisfy simultaneously two conditions: (i) clean difference maps and (ii) ADP parameters of the zinc ions similar to those of the adjacent atoms. The alkali cation binding sites were confirmed with *CheckMyMetal*[71]. Additionally, the Rb⁺ ions were clearly present in anomalous difference Fourier maps. The *COOT* program[72] was used for manual modeling in electron density maps. Stereochemical quality of the models was assessed using the wwPDB validation pipeline[73]. Final refinement statistics for all four crystal structures are reported in Supplementary Table 1.

Other software used.   The *SSM* algorithm[74] was used for Cα superposition of protein models. Molecular figures were generated in *PyMOL*[75]. The multipole sequence alignment was calculated in *Clustal Omega*[76].

Data availability.   Atomic coordinates and ADP parameters, as well as structure factors have been deposited in the Protein Data Bank (PDB) with the accession codes 6F3M (Ado/K⁺/Zn²⁺), 6F3O (2′-dAdo/K⁺/Zn²⁺), 6F3P (3′-dAdo/K⁺), and 6F3Q (2′-dAdo/Rb⁺). Raw diffraction images were deposited in the Integrated Resource for Reproducibility in Macromolecular Crystallography (ProteinDiffraction.org) with the following DOIs: https://doi.org/10.18430/M36F3M (Ado/K⁺/Zn²⁺), https://doi.org/10.18430/M36F3O (2′-dAdo/K⁺/Zn²⁺), https://doi.org/10.18430/M36F3P (3′-dAdo/K⁺) and https://doi.org/10.18430/M36F3Q (2′-dAdo/Rb⁺).

References

1. Richards, H. H., Chiang, P. K. & Cantoni, G. L. Adenosylhomocysteine hydrolase. *Crystallization of the purified enzyme and its properties. J Biol Chem* **253**, 4476–4480 (1978).
2. Poulton, J. E. & Butt, V. S. Purification and properties of S-adenosyl-ʟ-methionine: caffeic acid *O*-methyltransferase from leaves of spinach beet (*Beta vulgaris* L.). *Biochim Biophys Acta* **403**, 301–314 (1975).
3. Chiang, P. K. & Cantoni, G. L. Perturbation of biochemical transmethylations by 3-deazaadenosine *in vivo*. *Biochem Pharmacol* **28**, 1897–1902 (1979).
4. Chiang, P. K. Biological effects of inhibitors of *S*-Adenosylhomocysteine hydrolase. *Pharmacol Ther* **77**, 115–134 (1998).
5. Hershfield, M. S. Apparent suicide inactivation of human lymphoblast *S*-adenosylhomocysteine hydrolase by 2′-deoxyadenosine and adenine arabinoside. A basis for direct toxic effects of analogs of adenosine. *J Biol Chem* **254**, 22–25 (1979).
6. Brzezinski, K., Dauter, Z. & Jaskolski, M. High-resolution structures of complexes of plant S-adenosyl-ʟ-homocysteine hydrolase (*Lupinus luteus*). *Acta Crystallogr D Biol Crystallogr* **68**, 218–231 (2012).
7. Turner, M. A. *et al*. Structure determination of selenomethionyl *S*-adenosylhomocysteine hydrolase using data at a single wavelength. *Nat Struct Biol* **5**, 369–376 (1998).
8. Hu, Y. *et al*. Crystal structure of *S*-adenosylhomocysteine hydrolase from rat liver. *Biochemistry* **38**, 8323–8333 (1999).
9. Tanaka, N. *et al*. Crystal structure of S-adenosyl-ʟ-homocysteine hydrolase from the human malaria parasite *Plasmodium falciparum*. *J Mol Biol* **343**, 1007–1017 (2004).
10. Reddy, M. C. M. *et al*. Crystal structures of *Mycobacterium tuberculosis* S-adenosyl-ʟ-homocysteine hydrolase in ternary complex with substrate and inhibitors. *Protein Sci* **17**, 2134–2144 (2008).

11. Manszewski, T., Singh, K., Imiolczyk, B. & Jaskolski, M. An enzyme captured in two conformational states: crystal structure of *S*-adenosyl-L-homocysteine hydrolase from *Bradyrhizobium elkanii*. *Acta Crystallogr D Biol Crystallogr* **71**, 2422–2432 (2015).

12. Zheng, Y. *et al.* Crystal structures of *S*-adenosylhomocysteine hydrolase from the thermophilic bacterium *Thermotoga maritima*. *J Struct Biol* **190**, 135–142 (2015).

13. Brzezinski, K. *et al.* S-adenosyl-L-homocysteine hydrolase from a hyperthermophile (*Thermotoga maritima*) is expressed in *Escherichia coli* in inactive form - Biochemical and structural studies. *Int J Biol Macromol* **104**, 584–596 (2017).

14. Kusakabe, Y. *et al.* Structural insights into the reaction mechanism of S-adenosyl-L-homocysteine hydrolase. *Sci Rep* **5**, 16641 (2015).

15. Czyrko, J., Jaskólski, M. & Brzezinski, K. Crystal Structure of S-adenosyl-l-homocysteine hydrolase from *Cytophaga hutchinsonii*, a case of combination of crystallographic and noncrystallographic symmetry. *Croat Chem Acta* **91** (2018).

16. Palmer, J. L. & Abeles, R. H. The mechanism of action of *S*-adenosylhomocysteinase. *J Biol Chem* **254**, 1217–1226 (1979).

17. Li, M. *et al.* Copper ions inhibit S-adenosylhomocysteine hydrolase by causing dissociation of NAD$^+$ cofactor. *Biochemistry* **46**, 11451–11458 (2007).

18. Komoto, J. *et al.* Effects of site-directed mutagenesis on structure and function of recombinant rat liver *S*-adenosylhomocysteine hydrolase. Crystal structure of D244E mutant enzyme. *J Biol Chem* **275**, 32147–32156 (2000).

19. Manszewski, T., Szpotkowski, K. & Jaskolski, M. Crystallographic and SAXS studies of S-adenosyl-L-homocysteine hydrolase from *Bradyrhizobium elkanii*. *IUCrJ* **4**, 271–282 (2017).

20. Yuan, C. S., Yeh, J., Liu, S. & Borchardt, R. T. Mechanism of inactivation of *S*-adenosylhomocysteine hydrolase by (Z)−4′,5′-didehydro-5′-deoxy-5′-fluoroadenosine. *J Biol Chem* **268**, 17030–17037 (1993).

21. Yuan, C. S., Ault-Riché, D. B. & Borchardt, R. T. Chemical modification and site-directed mutagenesis of cysteine residues in human placental *S*-adenosylhomocysteine hydrolase. *J Biol Chem* **271**, 28009–28016 (1996).

22. Lozada-Ramírez, J. D., Martínez-Martínez, I., Sánchez-Ferrer, A. & García-Carmona, F. A colorimetric assay for *S*-adenosylhomocysteine hydrolase. *J Biochem Biophys Meth* **67**, 131–140 (2006).

23. Turner, M. A. *et al.* Structure and function of *S*-adenosylhomocysteine hydrolase. *Cell Biochem Biophys* **33**, 101–125 (2000).

24. Wang, M. *et al.* Effects of Ligand Binding and Oxidation on Hinge-Bending Motions in S-adenosyl-L-homocysteine Hydrolase. *Biochemistry* **45**, 7778–7786 (2006).

25. Clausen, M. J. V. & Poulsen, H. Sodium/Potassium Homeostasis in the Cell. *Met Ions Life Sci* **12**, 41–67 (2013).

26. Stepkowski, T., Brzeziński, K., Legocki, A. B., Jaskólski, M. & Béna, G. Bayesian phylogenetic analysis reveals two-domain topology of *S*-adenosylhomocysteine hydrolase protein sequences. *Mol Phylogenet Evol* **34**, 15–28 (2005).

27. Yang, X. *et al.* Catalytic strategy of S-adenosyl-L-homocysteine hydrolase: transition-state stabilization and the avoidance of abortive reactions. *Biochemistry* **42**, 1900–1909 (2003).

28. Yin, D. *et al.* Substrate binding stabilizes *S*-adenosylhomocysteine hydrolase in a closed conformation. *Biochemistry* **39**, 9811–9818 (2000).

29. Schomburg, I. *et al.* The BRENDA enzyme information system–From a database to an expert system. *J. Biotechnol.* **261**, 194–206 (2017).

30. Shannon, R. D. Revised effective ionic radii and systematic studies of interatomic distances in halides and chalcogenides. *Acta Crystallogr Sect A* **32**, 751–767 (1976).

31. Outten, C. E. Femtomolar Sensitivity of Metalloregulatory Proteins Controlling Zinc Homeostasis. *Science* **292**, 2488–2492 (2001).

32. Jacobsen, F. E., Kazmierczak, K. M., Lisher, J. P., Winkler, M. E. & Giedroc, D. P. Interplay between manganese and zinc homeostasis in the human pathogen *Streptococcus pneumoniae*. *Met Integr Biometal Sci* **3**, 38–41 (2011).

33. Begg, S. L. *et al.* Dysregulation of transition metal ion homeostasis is the molecular basis for cadmium toxicity in *Streptococcus pneumoniae*. *Nat Commun* **6** (2015).

34. Capdevila, D. A., Wang, J. & Giedroc, D. P. Bacterial Strategies to Maintain Zinc Metallostasis at the Host-Pathogen Interface. *J Biol Chem* **291**, 20858–20868 (2016).

35. Patzer, S. I. & Hantke, K. The ZnuABC high-affinity zinc uptake system and its regulator Zur in *Escherichia coli*. *Mol Microbiol* **28**, 1199–1210 (1998).

36. Bethin, K. E., Petrovic, N. & Ettinger, M. J. Identification of a major hepatic copper binding protein as *S*-adenosylhomocysteine hydrolase. *J Biol Chem* **270**, 20698–20702 (1995).

37. McArdle, H. J., Bingham, M. J., Summer, K. & Ong, T. J. Cu metabolism in the liver. *Adv Exp Med Biol* **448**, 29–37 (1999).

38. Mansoor, M. A. *et al.* Correlation between plasma total homocysteine and copper in patients with peripheral vascular disease. *Clin Chem* **46**, 385–391 (2000).

39. Chen, J. & Liu, Q. Copper ion' inhibition on activity of S-Adenosylhomocysteine hydrolase. *Chin Sci Bull* **47**, 421–424 (2002).

40. Li, Y., Chen, J., Liu, J., Yang, X. & Wang, K. Binding of Cu^{2+} to S-adenosyl-L-homocysteine hydrolase. *J Inorg Biochem* **98**, 977–983 (2004).

41. Gohara, D. W. & Di Cera, E. Molecular Mechanisms of Enzyme Activation by Monovalent Cations. *J Biol Chem* **291**, 20840–20848 (2016).

42. Larsen, T. M., Laughlin, L. T., Holden, H. M., Rayment, I. & Reed, G. H. Structure of rabbit muscle pyruvate kinase complexed with Mn^{2+}, K$^+$, and pyruvate. *Biochemistry* **33**, 6301–6309 (1994).

43. Viitanen, P. V. *et al.* Chaperonin-facilitated refolding of ribulosebisphosphate carboxylase and ATP hydrolysis by chaperonin 60 (groEL) are K$^+$ dependent. *Biochemistry* **29**, 5665–5671 (1990).

44. Villeret, V., Huang, S., Fromm, H. J. & Lipscomb, W. N. Crystallographic evidence for the action of potassium, thallium, and lithium ions on fructose-1,6-bisphosphatase. *Proc Natl Acad Sci USA* **92**, 8916–8920 (1995).

45. Komoto, J., Yamada, T., Takata, Y., Markham, G. D. & Takusagawa, F. Crystal structure of the *S*-adenosylmethionine synthetase ternary complex: a novel catalytic mechanism of *S*-adenosylmethionine synthesis from ATP and Met. *Biochemistry* **43**, 1821–1831 (2004).

46. Wu, Y., He, Y., Moya, I. A., Qian, X. & Luo, Y. Crystal structure of archaeal recombinase RADA: a snapshot of its extended conformation. *Mol Cell* **15**, 423–435 (2004).

47. Toraya, T., Sugimoto, Y., Tamao, Y., Shimizu, S. & Fukui, S. Propanediol dehydratase system. Role of monovalent cations in binding of vitamin B12 coenzyme or its analogs to apoenzyme. *Biochemistry* **10**, 3475–3484 (1971).

48. Wheatley, R. W., Juers, D. H., Lev, B. B., Huber, R. E. & Noskov, S. Y. Elucidating factors important for monovalent cation selectivity in enzymes: *E. coli* β-galactosidase as a model. *Phys Chem Chem Phys* **17**, 10899–10909 (2015).

49. Marcus, F. & Hosey, M. M. Purification and properties of liver fructose 1,6-bisphosphatase from C57BL/KsJ normal and diabetic mice. *J Biol Chem* **255**, 2481–2486 (1980).

50. Wu, Y., Qian, X., He, Y., Moya, I. A. & Luo, Y. Crystal structure of an ATPase-active form of Rad51 homolog from *Methanococcus voltae*. Insights into potassium dependence. *J Biol Chem* **280**, 722–728 (2005).

51. Paul, R., Patra, M. D. & Sen, U. Crystal structure of apo and ligand bound *Vibrio cholerae* ribokinase (Vc-RK): role of monovalent cation induced activation and structural flexibility in sugar phosphorylation. *Adv Exp Med Biol* **842**, 293–307 (2015).

52. Hohenester, E., Keller, J. W. & Jansonius, J. N. An alkali metal ion size-dependent switch in the active site structure of dialkylglycine decarboxylase. *Biochemistry* **33**, 13561–13570 (1994).

53. AEvarsson, A. *et al.* Crystal structure of human branched-chain alpha-ketoacid dehydrogenase and the molecular basis of multienzyme complex deficiency in maple syrup urine disease. *Structure* **8**, 277–291 (2000).

54. Woehl, E. U. & Dunn, M. F. Monovalent metal ions play an essential role in catalysis and intersubunit communication in the tryptophan synthase bienzyme complex. *Biochemistry* **34**, 9466–9476 (1995).
55. Peracchi, A., Mozzarelli, A. & Rossi, G. L. Monovalent cations affect dynamic and functional properties of the tryptophan synthase alpha 2 beta 2 complex. *Biochemistry* **34**, 9459–9465 (1995).
56. Dunn, M. F. Allosteric regulation of substrate channeling and catalysis in the tryptophan synthase bienzyme complex. *Arch Biochem Biophys* **519**, 154–166 (2012).
57. Vogt, A. D., Bah, A. & Di Cera, E. Evidence of the E*-E equilibrium from rapid kinetics of Na$^+$ binding to activated protein C and factor Xa. *J Phys Chem B* **114**, 16125–16130 (2010).
58. Vogt, A. D., Chakraborty, P. & Di Cera, E. Kinetic dissection of the pre-existing conformational equilibrium in the trypsin fold. *J Biol Chem* **290**, 22435–22445 (2015).
59. Lechtenberg, B. C., Johnson, D. J. D., Freund, S. M. V. & Huntington, J. A. NMR resonance assignments of thrombin reveal the conformational and dynamic effects of ligation. *Proc Nat. Acad Sci USA* **107**, 14087–14092 (2010).
60. Klock, H. E., Koesema, E. J., Knuth, M. W. & Lesley, S. A. Combining the polymerase incomplete primer extension method for cloning and mutagenesis with microscreening to accelerate structural genomics efforts. *Proteins* **71**, 982–994 (2008).
61. Cer, R. Z., Mudunuri, U., Stephens, R. & Lebeda, F. J. IC_{50}-*to*-K_i; a web-based tool for converting IC50 to Ki values for inhibitors of enzyme activity and ligand binding. *Nucleic Acids Res* **37**, W441–W445 (2009).
62. Otwinowski, Z. & Minor, W. Processing of X-ray diffraction data collected in oscillation mode. *Methods Enzymol* **276**, 307–326.
63. Sparta, K. M., Krug, M., Heinemann, U., Mueller, U. & Weiss, M. S. *XDSAPP2.0. J Appl Crystallogr* **49**, 1085–1092 (2016).
64. Kabsch, W. *XDS. Acta Crystallogr D Biol Crystallogr* **66**, 125–132 (2010).
65. McCoy, A. J. *et al. Phaser* crystallographic software. *J Appl Crystallogr* **40**, 658–674 (2007).
66. Winn, M. D. *et al.* Overview of the CCP4 suite and current developments. *Acta Crystallogr D Biol Crystallogr* **67**, 235–242 (2011).
67. Langer, G., Cohen, S. X., Lamzin, V. S. & Perrakis, A. Automated macromolecular model building for X-ray crystallography using ARP/wARP version 7. *Nat Protoc* **3**, 1171–1179 (2008).
68. Murshudov, G. N. *et al. REFMAC* 5 for the refinement of macromolecular crystal structures. *Acta Crystallogr D Biol Crystallogr* **67**, 355–367 (2011).
69. Winn, M. D., Isupov, M. N. & Murshudov, G. N. Use of TLS parameters to model anisotropic displacements in macromolecular refinement. *Acta Crystallogr D Biol Crystallogr* **57**, 122–133 (2001).
70. Painter, J. & Merritt, E. A. *TLSMD* web server for the generation of multi-group TLS models. *J Appl Crystallogr* **39**, 109–111 (2006).
71. Zheng, H. *et al. CheckMyMetal*: a macromolecular metal-binding validation tool. *Acta Crystallogr D Struct Biol* **73**, 223–233 (2017).
72. Emsley, P., Lohkamp, B., Scott, W. G. & Cowtan, K. Features and development of *Coot. Acta Crystallogr D Biol Crystallogr* **66**, 486–501 (2010).
73. Berman, H., Henrick, K. & Nakamura, H. Announcing the worldwide Protein Data Bank. *Nat Struct Biol* **10**, 980–980 (2003).
74. Krissinel, E. & Henrick, K. Secondary-structure matching (SSM), a new tool for fast protein structure alignment in three dimensions. *Acta Crystallogr D Biol Crystallogr* **60**, 2256–2268 (2004).
75. Schrödinger, LLC. The PyMOL Molecular Graphics System. *Version* 1.8. (2015).
76. Sievers, F. *et al.* Fast, scalable generation of high-quality protein multiple sequence alignments using Clustal Omega. *Mol Syst Biol* **7**, 539 (2011).

Acknowledgements

Author Contributions

J.C. expressed and purified the enzyme, performed enzyme kinetics and inhibition studies, J.S. performed isothermal titration calorimetry experiments, B.I. expressed and purified the mutated enzyme, Z.G. performed ^{23}Na NMR analysis, M.J. analyzed the data and wrote the paper, K.B. designed all experiments, performed the crystallographic studies, analyzed the data, and wrote the paper.

Additional Information

Supplementary information accompanies this paper at https://doi.org/10.1038/s41598-018-29535-y.

Competing Interests: The authors declare no competing interests.

Publisher's note: Springer Nature remains neutral with regard to jurisdictional claims in published maps and institutional affiliations.

Electronic Supplementary Information for

Metal-cation regulation of enzyme dynamics is a key factor influencing the activity of
S-adenosyl-L-homocysteine hydrolase
from *Pseudomonas aeruginosa*

Justyna Czyrko[1], Joanna Sliwiak[2], Barbara Imiolczyk[2], Zofia Gdaniec[3], Mariusz Jaskolski[2,4], & Krzysztof Brzezinski[1*]

[1] Laboratory of Biochemistry and Structural Biology, Institute of Chemistry, University of Bialystok, Poland

[2] Center for Biocrystallographic Research, Institute of Bioorganic Chemistry, Polish Academy of Sciences, Poznan, Poland

[3] Laboratory of Biomolecular NMR, Institute of Bioorganic Chemistry, Polish Academy of Sciences, Poznan, Poland

[4] Department of Crystallography, Faculty of Chemistry, A. Mickiewicz University, Poznan, Poland

*To whom correspondence should be addressed,
Email: k.brzezinski@uwb.edu.pl

Table of Contents

Table S1. Crystallographic data, data collection and structure refinement statistics. Values in parentheses are for the last resolution shell.

Added ligand/present cation(s)	Ado/K^+/Zn^{2+}	2'-dAdo/K^+/Zn^{2+}	3'-dAdo/K^+	2'-dAdo/Rb^+
Data collection				
Beamline	BESSY 14.2	BESSY 14.3	APS 22-ID	BESSY 14.1
Wavelength (Å)	0.9184	0.8950	1.0000	0.8077
Temperature (K)	100	100	100	100
Space group	*C*2	*C*2	*C*2	*C*2
Unit-cell parameters (Å,°)				
a	175.98	170.84	142.90	170.49
b	104.14	99.61	85.74	99.44
c	107.63	111.82	112.01	111.71
β	100.7	102.0	122.2	101.9
Resolution (Å)	50.0 – 1.60 (1.69 – 1.60)	25.0 – 1.75 (1.81 – 1.75)	30.0 – 1.35 (1.40 – 1.35)	50.0 – 1.45 (1.54 – 1.45)
Mosaicity (°)	0.1	0.4	0.6	0.1
Completeness (%)	97.8 (90.0)	99.9 (99.5)	98.6 (95.8)	98.6 (97.7)
Multiplicity	3.2 (2.8)	4.2 (4.2)	2.9 (2.6)	4.0 (4.0)
$\langle I/\sigma(I)\rangle$	14.9 (3.0)	17.6 (3.2)	13.1 (2.0)	16.6 (3.3)
R_{merge}†	0.061 (0.403)	0.078 (0.415)	0.066 (0.481)	0.049 (0.340)
Refinement statistics				
Working/test reflections	242459/2450	181035/1806	244097/1220	315012/3343
R/R_{free}‡	0.151/0.174	0.140/0.167	0.101/0.127	0.093/0.124
No. of atoms				
Protein	14335	14445	7401	14554
Ligand	76	40	36	40
NAD^+	176	176	88	176
Water	2021	1632	1132	2166
Phosphate ions	4	8	2	8
Cl^- ions	-	-	2	-
K^+ ions	4	4	2	-
Zn^{2+} ions	4	2	-	-
Rb^+ ions	-	-	-	5
Glycerol molecules	3	1	-	1
PEG molecules	-	-	-	1
R.m.s.d. from ideality				
bond lengths (Å)	0.013	0.015	0.016	0.018
bond angles (°)	1.58	1.66	1.77	1.80
Average B factor (Å²)	27.0	26.0	19.0	17.0
Ramachandran statistics (%)				
Most favored regions	98	98	98	98
Allowed regions	2	2	2	2
PDB code	6F3M	6F3O	6F3P	6F3Q

Table S2. Polar interactions with the ligand molecules bound in active site of PaSAHase, with the corresponding donor-acceptor distances (Å) in parentheses. Amino acid residues from the substrate (*) and cofactor (#) binding domains, as well as the monovalent cation coordinating loop ($) are involved in ligand binding. The interactions in all four subunits are almost identical; therefore, the distances are only listed for subunit A.

Protein/Phosphate atom	Ado/K$^+$/Zn^{2+} Adenosine atom	2'-dAdo/K$^+$/Zn^{2+} Adenine/Phosphate atom	2'-dAdo/Rb$^+$ Adenine/Phosphate atom	3'-dAdo/K$^+$ Cordycepin atom
*T63 Oγ	N1 (2.75)	N1 (2.74)	N1 (2.69)	N1 (2.73)
*Q65 Oε	N6 (2.85)	N6 (2.84)	N6 (2.87)	N6 (2.87)
$H382 O	N6 (3.11)	N6 (3.12)	N6 (3.04)	N6 (3.09)
$H382 N	N7 (2.95)	N7 (2.89)	N7 (2.93)	N7 (2.94)
Phosphate O2	-	N9 (3.18)	N9 (3.16)	-
Phosphate O4	-	N9 (2.96)	N9 (2.93)	-
*E164 Oε2	O2' (2.67)	O3 (2.59)	O3 (2.49)	O2' (2.61)
#D198 Oδ1	-	O2 (2.87)	O2 (2.76)	-
#D198 Oδ2	O2' (2.50)	O3 (2.65)	O3 (2.49)	O2' (2.56)
*T165 Oγ	O3' (2.70)	O1 (2.72)	O1 (2.79)	-
#K194 Nζ	O3' (2.78)	O1 (2.78)	O1 (2.68)	-
*H61 Nε2	O5' (2.77)	-	-	O5' (2.90)
*D139 Oδ1	O5' (2.76)	-	-	O5' (2.66)
*D139 Oδ2	-	O4 (2.71)	O4 (2.62)	-
#H323 Nδ1	O5' (2.68)	-	-	O5' (2.63)

Table S3. Details of alkali cation coordination near the active site of PaSAHase in all four complex structures with the corresponding cation-ligand distances in Å. The distances are listed for all chains (A-D).

Ligand atom:	Q65 Oε1	T380 O	T380 Oγ	H382 O	Wat1	Wat2	Wat3
Ado/K$^+$/Zn^{2+}							
A	3.21	2.71	2.83	2.74	2.74	3.09	2.82
B	3.18	2.68	2.90	2.74	2.75	3.06	2.80
C	3.20	2.70	2.86	2.73	2.78	3.06	2.84
D	3.19	2.68	2.83	2.76	2.80	3.08	2.76
2'-dAdo/K$^+$/Zn^{2+}							
A	3.20	2.70	2.80	2.78	2.81	2.95	2.86
B	3.18	2.62	2.85	2.81	2.82	3.01	2.83
C	3.17	2.65	2.88	2.80	2.76	3.07	2.83
D	3.19	2.61	2.89	2.77	2.80	2.96	2.76
3'-dAdo/K$^+$							
A	3.20	2.72	2.84	2.75	2.74	3.08	2.78
C	3.17	2.71	2.84	2.73	2.76	3.09	2.81
2'-dAdo/Rb$^+$							
A	3.22	2.84	2.88	2.87	2.94	3.12	3.01
B	3.20	2.84	2.90	2.88	2.90	3.18	2.97
C	3.21	2.84	2.88	2.88	2.92	3.14	2.99
D	3.22	2.83	2.91	2.89	2.92	3.14	2.98

Table S4. Comparison of the monovalent cation interactions with the anchoring glutamine or glutamate residue near the active site of selected SAHase models in the closed conformation.

Enzyme source	PDB ID	approaching residue	cation	type of interaction
P. aeruginosa	this work	Q65	K^+	direct
B. melitensis	3N58	Q59	K^+	direct
B. elkani	4LVC	Q62	NH_4^+	*via* water molecule
B. elkani	5M5K	Q62	Na^+	direct
M. tuberculosis	3CE6	Q73	Na^+	*via* water molecule
B. pseudomallei	3GLQ	Q66	Na^+	direct
L. luteus	3OND	Q66	Na^+	*via* water molecule
H. sapiens	1LI4	E59	Na^+ or NH_4^+	direct
P. falciparum	1V8B	E58	Na^+	*via* water molecule
N. fowleri	5V96	E63	Na^+	direct

Table S5. Details of zinc coordination in two complex structures, with the corresponding ligand-Zn^{2+} distances in Å. The interactions are listed for all four (A-D) subunits.

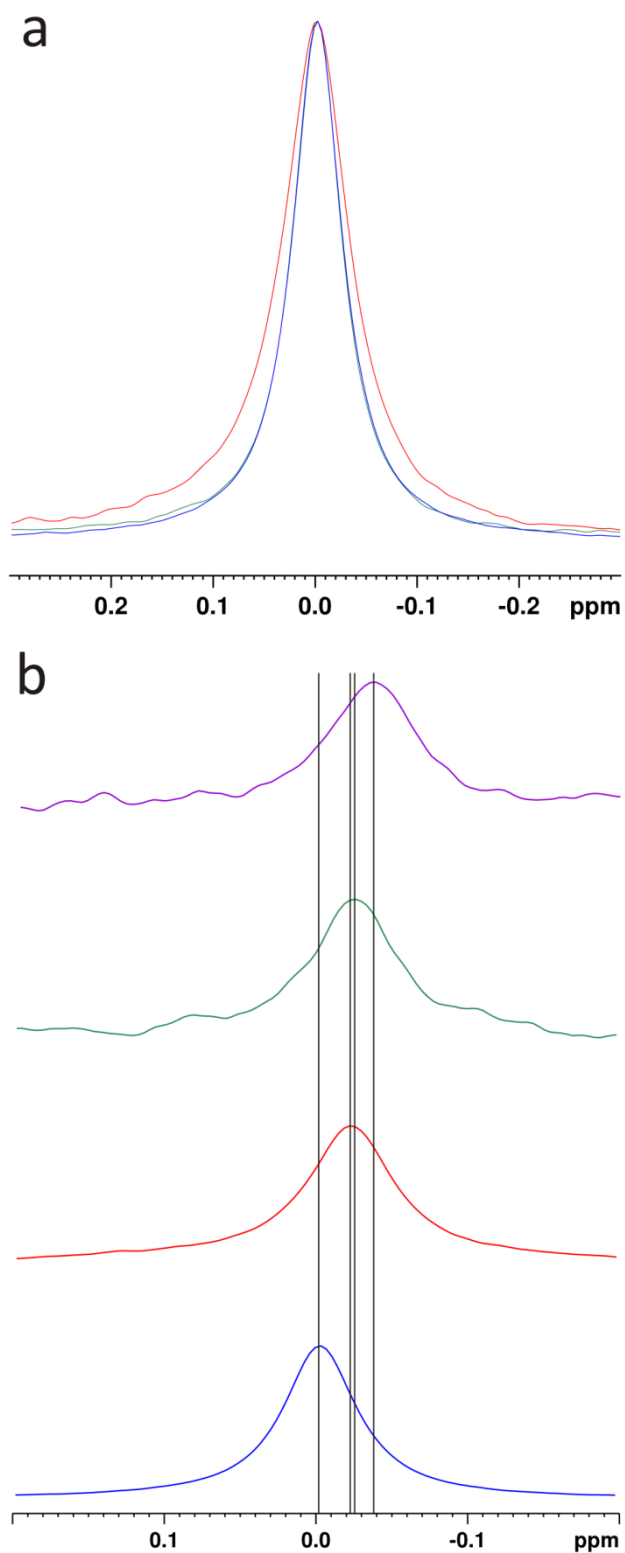| Ligand atom:	C85 Sγ	D139 O	D139 Oδ1	H323 Nε1	Zn^{2+} occupancy
Ado/K^+/Zn^{2+}					
A	2.32	2.22	2.11	2.07	0.5
B	2.35	2.30	2.12	2.09	0.5
C	2.38	2.19	2.14	2.05	0.5
D	2.33	2.26	2.11	2.11	0.5
2'-dAdo/K^+/Zn^{2+}					
A	2.32	2.09	2.42	2.13	0.11
D	2.29	2.13	2.39	2.19	0.19

Figure S1. Comparison of ^{23}Na NMR spectra of solutions containing: (a) 5 mM NaCl (green), 5mM NaCl + 1 mM Ado (blue), and 5 mM NaCl + 0.3 mM PaSAHase (Enz, red); (b) 5 mM NaCl (blue), 0.3 mM Enz + 5 mM NaCl + 1 mM Ado ([Enz]/[Na$^+$]=1:16.7, red), 0.3 mM Enz + 0.6 mM NaCl + 1 mM Ado ([Enz]/[Na$^+$]=1:2, green), 0.3 mM Enz + 0.3 mM NaCl + 1 mM Ado ([Enz]/[Na$^+$]=1:1, purple). All samples were prepared in 50 mM Tris·HCl at pH 7.5.
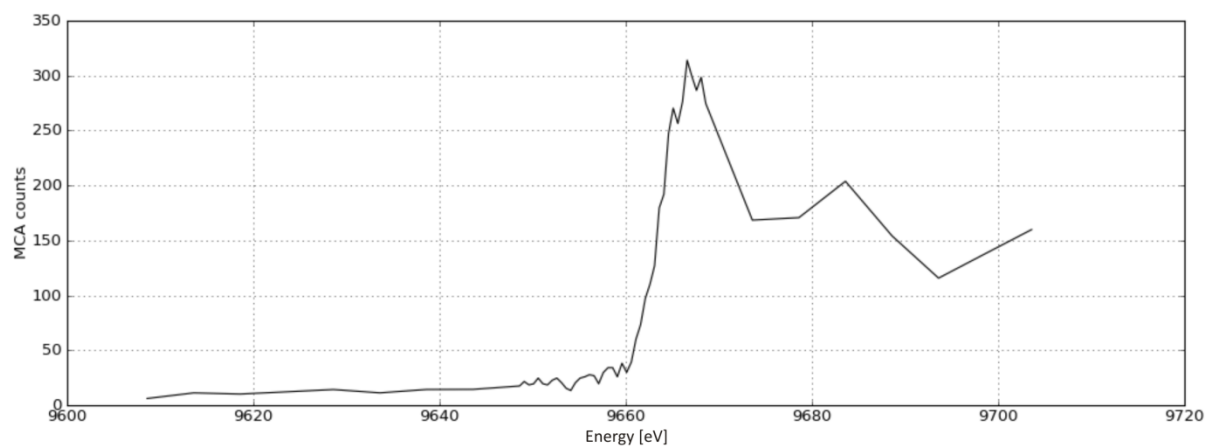
6

Figure S2. X-ray fluorescence spectrum recorded for PaSAHase sample co-purified with Zn^{2+} ions.

Crystal Structure of *S*-adenosyl-L-homocysteine Hydrolase from *Cytophaga hutchinsonii*, a Case of Combination of Crystallographic and Non-crystallographic Symmetry

Justyna Czyrko,[1] Mariusz Jaskolski,[2,3] Krzysztof Brzezinski[1,*]

[1] Laboratory of Biochemistry and Structural Biology, Institute of Chemistry, University of Bialystok, Poland

[2] Center for Biocrystallographic Research, Institute of Bioorganic Chemistry, Polish Academy of Sciences, Poznan, Poland

[3] Department of Crystallography, Faculty of Chemistry, A. Mickiewicz University, Poznań, Poland

[*] Corresponding author's e-mail address: k.brzezinski@uwb.edu.pl

THIS PAPER IS DEDICATED TO DR. BISERKA KOJIĆ-PRODIĆ ON THE OCCASION OF HER 80TH BIRTHDAY

Abstract: The majority of living organisms utilize *S*-adenosyl-L-homocysteine hydrolase (SAHase) as a key regulator of cellular methylation reactions. The unusual evolution history of SAHase genes is reflected in the phylogeny of these proteins, which are grouped into two major domains: mainly archaeal and eukaryotic/bacterial. Such a phylogeny is in contradiction to the three-domain topology of the tree of life, commonly based on 16S rRNA sequences. Within the latter domain, SAHases are classified as eukaryotic-only or bacterial-only clades depending on their origin and sequence peculiarities. A rare exception in this classification is SAHase from a cellulose-utilizing soil bacterium *Cytophaga hutchinsonii* (ChSAHase), as the phylogenetic analyses indicate that ChSAHase belongs to the animal clade. Here, the $P2_12_12$ crystal structure of recombinant ChSAHase in ternary complex with the oxidized form of the NAD^+ cofactor and a reaction product/substrate (adenosine) is presented. Additionally, a sodium cation was identified in close proximity of the active site. The crystal contains two translational NCS-related intimate dimers of ChSAHase subunits in the asymmetric unit. Two complete tetrameric enzyme molecules are generated from these dimers within the crystal lattice through the operation of crystallographic twofold axes in the *z* direction.

Keywords: cellular methylation, *S*-adenosyl-L-homocysteine (SAH), *S*-adenosyl-L-methionine (SAM), cellulose degradation, X-ray crystallography, crystallographic symmetry, non-crystallographic symmetry (NCS), translational non-crystallographic symmetry (tNCS).

INTRODUCTION

S-ADENOSYL-L-METHIONINE (SAM) is the most common donor of methyl group in cellular methylation of a wide range of small- and macromolecular substrates.[1] During the methyl-group transfer, SAM is converted to *S*-adenosyl-L-homocysteine (SAH), which is a strong, negative-feedback inhibitor of SAM-dependent methyl-transferases and must be therefore efficiently removed. *S*-adenosyl-L-homocysteine hydrolase (SAHase) serves this purpose by catalyzing the reversible decomposition of SAH to adenosine (Ado) and L-homocysteine (Hcy). The equilibrium of this reaction is shifted far into the direction of SAH synthesis. Moreover, the activity of SAHase is inhibited by adenosine, which is a product of the hydrolysis reaction.[2,3] However, under physiological conditions, Ado and Hcy are rapidly removed from the environment and the net result is SAH hydrolysis.

SAHases usually function as 222-symmetric homotetramers,[4–11] or sometimes as homodimers.[3,12] Each subunit of the enzyme contains a tightly but non-covalently bound nicotinamide adenine dinucleotide cofactor in its oxidized form, NAD^+. Each monomer is comprised of two large domains, namely the substrate- and cofactor-binding domains, which are separated by a deep interdomain cleft. Additionally, each subunit contains a

small C-terminal domain that plays a role in cofactor binding and protein oligomerization. The two principal domains (i.e., the substrate- and cofactor-binding domains) of the SAHase subunit are connected by two linker regions, folded as α-helical segments. During the catalytic cycle the enzyme oscillates between two conformational states: open (when ligand-free) and closed (ligand-bound). The open-closed movement of the domains is hinged upon the linker regions, which act like torsion-retorsion springs. The substrate/product delivery to/from the active site is regulated by a pair of highly conserved His-Phe residues, which function as a molecular gate.[3,7,8] Depending on the conformation of the gate, the entrance to the substrate-pocket access channel can be open or shut. Additionally, in the closed conformation, the enzyme coordinates a monovalent cation in close proximity of one of the hinge regions and of the active site area.

SAHase genes are present in the majority of (but not all) simple and complex organisms, including prokaryotic and eukaryotic microorganism, as well as plants and animals. However, they have evolved in an unusual way, and therefore the phylogeny of these enzymes is in contradiction to the three-domain topology of the tree of life, commonly based on 16S rRNA sequences.[13] In the phylogenetic analyses, SAHases are grouped into two major families, containing mainly archaeal or mainly eukaryotic/bacterial enzymes. Within the latter family, SAHases are classified depending on their origin and form, as eukaryotic-only or bacterial-only clades. A rare exception in this classification is SAHase from *Cytophaga hutchinsonii* (ChSAHase), a cellulose-utilizing soil bacterium, as in phylogenetic sequence analyses it is grouped within the animal clade, which suggests a late event of horizontal gene transfer.

In the present study, we have determined the crystal structure of the recombinant ChSAHase enzyme. The structure shows not only the enzyme complexed with one of the products of its hydrolytic reaction (adenosine), but also presents a case of a combination of crystallographic and non-crystallographic (NCS) symmetry. Although the asymmetric unit of the ChSAHase crystal contains indeed four subunits of the enzyme, they do not form one functional tetrameric unit. Instead, they are assembled into two dimers, located at two different crystallographic twofold axes, whose operation recreates two tetramers that are related by non-crystallographic translation (tNCS).

RESULTS AND DISCUSSION

Preparation and Crystallization of Recombinant ChSAHase

The expression and purification procedure was adjusted in order to obtain active, pure and homogeneous

ChSAHase samples. Due to the fact that ChSAHase has a tendency to precipitate suddenly at higher concentrations, is was important to keep all the enzyme solutions at concentrations below 8 mg/mL. A similar effect of protein concentration on its stability in solution was observed for plant SAHase from yellow lupine.[3,14] Typical yields of ChSAHase were 10 mg of pure enzyme from 1 liter of expression culture. The effects of protein concentration and crystallization drop volume were investigated for optimization of the crystallization process. The best, diffraction-quality crystals were obtained using the hanging-drop vapor-diffusion method by mixing 2.5 μL of protein solution at 7.5 mg/mL, preincubated at 1:13 molar ratio with adenosine, with 2.5 μL of reservoir solution containing 15 % (*w/v*) PEG 8000 and 0.5 M Li_2SO_4. Under the optimized conditions, diffraction-quality crystals grew within ten days. The crystals are orthorhombic, space group $P2_12_12$ with unit cell parameters a = 96.28, b = 102.44, and c = 188.92 Å. The Matthews coefficient[15] was consistent with four protein chains of this tetrameric enzyme in the asymmetric unit (V_M = 2.43 Å^3/Da, solvent content 49.4 %). The native Patterson function showed a strong non-origin peak with 47 % of the origin peak height and located at 0, 0.5, 0.424, indicating translational non-crystallographic symmetry (tNCS) with a translation vector of ≈95 Å (Figure 1).

Determination of the Oligomerization State

SAHases are typically active as homotetramers. Recombinant ChSAHase is not an exception in this respect, as confirmed by ultrafiltration and SEC-FPLC (Figures 2A, 2B). For the enzyme concentration steps, we used ultracentrifugation membranes with 100 kDa cutoff and no protein was detected in the supernatant. This experiment clearly indicated that ChSAHase does not exist as a monomer (48 kDa) or dimer (96 kDa) in solution. The last step of protein purification was carried out using size exclusion chromatography (SEC). In this experiment, the recombinant enzyme was eluted in fractions corresponding to molecular mass of ≈200 kDa, indicating again the tetrameric state of ChSAHase (192 kDa).

Enzymatic Studies

Enzymatic activity assays with recombinant ChSAHase were performed in the direction of SAH hydrolysis and the following kinetic parameters were determined: the catalytic rate (k_{cat}) of the reaction is 0.042 ± 0.003 s^{-1}, substrate affinity (K_M) is 15.2 ± 1.6 μM, and the maximum velocity (V_{max}) is 2.60 ± 0.15 μM s^{-1}. The results of the kinetic analysis are shown in Figure 3.
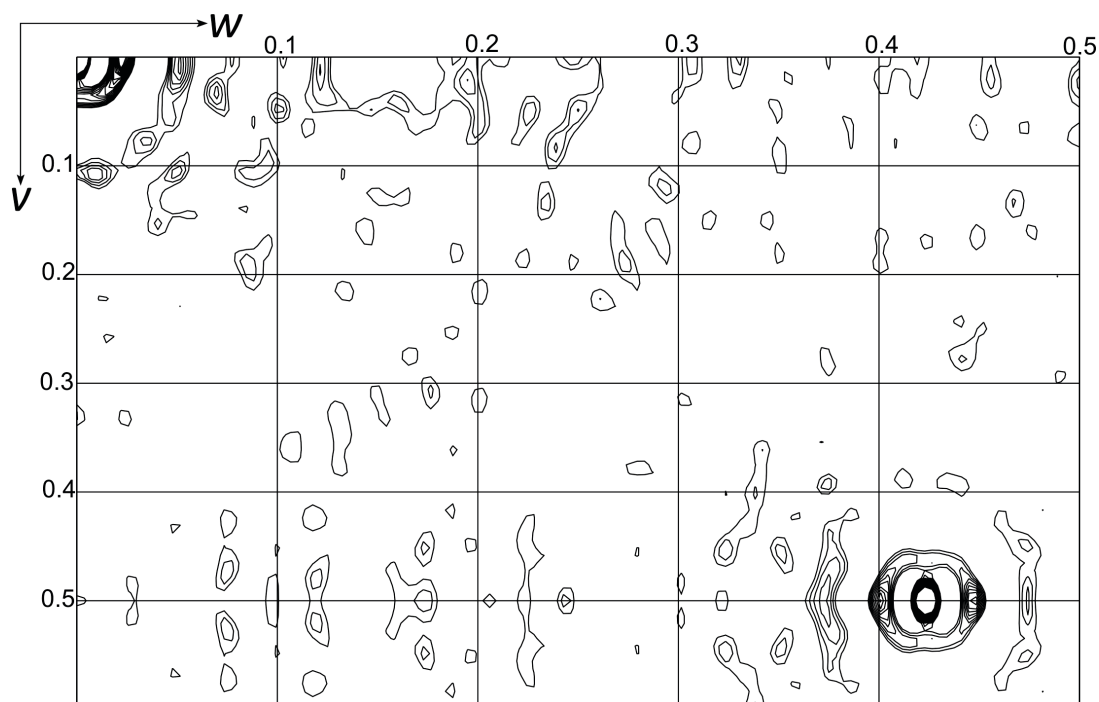
Figure 1. Section $u = 0$ of native Patterson function reveals a very significant non-origin peak at 0, 0.5, 0.424 which indicates the presence of tNCS corresponding to a translational vector of ≈95 Å.
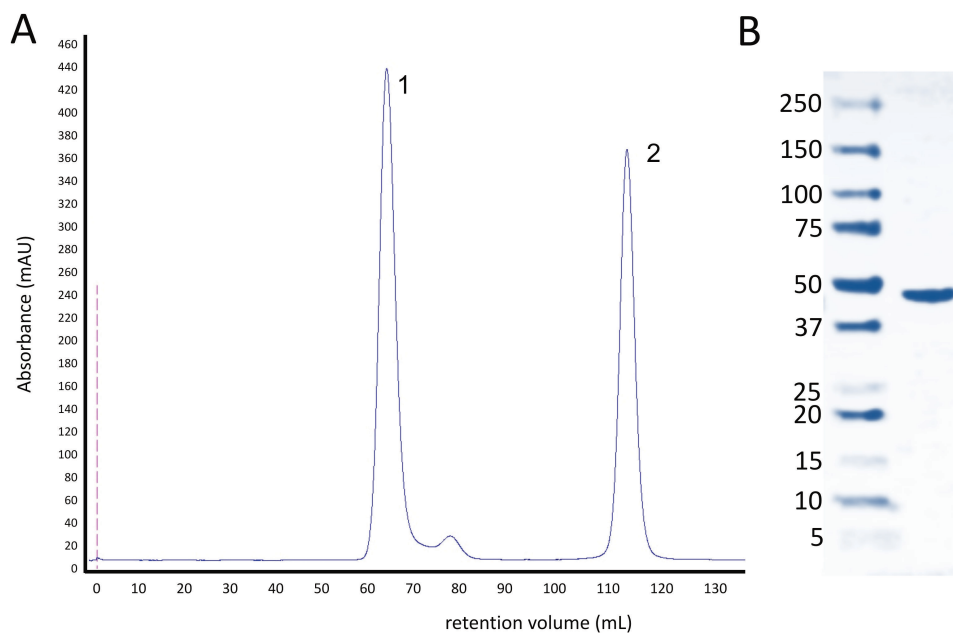

Figure 2. Purification and initial characterization of ChSAHase samples. (A) The final size exclusion chromatographic purification step recorded at 280 nm. Peak 1 corresponds to the tetrameric form of ChSAHase with the approximate molecular mass of ≈200 kDa, whereas peak 2 contains excess of the NAD+ cofactor used for saturation of the apo form of the enzyme. (B) Chromatographic peak 1 fractions analyzed by SDS-PAGE (right lane) to confirm the correct size of the monomer of the recombinant ChSAHase protein. Molecular mass markers are shown in the left lane.
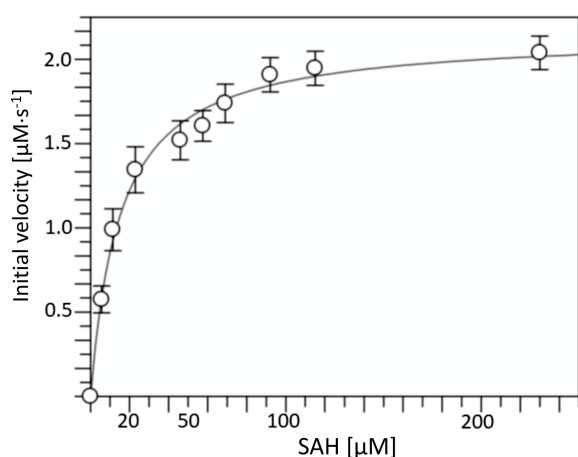
Figure 3. Kinetic analysis of recombinant ChSAHase determined using variable concentrations (from 0 to 230 µM) of *S*-adenosyl-ʟ-homocysteine (SAH) as a substrate. Conversion of Hcy to Hcy-TNB was monitored spectrophotometrically at 412 nm. Initial velocities (in µM s⁻¹) were estimated from the linear region of the recorded curve. The values were obtained as averages of two replicates, bars represent standard error of the mean values (SEM).

Overall Structure of ChSAHase

ChSAHase crystalizes in space group $P2_12_12$ with two tNCS-related intimate dimers (labeled AB and CD) in the asymmetric unit (Figure 4). The conformation of the dimers is virtually identical, as illustrated by the r.m.s. deviation of 0.18 Å for the superposition of their 863 Cα atoms. Also the superposition of the individual subunits in each dimer is characterized by a similar r.m.s.d. value, at a rotation of ≈179.7° in each case, indicating a nearly perfect non-crystallographic symmetry of the intimate dimers. Each subunit, comprised of 435 amino acid residues, with a molecular mass of about 48 kDa, binds one adenosine (Ado, substrate or product) molecule and one NAD⁺ (cofactor) molecule, as well as one sodium cation in the active site area. The structural organization of the subunit is similar to other SAHases and is shown in Figure 5. The fold consists of two large, well-separated main domains, the substrate-binding domain (residues 1–183 and 361–388) and the cofactor-binding domain (residues 196–355), plus an additional, small C-terminal dimerization domain (389–435). In the present crystal structure, each ChSAHase subunit adopts an adenosine-induced closed conformation. The precise location of the interdomain hinge regions is
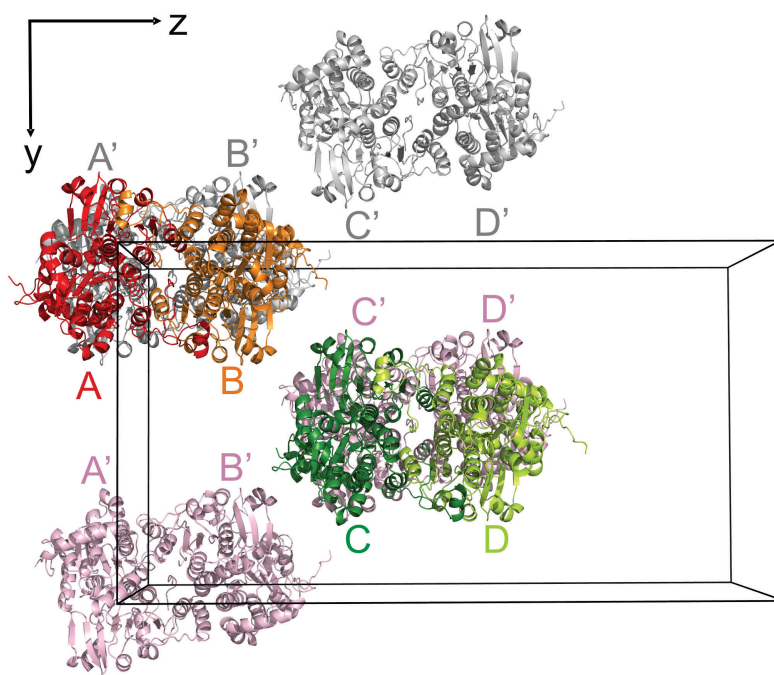

Figure 4. The two independent tNCS-related intimate dimers of ChSAHase forming the asymmetric part of the unit cell (outline), shown in a view along the *x* axis using ribbon representations colored red/orange (AB) and green/lime (CD). The two complete ChSAHase homotetramers are generated within the crystal lattice through the operation of crystallographic twofold axes along the *z* direction. Symmetry-related molecules A′B′ and C′D′ generated by crystallographic twofold axes at 0, 0 and 0, 0.5 are shown in gray and light pink, respectively.
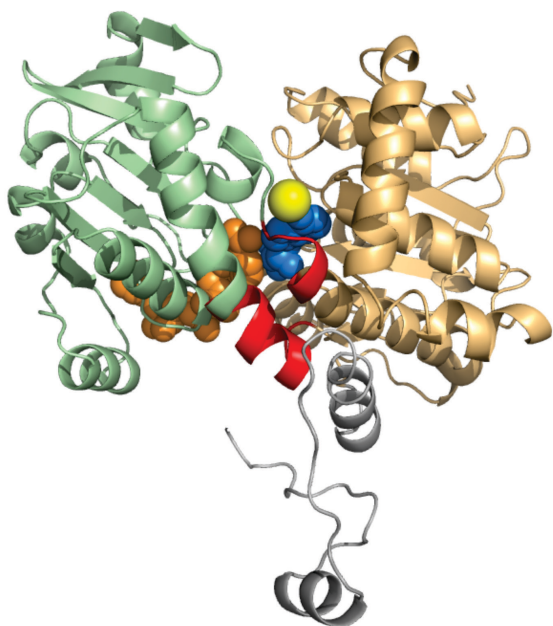
Figure 5. A ribbon diagram presenting the structure of one subunit (A) of ChSAHase in the closed conformation with the domains color-coded as follows: the substrate-binding domain (residues 1–183 and 361–388) is shown in light orange, the cofactor binding domain (residues 196–355) is shown in green, and the C-terminal domain (residues 389–435) is shown in gray. The two interdomain hinges (residues 184–195 and 356–360) linking the substrate and cofactor domains are shown in red. The NAD$^+$ cofactor (orange), adenosine (blue) and sodium cation (yellow) are shown in space-filling representation.

usually established by comparison of the open and closed conformations. Since this is not possible for ChSAHase, its linker segments (D184–K195 and H356–V360) were demarcated by sequence alignment with another bacterial SAHase, from *Bradyrhizobium elkanii*.[8,16]

A striking difference between the two tNCS-related intimate dimers AB and CD is visible in their mobility. The AB dimer is less flexible with the mean ADP (atomic displacement parameter) for main-chain atoms of 32.1 Å^2. The corresponding mean ADP value for the CD dimer is higher, 53.7 Å^2 Additionally, in the structure of the CD dimer significantly more side-chains (95 *vs* 40 in AB) were modeled with partial occupancy because of poorly defined electron density, which is usually a hallmark of high mobility and disorder. Despite the higher mobility of the CD dimer, the electron density maps were of very good quality, allowing unambiguous tracing of the main chain of all subunits. The exceptions are the N-terminal segments of chains A (M1-D3) and C (M1-F5) as well as all the artifactual cloning tripeptides, which could not be modeled because of disorder.

Table 1. Polar interactions with the adenosine molecule bound in the active site of ChSAHase, with the corresponding donor-acceptor distances (Å) in parentheses. Amino acid residues from the substrate (*) and cofactor (#) binding domains, as well as the monovalent cation coordinating loop ($) are involved in ligand binding. The interactions in all four subunits are almost identical; therefore, the distances are listed only for subunit A

Protein atom	Adenosine atom
*T58 Oγ	N1 (2.79)
*Q60 Oε	N6 (2.98)
$H356 O	N6 (3.15)
$H356 N	N7 (2.90)
*E159 Oε2	O2' (2.83)
#D193 Oδ2	O2' (2.63)
*T160 Oγ	O3' (2.84)
#K189 Nζ	O3' (2.99)
*H56 Nε2	O5' (2.96)
*D134 Oδ1	O5' (2.70)
#H304 Nδ1	O5' (2.62)

Within the crystal lattice, crystallographic symmetry generates two complete ChSAHase tetramers, ABA'B' and CDC'D', through the operation of two different twofold axes, both along the *z* direction (Figure 4). Since the structure of the ABA'B' tetramer is more rigid and complete, it will be used for further descriptions and comparisons, unless stated otherwise.

Enzyme-ligand Interactions

The crystal structure of ChSAHase was determined for a ternary complex with Ado substrate/product and NAD$^+$ cofactor. These two ligands are present in all subunits and are located in the active site (Ado) or in the crevice between the substrate- and cofactor-binding domains (NAD$^+$). Their ligand binding modes are presented in Table 1 (Ado) and Table 2 (NAD$^+$), and in Figures 6A and 6B, respectively. Additionally, one sodium cation is found in each subunit in close proximity of the active site. Its coordination mode is presented in Table 3 and Figure 6C. SAHases are highly conserved proteins, therefore it is not surprising that their interactions with both ligands, as well as with the monovalent cation are very similar among SAHases of various origin.[3,4,6–9,11,16]

The Mode of Adenosine Binding

The substrate-binding site of SAHases is formed by highly conserved amino acid residues. Therefore, the binding mode of Ado is similar to those observed in SAHases of various origin complexed with adenosine or its analogs. The amino acid residues involved in Ado binding are contributed by the two principal domains (Figure 6A). The

Table 2. Polar interactions with the NAD⁺ molecule bound in the cofactor binding site of ChSAHase with the corresponding donor-acceptor distances (Å) in parentheses. Amino acid residues from the substrate (*) and cofactor (#) binding domains, as well as the C-terminal oligomerization domain from the adjacent subunit (@) are involved in cofactor binding. The interactions in all subunits are almost identical; therefore, the distances are listed only for subunit A and the adjacent subunit B

Protein atom	NAD⁺ atom
*T160 Oγ	O2D (2.69)
*T161 Oγ	O1N (2.78)
*T162 Oγ	O3D (2.66)
*T162 N	O2D (3.17)
#N194 Nδ2	O1N (2.92)
#N227 N	O2N (2.90)
#E246 Oε1	O3B (2.48)
#E246 Oε2	O2B (2.72)
#N281 Nδ2	N7A (2.97)
#I302 O	N7N (2.93)
#H304 N	O3D (2.88)
#N349 Oδ1	N7N (3.08)
#N349 Nδ2	O7N (2.96)
@K429 Nζ	O2B (3.04)
@K429 Nζ	O3B (2.97)
@Y433 Oη	O2A (2.60)

purine ring is anchored in the binding site by several hydrogen bonds. The N6 atom is a donor in two hydrogen bonds, to the carbonyl group of H356 and the side-chain oxygen atom of Q60. It is of note that the latter residue is located in close proximity of the Na⁺ ion . The main-chain N atom of H356 and the side-chain O atom of T58 are involved in hydrogen bonding with the N7 and N1 atoms, respectively. Additionally, the side chains of L350 and M361 constrict the binding cavity and stabilize the position of the ligand through, respectively, C–H⋯π and hydrophobic interactions with the purine ring. The O2' hydroxyl group of the ribose moiety interacts with the side chain oxygen atoms of E159 and D193. Additionally, the side chains of T160 and K189 form hydrogen bonds with the O3' atom. Finally, the carboxylate group of D134 and the side chains of H56 and H304 form a network of interactions with the ribose O5' atom. The latter residue is an element of the molecular gate formed by a tandem of the highly conserved H304-F305 residues which restrict access to the active site from the solvent region. In the present ChSAHase the molecular gate is in the shut state in all subunits.

The Mode of NAD⁺ Binding

One NAD⁺ cofactor molecule is found in each subunit of the ChSAHase model. It is located in the crevice between the
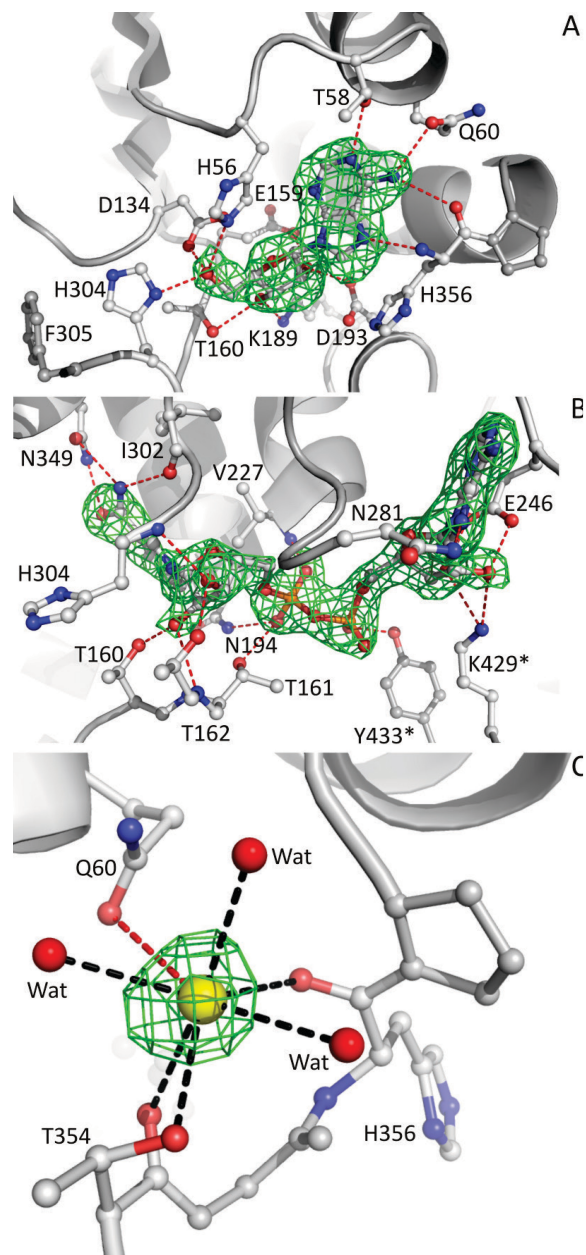

Figure 6. The modes of (A) adenosine, (B) NAD⁺ cofactor, and (C) Na⁺ cation binding in the area of the ChSAHase active site (shown for subunit A). Possible polar interactions are indicated by red dash lines, and the coordination bonds around the Na⁺ cation (yellow sphere) as black dash lines. Water molecules are depicted as red spheres. Two amino acid residues from the adjacent subunit B (K429 and Y433) are marked with a star. The mF_o-DF_c OMIT difference electron density maps are contoured at 2.5σ (adenosine) or 3.0σ (NAD⁺ and Na⁺).

two major domains and its binding mode, presented in Figure 6B, is very similar to that observed in other SAHases.

Table 3. Details of Na$^+$ ion coordination near the active site of ChSAHase with the corresponding cation-ligand distances (Å) listed for all chains (A–D)

Ligand atom:	T354 O	T354 Oγ	H356 O	Wat1	Wat2	Wat3
A	2.88	2.84	2.94	2.87	2.95	2.96
B	2.88	2.95	2.88	2.80	2.81	2.98
C	3.06	3.01	2.95	2.83	2.85	2.92
D	2.94	2.91	3.00	2.79	2.86	3.14

In the present structure, amino acid residues from both the cofactor- and substrate-binding domains are involved in hydrogen-bonding interactions with the NAD$^+$ molecule. Additionally, two residues from the C-terminal oligomerization domain from the adjacent subunit of the intimate dimer also participate in polar interactions with the cofactor. These interactions engage the main- and side-chain atoms of T160 (Oγ···O2D), T161 (Oγ···O2N) and T162 (N···O2D and Oγ···O3D) from the substrate-binding domain; of N194 (Nδ2···O2N), N227 (N···O1N), E246 (Oε1···O2B and Oε2···O3B), N281 (Nδ2···N7A), I302(O···N7N), H304 (N···O3D) and N349 (Nδ2···O7N and Oδ1···N7N) from the cofactor-binding domain; as well as K429 (Nζ···O2B and Nζ···O3B) and Y433 (Oη···O2A) from the adjacent C-terminal domain. The adenine moiety of the cofactor is sandwiched in a narrow cavity, restricted by the side chains of I247 and T279 which form vise-type C–H···π interactions with the purine ring. Additionally, seven water molecules participates in polar interactions with the cofactor molecule.

The Monovalent Cation Coordinated by ChSAHase

In the model of ChSAHase, all subunits exist in the closed conformation, with the substrate and cofactor domains clasped over the Ado substrate/product. In addition to the Ado molecule, each subunit coordinates a sodium cation in the substrate binding area. The Na$^+$ cation is found in the monovalent cation coordinating loop (T354–S356) in close proximity of the purine ring of the nucleoside, but it does not interact with the ligand directly. The coordination sphere of the sodium cation is a distorted octahedron formed by two main-chain carbonyl oxygen atoms provided by the T354 and H356 residues, as well as by the side-chain oxygen atom of T354. Finally, three water molecules complete the Na$^+$ coordination sphere. It is of note that the side chain oxygen atom of the Q60 residue located close to the sodium cation is involved in a cation-dipole interaction (Figure 6C). The Q60 residue is also involved in adenosine binding. A very similar coordination geometry of the Na$^+$ cation was observed in the crystal structures of other sodium-containing SAHases.[3,6,7,16]

Crystal Packing of ChSAHase

Although the asymmetric unit contains four subunits of ChSAHase, they are assembled into two unrelated dimers.

The dimers are located at two different twofold axes along the *z* direction: AB at 0, 0 and CD at 0, ½, which generate from each of them a full 222-symmetric tetrameric molecule possessing both crystallographic and non-crystallographic symmetry. The two dimers selected in the asymmetric unit (AB and CD) are of the same type within the 222-symmetric homotetramer, i.e., they correspond to the so-called intimate dimers, which are mutually hooked into a tight structure by swapping of the C-terminal dimerization domains. It is interesting to note that the dimerization domain of subunit A participates in the formation of the cofactor binding site of subunit B and vice versa, and the same is of course true of the CD dimer.

In addition to the translation of Δ*y* = ½ connected with the location of the point symmetry elements, the AB and CD dimers are also related by a translation of ≈80 Å along the *z* direction, which is equal to ≈0.42 of the *c* parameter of the unit cell. This translational non-crystallographic symmetry is clearly visible in the Patterson map (Figure 1), in which the highest non-origin peak (47 % of the origin) is located at 0, 0.5, 0.424. The combined AB-to-CD translation is equal to ≈95 Å and is coupled with a rotation of ≈1°, making this NCS symmetry of essentially translational type.

The non-crystallographic dyads of the ABA'B' tetramer, obviously parallel to the *xy* plane, are rotated by 7.9° from the crystallographic screws, as calculated by *ALIGN*.[17] In this alignment, the pseudo twofold axis of the 222 molecular symmetry that operates within the intimate AB dimer is nearly parallel to the crystallographic [100] direction. Similarly, the non-crystallographic dyads of the CDC'D' tetramer are rotated by 9.4° from the crystallographic screws, with the pseudo dyad relating C and D nearly parallel to [100]. A view of the molecular packing of the ChSAHase crystal is shown in Figure 4.

METHODS

Cloning, Expression, and Purification of ChSAHase

The coding sequence of the *sahH* gene was amplified by PCR from genomic DNA of *Cytophaga hutchinsonii* strain ATCC 33406 with the following primers: 5'-TACTTCCAATC-CAATGCCATGGTAGACACATTTGTAAAGCACAAAGTAAAAG

and 5'-TTATCCACTTCCAATGTTATTAGTATCTGTATTCGTCG-TTTTTATATGGGC. Subsequently, the amplicon was cloned into the pMCSG57 expression vector using the ligation independent cloning reaction. The correctness of the clone was confirmed by sequencing. The construct carrying the coding sequence of ChSAHase was used for transformation of BL21-CodonPlus(DE3)®-RIPL *Escherichia coli* cells and expressed. Briefly, 10 mL of TB medium containing 34 μg/mL chloramphenicol and 100 μg/mL ampicillin were inoculated and grown overnight at 310 K and the culture was used for inoculation of 1 L of TB medium that was cultivated with appropriate antibiotics to an OD_{600} of 1.0. The temperature was decreased to 291 K and protein expression was induced with IPTG at a final concentration of 0.3 mM. The cells were harvested 15 hours after induction and flash-frozen in liquid nitrogen.

The cell pellet was resuspended in 250 mL of buffer A (20 mM imidazole, 500 mM NaCl, 20 mM Tris·HCl pH 8.0, 10 % glycerol) with the addition of 0.5 mM TCEP·HCl and 100 μg/mL lysozyme. Cells were disrupted by sonication on ice and centrifuged at 277 K for 20 minutes at 4500 rpm. The supernatant was loaded onto a HisTrap column equilibrated with 0.1 M $NiSO_4$. The protein was eluted with 50 mL buffer containing 200 mM imidazole, 500 mM NaCl, 20 mM Tris·HCl pH 8.0, 10 % glycerol, and 1 mM TCEP·HCl. TEV Protease was added at a final concentration of 0.1 mg/mL and the protein solution was extensively dialyzed against buffer A. After overnight incubation at 277 K, the solution was loaded onto a HisTrap column equilibrated with 0.1 M $NiSO_4$ and the protein was eluted with buffer A, subsequently exchanged for buffer B (100 mM NaCl, 25 mM Tris·HCl pH 8.0, 1 mM TCEP·HCl) *via* dialysis. Next, a modified procedure of Yuan *et al.*[18] was used for the preparation of the apo form of the enzyme. Briefly, a solution containing 10 mg of recombinant ChSAHase dissolved in 5 mL of buffer B was gradually mixed with 10 mL of saturated solution of $(NH_4)_2SO_4$ at pH 3.3, and then stored for 10 min on ice. The mixture was centrifuged and the precipitate was dissolved in 5 mL of buffer B. The enzyme was precipitated again as above and the pellet was washed with saturated neutral solution of $(NH_4)_2SO_4$. Finally, the precipitated apo ChSAHase was dissolved in 2 mL of buffer C (100 mM NaCl, 25 mM Tris·HCl pH 8.0) and subsequently NAD^+ was added to a final concentration of 2 mM. After 30 minutes of incubation on ice, the mixture was loaded onto a Superdex 200 (Pharmacia) gel filtration column pre-equilibrated with buffer D (150 mM NaCl, 25 mM Tris·HCl pH 8.0, 1 mM TCEP·HCl). The protein was eluted with buffer D as a tetramer. Fractions with ChSAHase were concentrated to 7.5 mg/mL using Amicon Ultra 100 ultracentrifugation filters and subsequently passed through 0.22 μm filtration membrane. For all the subsequent experiments, fresh protein solutions were always used.

The purified protein is extended at the N-terminus by a short tripeptide (SNA-) cloning artifact. SDS-PAGE analysis confirmed the molecular weight of the expressed protein (≈48 kDa). Ultracentrifugation using filters with 100 kDa cutoff as well as size exclusion chromatography confirmed the tetrameric oligomerization state of ChSAHase in solution.

Assays for SAHase Activity

Assays for ChSAHase activity were performed in the hydrolytic direction. Enzymatic reactions were monitored spectrophotometrically and the rate of L-homocysteine (Hcy) formation was measured by monitoring its reaction with 5,5'-dithiobis(2-nitrobenzoic acid) (DTNB). Assays were performed in 3 mL volume in a buffer containing 100 mM KCl and 25 mM HEPES·KOH pH 7.5. The buffer was supplemented with six units of adenosine deaminase, 100 μM DTNB, and 0.35 μM of ChSAHase. The reaction was initiated by the addition of *S*-adenosyl-L-homocysteine (SAH) at a final concentration from 5.75 to 230 μM. The conversion of Hcy to Hcy-TNB was carried out at 295 K. The reaction progress was measured for one minute and monitored at 412 nm using a Hitachi U-3900H spectrophotometer. Initial velocity parameters were estimated from the linear region of the recorded curve. The experimental data were analyzed with the *GraFit* 7.0 software (Erithacus) to obtain the following kinetic parameters of the enzymatic reactions: substrate affinity (K_M), activity (V_{max}), as well as the catalytic rate (k_{cat}). All measurements were performed in duplicates.

Crystallization and X-ray Data Collection

Protein solution (5 mg/mL, measured spectrophotometrically at 280 nm) in buffer D was incubated overnight with 2 mM adenosine (1:13 molar ratio) at 277 K. The mixture was used for screening for crystallization conditions with a sparse-matrix screen[19] from Molecular Dimensions (Structure Screen 1). Crystallization drops for the screening experiments were mixed from 0.6 μL of the protein solution and 0.6 μL of the reservoir solution. Initial crystals were obtained at 292 K from 15 % (*w/v*) PEG 8000 and 0.5 M Li_2SO_4 using the sitting-drop vapor-diffusion method. The crystallization conditions were tuned by adjusting the protein concentration and volume of the crystallization drop. The best crystals were obtained at protein concentration of 7.5 mg/mL. They were grown using the hanging-drop vapor-diffusion method by mixing 2.5 μL of a ChSAHase-Ado solution with 2.5 μL of precipitating solution on a siliconized coverslide and equilibrating the drop against 1.0 mL of the precipitant solution. Diffraction-quality crystals appeared within ten days.

X-Ray diffraction data were measured at the BESSY synchrotron beamline 14.1 of the Helmholtz-Zentrum

Table 4. Crystallographic data, data collection and structure refinement statistics. Values in parentheses are for the last resolution shell

Data collection and processing	
Beamline	BESSY 14.1
Wavelength (Å)	0.91841
Temperature (K)	100
Space group	$P2_12_12$
Unit-cell parameters (Å)	
a	96.28
b	102.44
c	188.92
Resolution (Å)	50.0 – 2.09
	(2.21 – 2.09)
Mosaicity (°)	0.12
Completeness (%)	99.6 (98.9)
Multiplicity	4.5 (4.6)
$<I/\sigma(I)>$	13.0 (2.4)
R_{merge}	0.090 (0.731)
Refinement statistics	
Working/test reflections	108795/2101
R/R_{free}	0.210/0.231
No. of atoms / $<B>$ (Å^2)	
Overall	14484/42.8
Protein	13457/43.5
Ado	76/36.5
NAD$^+$	176/38.4
Water	751/31.3
PEG	7/56.2
PG4	13/69.7
Na$^+$ ions	4/34.5
R.m.s.d. from ideality	
bond lengths (Å)	0.012
bond angles (°)	1.56
Ramachandran statistics (%)	
Most favored regions	98
Allowed regions	2
PDB code	6GBN

Berlin (HZB). A single crystal was soaked for a few seconds in the reservoir solution supplemented with 15 % (*v/v*) PEG 400, and then vitrified in liquid nitrogen prior to X-ray data collection. The diffraction data extend to 2.09 Å and were autoprocessed with *XDSAPP*[20] which makes use of *XDS*[21] and the *CCP4* suite.[22] The final data set is characterized in Table 4.

Structure Solution, Refinement, and Validation

The native Patterson map (Figure 1) showed a high non-origin peak at 0, 0.5, 0.424, implicating the existence of non-crystallographic translation of ≈95 Å in the unit cell. A preliminary solution of the crystal structure obtained by molecular replacement with the application of *PHASER*[23] from the *CCP4* suite and using chain A of *H. sapiens* SAHase[24] as the search model (PDB entry 1LI4) confirmed that the crystal packing indeed included two independent ChSAHase dimers located at two different crystallographic

twofold [001] axes, with an additional translation of ≈80 Å along *z*. This preliminary solution revealed that the crystallographic twofold symmetry was not involved in the generation of the unique intimate dimer at each location. In order to generate a consistent description of the asymmetric unit contents, the structure was solved again, this time using the intimate dimer of *H. sapiens* SAHase as the search model (PDB entry 1LI4, chain A and its symmetry-related counterpart). The *PHASER* program was run in this case in the translation search mode with a minimum length of the translational vector of 90 Å, as estimated from the Patterson function. (It should be noted that in variance with the present ChSAHase case, the intimate dimer of *H. sapiens* SAHase *is* generated by crystallographic twofold symmetry.) The final solution is described in space group $P2_12_12$ with two separate tNCS-related intimate dimers (AB and CD) in the asymmetric unit, from which two different crystallographic dyads along *z* (at 0, 0 for AB and at 0, ½ for CD) generate two complete ChSAHase homotetramers (ABA'B' and CDC'D'). Automatic model building was carried out with the online version of *ARP/wARP*.[25] Isotropic stereochemically-restrained structure-factor refinement was carried out in *REFMAC5*[26] with maximum-likelihood targets and with the inclusion of automatically generated local NCS restraints. After a few rounds of minimization, three TLS groups per protein chain, as suggested by the *TLSMD* server,[27] were included in the refinement procedure.[28] The placement of the model in the unit cell was standardized with the *ACHESYM* server.[29] The ligands were identified without ambiguity in mF_o-DF_c omit electron density maps phased with the contribution of the protein atoms only. The alkali cation binding sites were confirmed as Na$^+$ with *CheckMyMetal*.[30] Water molecules and other components of the buffer solution were added only when unambiguously confirmed by electron density maps. The *COOT* program[31] was used for manual modeling in electron density maps. The stereochemical quality of the model was assessed using the wwPDB validation pipeline.[32] Atomic coordinates and ADP parameters, as well as structure factors have been deposited in the Protein Data Bank (PDB) with the accession code 6GBN. Raw X-ray diffraction images for the crystal structure of the ChSAHase-NAD$^+$-Ado ternary complex have been deposited in the RepOD Repository at the Interdisciplinary Centre for Mathematical and Computational Modelling (ICM) of the University of Warsaw, Poland, with the Digital Object Identifier (DOI) doi:10.18150/repod.4000773, and are available for download to all interested researchers from http://dx.doi.org/10.18150/repod.4000773. The final refinement statistics are reported in Table 4.

REFERENCES

[1]   H. H. Richards, P. K. Chiang, G. L. Cantoni, *J. Biol. Chem.* **1978**, *253*, 4476.

[2]   P. K. Chiang, *Pharmacol. Ther.* **1998**, *77*, 115.

[3]   K. Brzezinski, Z. Dauter, M. Jaskolski, *Acta Crystallogr. D* **2012**, *68*, 218.

[4]   M. A. Turner, C. S. Yuan, R. T. Borchardt, M. S. Hershfield, G. D. Smith, P. L. Howell, *Nat. Struct. Biol.* **1998**, *5*, 369.

[5]   Y. Hu, J. Komoto, Y. Huang, T. Gomi, H. Ogawa, Y. Takata, M. Fujioka, F. Takusagawa, *Biochemistry* **1999**, *38*, 8323.

[6]   N. Tanaka, M. Nakanishi, Y. Kusakabe, K. Shiraiwa, S. Yabe, Y. Ito, Y. Kitade, K.T. Nakamura, *J. Mol. Biol.* **2004**, *343*, 1007.

[7]   M. C. M. Reddy, G. Kuppan, N. D. Shetty, J. L. Owen, T. R. Ioerger, J. C. Sacchettini, *Protein Sci.* **2008**, *17*, 2134.

[8]   T. Manszewski, K. Singh, B. Imiolczyk, M. Jaskolski, *Acta Crystallogr. D* **2015**, *71*, 2422.

[9]   Y. Zheng, C. -C. Chen, T. -P. Ko, X. Xiao, Y. Yang, C. -H. Huang, G. Qian, W. Shao, R. -T. Guo, *J. Struct. Biol.* **2015**, *190*, 135.

[10] K. Brzezinski, J. Czyrko, J. Sliwiak, E. Nalewajko-Sieliwoniuk, M. Jaskolski, B. Nocek, Z. Dauter, *Int. J. Biol. Macromol.* **2017**, *104*, 584.

[11] Y. Kusakabe, M. Ishihara, T. Umeda, D. Kuroda, M. Nakanishi, Y. Kitade, H. Gouda, K. T. Nakamura, N. Tanaka, *Sci. Rep.* **2015**, *5*, 16641.

[12] A. Guranowski, J. Pawelkiewicz, *Eur. J. Biochem.* **1977**, *80*, 517.

[13] T. Stepkowski, K. Brzeziński, A. B. Legocki, M. Jaskólski, G. Béna, *Mol. Phylogenet. Evol.* **2005**, *34*, 15.

[14] K. Brzezinski, G. Bujacz, M. Jaskolski, *Acta Crystallogr. F* **2008**, *64*, 671.

[15] B. W. Matthews, *J. Mol. Biol.* **1968**, *33*, 491.

[16] T. Manszewski, K. Szpotkowski, M. Jaskolski, *IUCrJ* **2017**, *4*, 271.

[17] G. E. Cohen, *J. Appl. Crystallogr.* **1997**, *30*, 1160.

[18] C. S. Yuan, J. Yeh, S. Liu, R. T. Borchardt, *J. Biol. Chem.* **1993**, *268*, 17030.

[19] J. Jancarik, S. H. Kim, *J. Appl. Crystallogr.* **1991**, *24*, 409.

[20] K. M. Sparta, M. Krug, U. Heinemann, U. Mueller, M. S. Weiss, *J. Appl. Crystallogr.* **2016**, *49*, 1085.

[21] W. Kabsch, *Acta Crystallogr. D* **2010**, *66*, 125.

[22] M. D. Winn, C. C. Ballard, K. D. Cowtan, E. J. Dodson, P. Emsley, P. R. Evans, R. M. Keegan, E. B. Krissinel, A. G. W. Leslie, A. McCoy, S. J. McNicholas, G. N. Murshudov, N. S. Pannu, E. A. Potterton, H. R. Powell, R. J. Read, A. Vagin, K. S. Wilson, *Acta Crystallogr. D* **2011**, *67*, 235.

[23] A. J. McCoy, R. W. Grosse-Kunstleve, P. D. Adams, M. D. Winn, L. C. Storoni, R. J. Read, *J. Appl. Crystallogr.* **2007**, *40*, 658.

[24] X. Yang, Y. Hu, D. H. Yin, M. A. Turner, M. Wang, R. T. Borchardt, P. L. Howell, K. Kuczera, R. L. Schowen, *Biochemistry* **2003**, *42*, 1900.

[25] G. Langer, S. X. Cohen, V. S. Lamzin, A. Perrakis, *Nat. Protoc.* **2008**, *3*, 1171.

[26] G. N. Murshudov, P. Skubák, A. A. Lebedev, N. S. Pannu, R. A. Steiner, R. A. Nicholls, M. D. Winn, F. Long, A. A. Vagin, *Acta Crystallogr. D* **2011**, *67*, 355.

[27] J. Painter, E. A. Merritt, *J. Appl. Crystallogr.* **2006**, *39*, 109.

[28] M. D. Winn, M. N. Isupov, G. N. Murshudov, *Acta Crystallogr. D* **2001**, *57*, 122.

[29] M. Kowiel, M. Jaskolski, Z. Dauter, *Acta Crystallogr. D* **2014**, *70*, 3290.

[30] H. Zheng, D. R. Cooper, P. J. Porebski, I. G. Shabalin, K. B. Handing, W. Minor, *Acta Crystallogr. D* **2017**, *73*, 223.

[31] P. Emsley, B. Lohkamp, W. G. Scott, K. Cowtan, *Acta Crystallogr. D* **2010**, *66*, 486.

[32] H. Berman, K. Henrick, H. Nakamura, *Nat. Struct. Biol.* **2003**, *10*, 980.

OŚWIADCZENIA WSKAZUJĄCE WKŁAD POSZCZEGÓLNYCH AUTORÓW W POWSTANIE PUBLIKACJI

PUBLIKACJA

D1

Białystok, 26-05-2020

dr hab. Krzysztof Brzeziński
Uniwersytet w Białymstoku
Wydział Chemii
ul. Ciołkowskiego 1K
15-245 Białystok

Oświadczenie współautora publikacji

Dotyczy publikacji:

Brzezinski, K., Czyrko, J., Sliwiak, J., Nalewajko-Sieliwoniuk, E., Jaskolski, M., Nocek, B. and Dauter, Z. (2017). *S*-adenosyl-L-homocysteine hydrolase from a hyperthermophile (*Thermotoga maritima*) is expressed in *Escherichia coli* in inactive form - Biochemical and structural studies. *International Journal of Biological Macromolecules* **104,** 584-596.

Oświadczam, że w pracy: **Brzezinski, K., Czyrko, J., Sliwiak, J., Nalewajko-Sieliwoniuk, E., Jaskolski, M., Nocek, B. and Dauter, Z. (2017).** *S*-adenosyl-L-homocysteine hydrolase from a hyperthermophile (*Thermotoga maritima*) is expressed in *Escherichia coli* in inactive form - Biochemical and structural studies. *International Journal of Biological Macromolecules* **104, 584-596.**, mój udział polegał na sformułowaniu problemu badawczego i koncepcji pracy, wykonaniu eksperymentów związanych z częścią biokrystalograficzną pracy, analizie wyników i współopracowaniu publikacji.

Białystok, 26-05-2020

mgr Justyna Czyrko-Horczak
Uniwersytet w Białymstoku
Wydział Chemii
ul. Ciołkowskiego 1K
15-245 Białystok

Oświadczenie współautora publikacji

Dotyczy publikacji:

Brzezinski, K., Czyrko, J., Sliwiak, J., Nalewajko-Sieliwoniuk, E., Jaskolski, M., Nocek, B. and Dauter, Z. (2017). *S*-adenosyl-L-homocysteine hydrolase from a hyperthermophile (*Thermotoga maritima*) is expressed in *Escherichia coli* in inactive form - Biochemical and structural studies. *International Journal of Biological Macromolecules* **104,** 584-596.

Oświadczam, że w pracy: **Brzezinski, K., Czyrko, J., Sliwiak, J., Nalewajko-Sieliwoniuk, E., Jaskolski, M., Nocek, B. and Dauter, Z. (2017).** *S*-adenosyl-L-homocysteine hydrolase **from a hyperthermophile (*Thermotoga maritima*) is expressed in *Escherichia coli* in inactive form - Biochemical and structural studies.** *International Journal of Biological Macromolecules* **104, 584-596.**, mój udział polegał na optymalizacji procedury oczyszczania rekombinowanego białka, analizie stanów oligomerycznych białka, ustaleniu stanu utlenienia kofaktora, opracowaniu i wykonaniu pomiarów aktywności katalitycznej z wykorzystaniem chromatografii HPLC, przeprowadzeniu analizy porównawczej modeli strukturalnych enzymu w formie aktywnej i nieaktywnej, analizie wyników i współopracowaniu publikacji.

Poznań, 10-11-2018

dr Joanna Śliwiak
Instytut Chemii Bioorganicznej PAN
Zakład Krystalografii
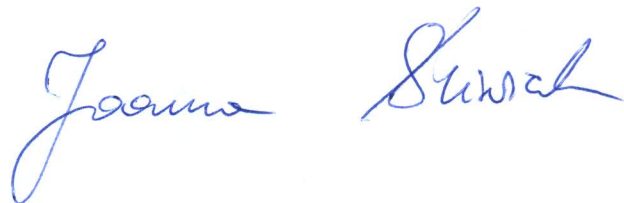Centrum Badań Biokrystalograficznych
ul. Noskowskiego 12/14
61-704 Poznań

Oświadczenie współautora publikacji

Dotyczy publikacji:

Brzezinski, K., Czyrko, J., Sliwiak, J., Nalewajko-Sieliwoniuk, E., Jaskolski, M., Nocek, B., Dauter, Z. (2017). *S*-adenosyl-L-homocysteine hydrolase from a hyperthermophile (*Thermotoga maritima*) is expressed in *Escherichia coli* in inactive form - Biochemical and structural studies. *International Journal of Biological Macromolecules* **104,** 584-596.

Oświadczam, że w pracy: **Brzezinski, K., Czyrko, J., Sliwiak, J., Nalewajko-Sieliwoniuk, E., Jaskolski, M., Nocek, B., Dauter, Z. (2017).** *S*-adenosyl-L-homocysteine hydrolase from a hyperthermophile **(***Thermotoga maritima***) is expressed in** *Escherichia coli* **in inactive form - Biochemical and structural studies.** *International Journal of Biological Macromolecules* **104, 584-596.,** mój udział polegał na przeprowadzeniu i analizie pomiarów dotyczących oddziaływań enzym-ligand metodą miareczkowania mikrokalorymetrycznego.

Białystok, 23-11-2018

Dr Edyta Nalewajko-Sieliwoniuk
Uniwersytet w Białymstoku
Wydział Biologiczno-Chemiczny
Instytut Chemii
ul. K. Ciołkowskiego 1K
15-245 Białystok

Oświadczenie współautora publikacji

Dotyczy publikacji:

Brzezinski, K., Czyrko, J., Sliwiak, J., Nalewajko-Sieliwoniuk, E., Jaskolski, M., Nocek, B. and Dauter, Z. (2017) *S*-adenosyl-L-homocysteine hydrolase from a hyperthermophile (*Thermotoga maritima*) is expressed in *Escherichia coli* in inactive form - Biochemical and structural studies. *International Journal of Biological Macromolecules* **104**, 584-596.

Oświadczam, że w pracy: **Brzezinski, K., Czyrko, J., Sliwiak, J., Nalewajko-Sieliwoniuk, E., Jaskolski, M., Nocek, B. and Dauter, Z. (2017)** *S*-adenosyl-L-homocysteine hydrolase from a hyperthermophile **(***Thermotoga maritima***)** is expressed in *Escherichia coli* in inactive form - Biochemical and structural studies. *International Journal of Biological Macromolecules* **104, 584-596.**, mój udział polegał na przeprowadzeniu testów aktywności enzymatycznej badanego białka.

Edyta Nalewajko-Sieliwoniuk

Poznań, 25-04-2020

Prof. dr hab. Mariusz Jaskólski
Uniwersytet im. Adama Mickiewicza w Poznaniu
Wydział Chemii
ul. Uniwersytetu Poznańskiego 8
61-614 Poznań

Oświadczenie współautora publikacji

Dotyczy publikacji:

Brzezinski, K., Czyrko, J., Sliwiak, J., Nalewajko-Sieliwoniuk, E., Jaskolski, M., Nocek, B. and Dauter, Z. (2017). *S*-adenosyl-L-homocysteine hydrolase from a hyperthermophile (*Thermotoga maritima*) is expressed in *Escherichia coli* in inactive form - Biochemical and structural studies. *International Journal of Biological Macromolecules* **104,** 584-596.

Oświadczam, że w pracy: **Brzezinski, K., Czyrko, J., Sliwiak, J., Nalewajko-Sieliwoniuk, E., Jaskolski, M., Nocek, B. and Dauter, Z. (2017)** *S*-**adenosyl-L-homocysteine hydrolase from a hyperthermophile (***Thermotoga maritima***) is expressed in** *Escherichia coli* **in inactive form - Biochemical and structural studies.** *International Journal of Biological Macromolecules* **104, 584-596.**, mój udział polegał na współopracowaniu publikacji.
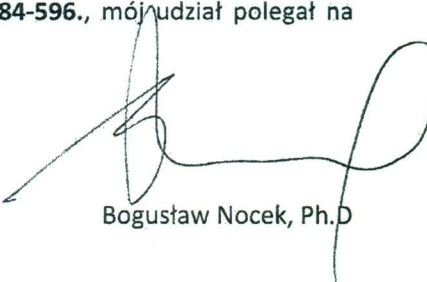
Mariusz Jaskólski

North Chicago, 26-11-2018

Dr Bogusław Nocek
Senior Scientist, Abbvie

Oświadczenie współautora publikacji

Dotyczy publikacji:

Brzezinski, K., Czyrko, J., Sliwiak, J., Nalewajko-Sieliwoniuk, E., Jaskolski, M., Nocek, B. and Dauter, Z. (2017) *S*-adenosyl-L-homocysteine hydrolase from a hyperthermophile (*Thermotoga maritima*) is expressed in *Escherichia coli* in inactive form - Biochemical and structural studies. *International Journal of Biological Macromolecules* **104**, 584-596.

Oświadczam, że w pracy: **Brzezinski, K., Czyrko, J., Sliwiak, J., Nalewajko-Sieliwoniuk, E., Jaskolski, M., Nocek, B. and Dauter, Z. (2017)** *S*-**adenosyl-L-homocysteine hydrolase from a hyperthermophile (***Thermotoga maritima***) is expressed in ***Escherichia coli*** in inactive form - Biochemical and structural studies.** *International Journal of Biological Macromolecules* **104, 584-596.**, mój udział polegał na współprzygotowaniu publikacji i analizie danych.
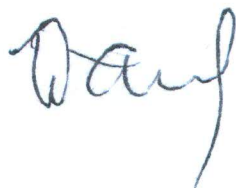
Bogusław Nocek, Ph.D

Dr hab. Zbigniew Dauter
National Cancer Institute
Macromolecular Crystallography Laboratory
Synchrotron Radiation Research Section
Argonne National Laboratory
Bldg. 202, Argonne, S. Cass Ave.
IL 60439, USA

Oświadczenie współautora publikacji

Dotyczy publikacji:

Brzezinski, K., Czyrko, J., Sliwiak, J., Nalewajko-Sieliwoniuk, E., Jaskolski, M., Nocek, B. and Dauter, Z. (2017) *S*-adenosyl-L-homocysteine hydrolase from a hyperthermophile (*Thermotoga maritima*) is expressed in *Escherichia coli* in inactive form - Biochemical and structural studies. *International Journal of Biological Macromolecules* **104,** 584-596.

Oświadczam, że w pracy: **Brzezinski, K., Czyrko, J., Sliwiak, J., Nalewajko-Sieliwoniuk, E., Jaskolski, M., Nocek, B. and Dauter, Z. (2017)** *S*-adenosyl-L-homocysteine hydrolase from a hyperthermophile **(***Thermotoga maritima***) is expressed in** *Escherichia coli* **in inactive form - Biochemical and structural studies.** *International Journal of Biological Macromolecules* **104, 584-596.**, mój udział polegał na analizie danych krystalograficznych.

PUBLIKACJA

D2

Białystok, 26-05-2020

mgr Justyna Czyrko-Horczak
Uniwersytet w Białymstoku
Wydział Chemii
ul. Ciołkowskiego 1K
15-245 Białystok

Oświadczenie współautora publikacji

Dotyczy publikacji:

Czyrko, J., Sliwiak, J., Imiolczyk, B., Gdaniec, Z., Jaskolski, M., Brzezinski, K. (2018). Metal-cation regulation of enzyme dynamics is a key factor influencing the activity of *S*-adenosyl-L-homocysteine hydrolase from *Pseudomonas aeruginosa*. *Scientific Reports* **8,** 11334.

Oświadczam, że w pracy: **Czyrko, J., Sliwiak, J., Imiolczyk, B., Gdaniec, Z., Jaskolski, M., Brzezinski, K. (2018). Metal-cation regulation of enzyme dynamics is a key factor influencing the activity of *S*-adenosyl-L-homocysteine hydrolase from *Pseudomonas aeruginosa*. *Scientific Reports* 8, 11334.,** mój udział polegał na optymalizacji procedury oczyszczania rekombinowanego białka, opracowaniu systemu klonowania i oczyszczania muteiny PaSAHazy Gln65Ala, analizie stanów oligomerycznych białka, ustaleniu stanu utlenienia kofaktora, przeprowadzeniu wszystkich eksperymentów związanych z kinetyką reakcji enzymatycznych oraz wpływem inhibitorów na aktywność katalityczną enzymu, analizie wyników i współopracowaniu publikacji.

Poznań, 10-11-2018

dr Joanna Śliwiak
Instytut Chemii Bioorganicznej PAN
Zakład Krystalografii
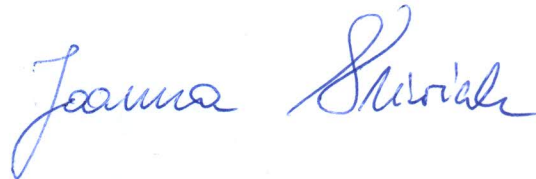Centrum Badań Biokrystalograficznych
ul. Noskowskiego 12/14
61-704 Poznań

Oświadczenie współautora publikacji

Dotyczy publikacji:

Czyrko, J., Sliwiak, j., Imiolczyk, B., Gdaniec, Z., Jaskolski, M., Brzezinski, K. (2018). Metal-cation regulation of enzyme dynamics is a key factor influencing the activity of *S*-adenosyl-L-homocysteine hydrolase from *Pseudomonas aeruginosa*. (2018). *Scientific Reports* **8,** 11334.

Oświadczam, że w pracy: **Czyrko, J., Sliwiak, j., Imiolczyk, B., Gdaniec, Z., Jaskolski, M., Brzezinski, K. (2018). Metal-cation regulation of enzyme dynamics is a key factor influencing the activity of *S*-adenosyl-L-homocysteine hydrolase from *Pseudomonas aeruginosa*. (2018). *Scientific Reports* 8, 11334.,** mój udział polegał na przeprowadzeniu i analizie pomiarów dotyczących oddziaływań enzym-ligand metodą miareczkowania mikrokalorymetrycznego.

Poznań, 2020-03-19

dr Barbara Imiołczyk
Instytut Chemii Bioorganicznej PAN
Zakład Krystalografii
Centrum Badań Biokrystalograficznych
ul. Noskowskiego 12/14
61-704 Poznań

Oświadczenie współautora publikacji

Dotyczy publikacji:

Czyrko J.,Sliwiak J., Imiolczyk B., Gdaniec Z., Jaskolski M., Brzezinski K. "Metal-cation regulation of enzyme dynamics is a key factor influencing the activity of S-adenosyl-L-homocysteine hydrolase from Pseudomonas aeruginosa" Scientific Reports 8, 11334 (2018).

Oświadczam, że w pracy **Czyrko J., Sliwiak J., Imiolczyk B., Gdaniec Z., Jaskolski M., Brzezinski K. "Metal-cation regulation of enzyme dynamics is a key factor influencing the activity of S-adenosyl-L-homocysteine hydrolase from Pseudomonas aeruginosa" Scientific Reports 8, 11334 (2018)** mój wkład w powstanie tej pracy polegał na: ekspresji i oczyszczeniu mutanta Q65A SAHazy z *Pseudomonas aeruginosa*.

Prof. dr hab. Zofia Gdaniec
Instytut Chemii Bioorganicznej PAN
Zakład Biomolekularnego NMR
ul. Noskowskiego 12/14
61-704 Poznań

Oświadczenie współautora publikacji

Dotyczy publikacji:

Czyrko, J., Sliwiak, j., Imiolczyk, B., Gdaniec, Z., Jaskolski, M., Brzezinski, K. (2018). Metal-cation regulation of enzyme dynamics is a key factor influencing the activity of *S*-adenosyl-L-homocysteine hydrolase from *Pseudomonas aeruginosa*. (2018). *Scientific Reports* **8,** 11334.

Oświadczam, że w pracy: **Czyrko, J., Sliwiak, j., Imiolczyk, B., Gdaniec, Z., Jaskolski, M., Brzezinski, K. (2018). Metal-cation regulation of enzyme dynamics is a key factor influencing the activity of *S*-adenosyl-L-homocysteine hydrolase from *Pseudomonas aeruginosa*. (2018). *Scientific Reports* 8, 11334.,** mój udział polegał na przeprowadzeniu i analizie pomiarów ^{23}Na NMR.

Prof. dr hab. Mariusz Jaskólski
Uniwersytet im. Adama Mickiewicza w Poznaniu
Wydział Chemii
ul. Uniwersytetu Poznańskiego 8
61-614 Poznań

<center>**Oświadczenie współautora publikacji**</center>

Dotyczy publikacji:

Czyrko, J., Sliwiak, j., Imiolczyk, B., Gdaniec, Z., Jaskolski, M., Brzezinski, K. (2018). Metal-cation regulation of enzyme dynamics is a key factor influencing the activity of *S*-adenosyl-L-homocysteine hydrolase from *Pseudomonas aeruginosa*. *Scientific Reports* **8,** 11334.

Oświadczam, że w pracy: **Czyrko, J., Sliwiak, j., Imiolczyk, B., Gdaniec, Z., Jaskolski, M., Brzezinski, K. (2018). Metal-cation regulation of enzyme dynamics is a key factor influencing the activity of *S*-adenosyl-L-homocysteine hydrolase from *Pseudomonas aeruginosa*. *Scientific Reports* 8, 11334.**, mój udział polegał na współopracowaniu publikacji.

Mariusz Jaskólski

Białystok, 26-05-2020

dr hab. Krzysztof Brzeziński
Uniwersytet w Białymstoku
Wydział Chemii
ul. Ciołkowskiego 1K
15-245 Białystok

Oświadczenie współautora publikacji

Dotyczy publikacji:

Czyrko, J., Sliwiak, J., Imiolczyk, B., Gdaniec, Z., Jaskolski, M., Brzezinski, K. (2018). Metal-cation regulation of enzyme dynamics is a key factor influencing the activity of *S*-adenosyl-L-homocysteine hydrolase from *Pseudomonas aeruginosa*. *Scientific Reports* **8,** 11334.

Oświadczam, że w pracy: **Czyrko, J., Sliwiak, J., Imiolczyk, B., Gdaniec, Z., Jaskolski, M., Brzezinski, K. (2018). Metal-cation regulation of enzyme dynamics is a key factor influencing the activity of *S*-adenosyl-L-homocysteine hydrolase from *Pseudomonas aeruginosa*. *Scientific Reports* 8, 11334.,** mój udział polegał na sformułowaniu problemu badawczego i koncepcji pracy, wykonaniu eksperymentów związanych z częścią biokrystalograficzną pracy, analizie wyników i współopracowaniu publikacji.

PUBLIKACJA

D3

Białystok, 26-05-2020

mgr Justyna Czyrko-Horczak
Uniwersytet w Białymstoku
Wydział Chemii
ul. Ciołkowskiego 1K
15-245 Białystok

Oświadczenie współautora publikacji

Dotyczy publikacji:

Czyrko J., Jaskolski M., Brzezinski K. (2018). Crystal structure of *S*-adenosyl-L-homocysteine hydrolase from *Cytophaga hutchinsonii*, a case of combination of crystallographic and non-crystallographic symmetry. *Croatica Chemica Acta* **91**, 153-162.

Oświadczam, że w pracy: **Czyrko J., Jaskolski M., Brzezinski K. (2018). Crystal structure of *S*-adenosyl-L-homocysteine hydrolase from *Cytophaga hutchinsonii*, a case of combination of crystallographic and non-crystallographic symmetry. *Croatica Chemica Acta* 91, 153-162.,** mój wkład polegał na wykonaniu wszystkich eksperymentów, analizie wyników i współopracowaniu publikacji.

Prof. dr hab. Mariusz Jaskólski
Uniwersytet im. Adama Mickiewicza w Poznaniu
Wydział Chemii
ul. Uniwersytetu Poznańskiego 8
61-614 Poznań

<div align="center">

Oświadczenie współautora publikacji

</div>

Dotyczy publikacji:

Czyrko J., Jaskolski M., Brzezinski K. (2018). Crystal structure of *S*-adenosyl-L-homocysteine hydrolase from *Cytophaga hutchinsonii*, a case of combination of crystallographic and non-crystallographic symmetry. *Croatica Chemica Acta* **91**, 153-162.

Oświadczam, że w pracy: **Czyrko J., Jaskolski M., Brzezinski K. (2018). Crystal structure of *S*-adenosyl-L-homocysteine hydrolase from *Cytophaga hutchinsonii*, a case of combination of crystallographic and non-crystallographic symmetry. *Croatica Chemica Acta* 91, 153-162.,** mój wkład polegał na analizie wyników i współopracowaniu publikacji.

Mariusz Jaskólski

Białystok, 26-05-2020

dr hab. Krzysztof Brzeziński
Uniwersytet w Białymstoku
Wydział Chemii
ul. Ciołkowskiego 1K
15-245 Białystok

Oświadczenie współautora publikacji

Dotyczy publikacji:

Czyrko J., Jaskolski M., Brzezinski K. (2018). Crystal structure of *S*-adenosyl-L-homocysteine hydrolase from *Cytophaga hutchinsonii*, a case of combination of crystallographic and non-crystallographic symmetry. *Croatica Chemica Acta* **91**, 153-162.

Oświadczam, że w pracy: **Czyrko J., Jaskolski M., Brzezinski K. (2018). Crystal structure of *S*-adenosyl-L-homocysteine hydrolase from *Cytophaga hutchinsonii*, a case of combination of crystallographic and non-crystallographic symmetry. *Croatica Chemica Acta* 91, 153-162.,** mój wkład polegał na analizie wyników i współopracowaniu publikacji.